BRL

AD

AD 7259998

CONTRACT REPORT NO. 37

3SR-201

HELP CODE SOLUTIONS TO TWO TEST
PROBLEMS IN ARMOR PENETRATION
TOPICAL REPORT

Prepared by

Systems, Science and Software
La Jolla, California

DDC

JUL 8 1971

RECEIVED

D

May 1971

This document has been approved for public release and sale;
its distribution is unlimited.

U.S. ARMY ABERDEEN RESEARCH AND DEVELOPMENT CENTER
BALLISTIC RESEARCH LABORATORIES
ABERDEEN PROVING GROUND, MARYLAND

165

DOCUMENT CONTROL DATA · R & D

(Security classification of title, body of abstract and indexing annotation must be entered when the overall report is classified)

1 ORIGINATING ACTIVITY *(Corporate author)*	2a. REPORT SECURITY CLASSIFICATION
Systems, Science and Software P.O. Box 1620 La Jolla, California 92123	Unclassified
	2b. GROUP

3. REPORT TITLE

HELP Code Solutions to Two Test Problems in Armor Penetration

4. DESCRIPTIVE NOTES *(Type of report and inclusive dates)*

Topical Report

5. AUTHOR(S) *(First name, middle initial, last name)*

L. J. Hageman
J. M. Walsh

6. REPORT DATE	7a. TOTAL NO. OF PAGES	7b. NO. OF REFS
May 1971	163	3

8a. CONTRACT OR GRANT NO. DAAG 07-68-C-0931	9a. ORIGINATOR'S REPORT NUMBER(S) 3SR-201
b. PROJECT NO. RDT&E 1T650212D620	
c.	9b. OTHER REPORT NO(S) *(Any other numbers that may be assigned this report)* BRL Contract Report No. 37
d.	

10. DISTRIBUTION STATEMENT

This document has been approved for public release and sale;
its distribution is unlimited.

11. SUPPLEMENTARY NOTES	12. SPONSORING MILITARY ACTIVITY
	USA Aberdeen Research & Development Center Ballistic Research Laboratories Aberdeen Proving Ground, Maryland 21005

13. ABSTRACT

Two test problems, each the impact of a right circular cylinder on a target plate of finite thickness, at a velocity in the ballistic range, are solved using an Eulerian computer program, HELP, for the solution of axisymmetric time-dependent flows. Test Problem Number 1 is an iron-on-iron impact and Test Problem Number 2 is an iron projectile impacting aluminum. In all cases the materials are treated as compressible and deviatoric stresses are obtained using an elastic-plastic constitutive equation.

Computed results from these first two HELP problems are given in considerable detail in order that quantitative comparisons of these solutions can be made with Lagrangian calculations being performed by other research teams.

DD FORM **1473** REPLACES DD FORM 1473, 1 JAN 64, WHICH IS OBSOLETE FOR ARMY USE.

KEY WORDS	LINK A		LINK B		LINK C	
	ROLE	WT	ROLE	WT	ROLE	WT
Impact						
Armor Penetration						
Numerical Solutions						
Material Response						

BALLISTIC RESEARCH LABORATORIES

CONTRACT REPORT NO. 37

3SR-201

MAY 1971

HELP CODE SOLUTIONS TO TWO TEST PROBLEMS IN ARMOR PENETRATION

TOPICAL REPORT

L. J. Hageman
J. M. Walsh

Prepared By:

SYSTEMS, SCIENCE AND SOFTWARE
La Jolla, California

ABERDEEN PROVING GROUND, MARYLAND

BALLISTIC   RESEARCH   LABORATORIES

CONTRACT REPORT NO. 37

3SR-201

LJHageman/JMWalsh
Aberdeen Proving Ground, Md.
May 1971

HELP CODE SOLUTIONS TO TWO TEST
PROBLEMS IN ARMOR PENETRATION

TOPICAL REPORT

ABSTRACT

Two test problems, each the impact of a right circular cylinder on
a target plate of finite thickness, at a velocity in the ballistic range,
are solved using an Eulerian computer program, HELP, for the solution of
axisymmetric time-dependent flows. Test Problem Number 1 is an iron-on-
iron impact and Test Problem Number 2 is an iron projectile impacting
aluminum. In all cases the materials are treated as compressible and
deviatoric stresses are obtained using an elastic-plastic constitutive
equation.

Computed results from these first two HELP problems are given in
considerable detail in order that quantitative comparisons of these
solutions can be made with Lagrangian calculations being performed by
other research teams.

CONTENTS

CONTENTS (continued)

I. INTRODUCTION

General objectives which have been assigned to S^3 in the present armor penetration program consist of:

(1) The development of certain advanced Eulerian numerical techniques for the solution of problems in armor penetration.

(2) The application of these techniques to a range of problems. These applications incorporate accurate material descriptions and configurations of practical concern in an effort to provide a realistic theoretical description of th _rmor penetration process.

(3) The solution of two specified test problems. These test problems are not intended to represent realistic armor penetrations, since use is made of simple highly-idealized material properties and projectiles that are right circular cylinders. The objective of this work, requested by the Joint Technical Coordinating Group for Munitions Effectiveness (JTCG/ME), is to provide solutions to problems which are very well defined so that meaningful comparisons can be made between the Eulerian solutions by S^3 and the Lagrangian results by other research groups participating in the JTCG/ME program.

The purpose of the present paper is to report the Eulerian solutions to the problems assigned by the JTCG/ME, Item (3) above. In Section II below, the problems are stated and the requested information is listed. In Section III the solutions are given. All of the information requested by the JTCG/ME is presented in that section.

1

Both of the solutions given in Section III were computed using the HELP code, a hydrodynamic elastic-plastic multi-material program which is being developed and tested under Task (1) above. The HELP code used as its starting point the code RPM, a compressible hydrodynamic rigid-plastic one-material Eulerian code which was developed under auspices of the Ballistic Research Laboratories and which is used extensively in S^3 programs.

A considerable amount of related research, not required to meet the JTCG/ME specifications, will be mentioned briefly but will not be detailed in the present report. This work consists of Eulerian solutions obtained using alternative physical models and/or Eulerian programs. One of these is an incompressible rigid-plastic solution to Test Problem No. 1 (a like-material impact). This solution made use of the SLUG code, a program developed as part of this effort by adding a rigid-plastic capability to the S^3 incompressible Eulerian code SURGE. The SLUG calculation has been described in previous reports and discussed at JTCG/ME meetings. Also, a solution to Test Problem No. 2 (an unlike-material impact) using the DORF code, was obtained and reported in early 1969. DORF is a two-material compressible hydrodynamic code with strength included in the rigid-plastic approximation. Results from these and other Eulerian variations of the test problems are, in most respects, in substantial agreement with the HELP solutions given in Section III. Some differences, e.g., the absence of tensions in the incompressible model, have been noted previously. The HELP solutions are presented in Section III, however, because they include the full range of physical phenomena (compressibility, an elastic as well as a plastic regime, and sharp Eulerian interfaces) which occur in the problems as stated by the JTCG/ME.

2

II. STATEMENT OF PROBLEMS

A. INITIAL CONDITIONS

1. Test Problem No. 1

Test Problem No. 1 is an axisymmetric iron-on-iron impact in which a right circular cylinder (radius 0.375 cm, length 1.15 cm) impinges at 9.0×10^4 cm/sec on a flat plate target of thickness 1.5 cm.

3
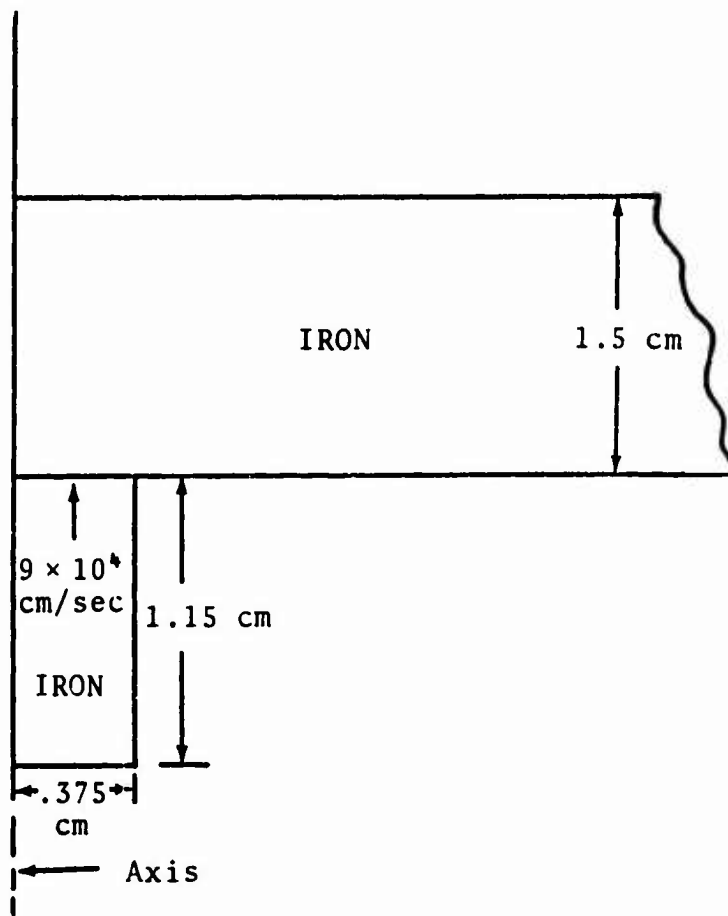
These initial conditions are illustrated in the preceding sketch. Equation-of-state and constitutive equations are specified in (b) and (C) below.

2. Test Problem No. 2

This problem differs from the preceding one only in regard to the target, which becomes a 1.0-cm-thick aluminum plate, as sketched below.

1.0 cm   ALUMINUM

9×10^4
cm/sec

IRON

4
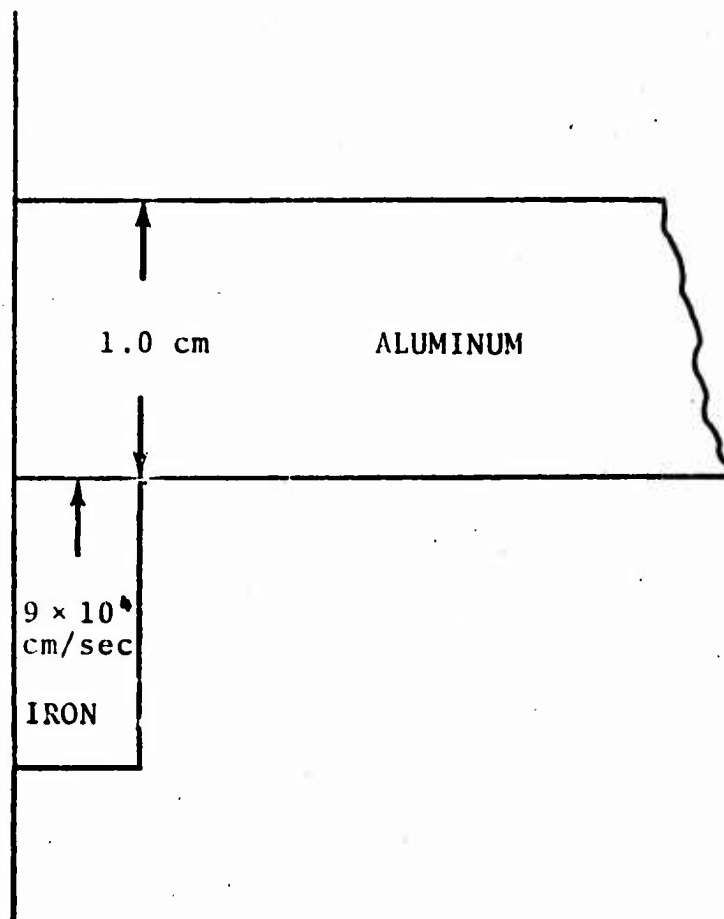
B. MATERIAL EQUATIONS OF STATE: THE HYDROSTATIC STRESS

The equation of state of the interacting materials is assumed to be of the form

$$P = \left(A_0 + A_1\mu + A_2\mu^2 + A_3\mu^3\right)\left(1 - A_4\mu\right)$$

$$+ \left(B_0 + B_1\mu + B_2\mu^2 + B_3\mu^3\right)E$$

(1)

where the A_i and B_i are constants, P is pressure, E is specific internal energy and $\mu = \left(\rho/\rho_0 - 1\right)$ is a measure of compression in terms of the density ρ and initial density ρ_0. This form is sufficiently general for representing metals over the pressure ranges of interest.

Values of the material constants for iron and aluminum are listed in Table 1.

C. THE DEVIATORIC STRESS

The specified relation for the deviatoric contribution to the stress is that of an elastic-perfectly plastic material for which the shear yield strength K satisfies the condition

$$K = K_0\left(1 - E/E_M\right) \qquad \text{for} \quad E < E_m$$

$$K = 0 \qquad \text{for} \quad E \geq E_M$$

(2)

i.e., reduction in the yield stress due to heating is accounted for by the simple linear term $\left(1 - E/E_M\right)$.

These conditions for the deviatoric stress are easily formulated along lines given in standard texts.[1] Starting with the usual definition of the strain rate deviator tensor $\dot{\epsilon}_{ij}$,

5

TABLE 1

	Iron	Aluminum
A_0	0.	0.
A_1	1.236×10^{12}	0.765×10^{12}
A_2	2.452×10^{12}	1.659×10^{12}
A_3	5.139×10^{12}	0.428×10^{12}
A_4	0.	0.
B_0	0.	0.
B_1	17.16	5.94
B_2	0.	0.
B_3	0.	0.
C_0 (g/cc)	7.8	2.79
K_0 (mbar)	0.006	0.003
E_M (ergs/g)	3.0×10^{10}	7.0×10^9
G (mbar)	1.93	0.274

6

one has in Cartesian notation

$$\dot{\varepsilon}_{ij} = \frac{1}{2}\left(\frac{\partial u_i}{\partial x_j} + \frac{\partial u_j}{\partial x_i}\right) - \frac{1}{3}\left(\frac{\partial u_k}{\partial x_k} \delta_{ij}\right) \tag{3}$$

For the elastic regime stress deviator increments $\left(\Delta\sigma_{ij} = \dot{\sigma}_{ij} \Delta t\right)$ are determined from the relation for elastic deformation

$$\dot{\sigma}_{ij} = 2G \dot{\varepsilon}_{ij} \tag{4}$$

where G is the rigidity modulus. This elastic relation is used to determine stress increments whenever the condition

$$\sigma_{ij} \sigma_{ij} < 2K^2 \tag{5}$$

is satisfied. When, however, the stresses given by (4) would cause (5) to be violated, one instead assumes perfectly plastic behavior for which the stresses satisfy the von Mises condition

$$\sigma_{ij} \sigma_{ij} = 2K^2 \tag{6}$$

and the stress increments are determined from the Prandtl-Reuss equations

$$\dot{\sigma}_{ij} = 2G \left(\dot{\varepsilon}_{ij} - \frac{\sigma_{k\ell} \sigma_{k\ell}}{2K^2} \sigma_{ij}\right) . \tag{7}$$

It is easy to show (multiplying (7) by σ_{ij} and performing the indicated summation) that the use of (7) to compute stress increments implies that $\sigma_{ij} \dot{\sigma}_{ij} = 0$, or $\frac{d}{dt}\left(\sigma_{ij} \sigma_{ij}\right) = 0$. Hence (7) is compatible with (6) in the sense that further deformation of the plastic type causes (6) to continue to be satisfied. (Application of (4) would cause (5) to be violated.)

Values of the material constants G, K , E_M for iron and aluminum are given in Table 1.

The above elastic-perfectly plastic constitutive equations are idealized versions of the material behavior. Such effects as the dependence of stresses on strain rates, and the increase of yield due to work hardening, have been ignored in these test problems in the interest of simplicity.

A detailed description of how the above equations are included in the computer program will be given when the HELP code development is reported as part of Task (1).

D. THE FAILURE CONDITION

The material is assumed to fail only due to hydrostatic tension. Specifically, the iron is assumed to fail at a relative volume $\left(V/V_0\right) = 1.03$ and the aluminum fails at $\left(V/V_0\right) = 1.015$. The assumed failure thresholds correspond to tensions of approximately 35 kilobars and 11 kilobars, for unheated iron and aluminum respectively.

More sophisticated failure models for cavitation or spalling could be introduced. During the past few years, a considerable amount of plane-wave research has been done at Sandia Corporation, Los Alamos, General Motors, and other laboratories, to determine the conditions for spallation failure in materials of interest. A summary discussion of experimental work and proposed mathematical criteria for spallation, together with plane wave calculations to test aspects of these models, is given in a recent S³ document.[2] It would not be difficult to incorporate a modern time-dependent spall criterion, such as the cumulative damage model[3] by Tuler and Butcher, into a two-dimensional calculation. Such a model would cause the material to fail at a tensile level which depends upon the local tensile history. The material would thereafter fail to support tensions, as in the simple instantaneous failure model.

8

A general two-dimensional treatment of the material failure, in which one predicts crack propagation directions and velocities, has been the subject of some attention in the present program, though additional work would be required to complete and test such a capability.

E. REQUESTED INFORMATION

For each problem plots at 0.5 μsec intervals were requested of the following information:

1. Total stress (axial direction) versus Y along axis of symmetry.

2. Axial velocity versus Y along axis of symmetry.

3. Relative volume $\frac{V}{V_0} \left(= \frac{\rho_0}{\rho} \right)$ versus radial distance at five levels in the target:

    (a) Target front surface

    (b) One-quarter way through target

    (c) One-half way through target

    (d) Three-quarters of the distance through the target

    (e) Back surface of the target

4. Specific internal energy at these positions.

5. Instantaneous plastic strain rate at these positions.

6. Total (integrated) plastic work at these positions.

These results were to be supplied for a time duration of 5 μsec in Problem No. 1, and for 3 μsec in Problem No. 2.

9

In regard to Items (3) through (6), the requested quantity (relative volume, specific internal energy, etc.) is plotted versus radial distance x, along that locus of moving mass elements which was originally (t=0) at the requested level in the target. Thus the plots refer to the original mass elements and are directly comparable to Lagrangian plots for the same problem.

III. NUMERICAL SOLUTIONS TO THE TEST PROBLEM

A. GENERAL REMARKS

Solutions have been obtained to 20 µsec in Test Problem No.1 and to 10 µsec in Test Problem No. 2 in addition to the 5 and 3 µsec physical times which were requested. Selected results will be presented for the extended times, but the requested detailed plots for comparison purposes are given only to 5 and 3 µsec.

No special difficulties were encountered in treating the later times and the calculations were stopped only to save computing costs.

A motion picture film has been made of automatic plots from Test Problem No. 2, showing the projectile-target configurations as the projectile penetrates the target. The last frame of the film is given in Section III-C as Fig. 22.

B. RESOLUTION AND COMPUTING TIME INFORMATION

1. Space and Time Resolution

For both of the problems space was divided into cells of dimensions $\Delta Z = 0.05$ cm and $\Delta R = 0.075$ cm, except at large radii where ΔR was increased to save computing costs in remote regions of the target. This zoning allowed five cells across the radius of the projectile in either problem, and 20 cells across the target in Problem No. 1.

The time step per cycle was taken to be the minimum value, for any cell in the mesh, of the quantity $0.4 \Delta X/(c+u)$, where ΔX is the cell dimension, c is sound speed and u is the absolute magnitude of the velocity components in the ΔX direction. Thus the problems were run at 0.4 times the maximum time step which is compatible with numerical stability.

2. Computing Time

Detailed computing time studies were made of Test Problem No. 2. At late times in the interaction, the computing time per average (short edit) cycle was 4.8 seconds. This time is partitioned among the major subroutines as follows.

CDT = 0.3 sec (Equation of State and Time Step)

EDIT = 0.2 sec (Energy Conservation Check and Edit)

PHASE 1 = 0.4 sec (Pressure Effects)

PHASE 3 = 1.0 sec (Strength Effects)

INFACE = 1.5 sec (Tracer Motion, plus calculation of mass transport from mixed and free surface cells)

PHASE 2 = 1.4 sec (Transport)

The additional time to treat this two-material flow, as compared to the analogous one-material problem run with RPM, is estimated at 2/3 the INFACE time. Thus the interface and free surface treatments increase the total cost of the calculation by about 20 percent. This percentage increase is not fixed from one problem to another, however, and can be substantially different for problems which contain a substantially different ratio of interface cells (free surface or multi-material) to pure cells.

The above 4.8 seconds per cycle implies 8.5 minutes for the time required to extend the problem time by 3 μsec. The actual computing time for the first 3 μsec was 8.0 minutes, including considerable time in long edits. (This time is slightly shorter than that for a 3 μsec extension at later times, because the entire grid is not yet active at the earlier times.)

12

Such detailed timing studies are not available on
Problem No. 1 but the total computing time for the first
5.0 μsec was 11.0 minutes (i.e., by interpolation, 6.6 minutes
for 3.0 μsec). This problem is somewhat simpler (no material
interface nor pressure iteration for mixed cells) than Problem
No. 2 and therefore requires less computing time.

The above timing studies were made on a UNIVAC 1108
computer.

Economy of operation, and the associated freedom to
perform parameter studies with modest computing costs, is
one of the strong features of Eulerian hydrodynamics.

C. PROJECTILE-TARGET CONFIGURATIONS VERSUS TIME

1. Test Problem No. 1

Automatic plots of the projectile-target configura-
tions, at one-half microsecond intervals, are given for Test
Problem No. 1 as Figs. 1 to 11. Only one-half of the inter-
action is shown, the left border being the axis of symmetry.

These plots are constructed using the positions of the
moving tracer particles. The tracer particle interior to
the target are plotted as points. These tracers are passive
in the sense that they do not "interact" with the Eulerian
solution but merely move with the local fluid velocity. For
the projectile, the interior tracers are connected by straight
line segments and are also passive in the sense described
above. The interior tracers were located initially in the
lower left corner of every block of four cells. Their loca-
tions at any time gives a quick impression of the displace-
ments and distortion which the materials have undergone.

Interface tracers, initially five per Eulerian cell
dimension, denote the position of the moving free surfaces.
(In the plots the free surfaces are obtained by connecting

13

adjacent tracers with straight line segments.) These inter-
face tracers, which are also advanced with the velocity of the
local fluid, are not passive since they actively affect the
basic Eulerian solution. Transport to and from free surface
cells, for example, takes account of where the free surface
intersects the cell boundaries; further, cells are evacuated
when the surface leaves and empty cells receive no mass trans-
port until entered by a free surface. The tracers denoting
the projectile-target interface, in this like-material impact,
are passive since no particular treatment of the cells con-
taining this interface is required.

Cells which have spalled, due to the prescribed failure
condition, are marked in as dark rectangles. Thus peripheral
rarefactions have caused some cavitation at the interface at
1.5 microseconds. And the projectile opens internally near
the axis between 2.0 and 3.0 μsec, only to close again before
3.5 μsec. In this latter case, the oncoming projectile has
filled the void caused by the rarefaction from the sides of
the projectile.

2. Test Problem No. 2

Similar plots of the iron-aluminum impact are seen as
Figs. 12 through 22. Here the plots 12-18 show the interaction
at one-half microsecond intervals to 3.0 μsec, and times 5,
7.5 and 10 μsec are shown in subsequent plots. The plots
12-21 show the fixed Eulerian grid with superimposed contours
of the moving surfaces and the projectile target interface.
Figure 22 omits the grid and depicts the positions of the
array of passive tracers which were originally at cell centers
within the projectile and target. This figure shows severe
distortion of both projectile and target near the interface
and at the target lip.

14

In this two-material interaction the tracer particles which denote the projectile-target interface have an active role in the Eulerian solution. In the calculation, the mass, momentum and energy transports (associated with the moving steel and aluminum) take account of the interface position (obtained by interpolating between tracers).

Spalled cells are darkened in the plots. It is seen that spall begins, again, near the interface at the projectile edge, a process which starts at 1.0 μsec and increases throughout. (The projectile does not fail near the axis, as in Problem No. 1.) Back surface target spall is evident, beginning at 2.0 μsec, reaching a maximum at 2.5 to 3.0 μsec, and diminishing somewhat at later times as the target material begins to overtake the spalled material. This back surface spall is also evident (as tracer particle separation) in the motion picture which was referred to in (A) above.

D. **PLOTS OF REQUESTED INFORMATION**

1. **Problem No. 1**

   (a) **Total Stress (Axial Direction)
         Versus Y Along Axis of Symmetry**

These results are plotted, for half-microsecond intervals to 5 μsec, as Figs. 23 through 32. In all plots the initial position of the interface is at 1.4 cm and distance into the target increases to the right. At the earliest time, 0.5 μsec, nearly symmetrical 150 kbar shocks have propagated into both the target and projectile. At 1.0 μsec these shocks have attenuated to approximately half this strength due to shock divergence and to rarefactions from the free surfaces. By 1.5 μsec, a substantial tensile region (20 kbars) is seen on the axis; this tensile region is predominantly in the projectile material, near the projectile-target interface. The

15

plot at 2.0 μsec shows the effect of cavitation failure on the projectile axis, occurring between 1.5 and 2.0 μsec when tensions exceed some 35 kbars (see Section II-2 for the assumed failure condition). This tension results in a rarefaction into the neighboring material, and slight noise in the solution due to the sudden increase of pressure to zero when the failure condition is satisfied. Tensions are also evident in the rear of the projectile at 2.5 μsec, but these are seen later to be insufficient to cause cavitation. By 3.5 μsec, further, the oncoming projectile has caused the previously spalled cells to again be compressed, and positive pressures are seen at all positions on the axis. At 5 μsec the stresses are compressive and the maximum stress, approximately 20 kbars, is in a region approximately one-fourth through the target.

(b) Velocity Versus Y Along Axis of Symmetry

The axial velocity plots are seen as Figs. 33 through 43. These plots are essentially self-explanatory. The results are believed to be realistic, except for the expected smearing of the shock front over several cells and the observed small oscillations in the velocity profile. It can be observed that, at the latest time of 5 μsec, the back of the projectile has decelerated only about six percent in velocity, from the original 9×10^4 cm/sec to 8.4×10^4 cm/sec. (At this time, the energy in the problem remains 57 percent kinetic, as indicated by the energy values given at the bottom of Fig. 11.)

(c) Relative Volume Versus Radial Distance at
Various Levels in the Target

Plots of relative volume $\frac{V}{V_0} \left(= \frac{\rho_0}{\rho} \right)$ are seen as Figs. 44 through 53. Compressions to $\frac{V}{V_0} = .9$ are seen at the earliest time (0.5 μsec) at the target front surface in

16

the vicinity of the axis. By 1.0 μsec the compression in this region has diminished by about a factor of five $\left(\frac{V}{V_0} = .98\right)$ and by 1.5 μsec the compression has become a distension $\left(\frac{V}{V_0} = 1.02\right)$, as seen in Fig. 46. This distension corresponds to the tension noted previously (Part (a) above) in connection with the results for stress as a function of distance along the axis of symmetry. By times of 2.5 to 5 μsec, small oscillations are evident in these plots of relative volume versus radial distance, especially at the target front surface. These oscillations are due primarily to the sudden discontinuity which occurs in the interaction whenever the material in a given cell reaches its failure threshold. (Somewhat similar effects were seen previously in the axial pressure plots.) To good accuracy at the stress levels in this problem, these plots of relative volume are equivalent to pressure plots at the same times and levels, since pressure is proportional to compression for small compressions of the cold material.

(d) Specific Internal Energy Versus Radial
Distance at Various Target Levels

These results are given as Figs. 54-63. The greatest specific internal energies, around 1.25×10^9 ergs/g, occur at early times (see Fig. 54, the 0.5 μsec plot) and are simply the specific internal energy of the initially shocked material. This particular energy (that due to the plane shock at early times) is very easily determined theoretically from the shock relation $\Delta E = \frac{1}{2}u_p^2$ where the shock particle velocity u_p, from symmetry, must be one-half the 9.0×10^5 velocity of impact. The resulting energy is 1.01×10^9 ergs/g. The agreement is reasonable, the difference between this exact value and those in Fig. 54 being due to transient oscillations in the early stages of the numerical solution.

17

At the later times, the energies are seen to diminish as pressures are relieved, and the material expands from its shocked state. Once the pressures have attenuated to low stress levels, as at the 5 μsec time depicted in Fig. 63, the observed specific internal energies are attributable to a combination of (a) shock heating, and (b) work done against the plastic forces (the additional mechanism of energy change, adiabatic expansion, being negligible at low stress levels.)

As seen in the late time plots, the specific internal energies, near the target front surface, peak at a radius of .3 or .4 cm, so that there is a (local) minimum of specific internal energy at the axis. This apparent anomaly, since one might expect a maximum at the axis of symmetry, has been the subject of a simple analysis. The effect arises because the work done against the plastic forces (plotted subsequently as Figs. 74 through 83) is a maximum for the high-shear region near the projectile edge (at radius .375 cm) and therefore has a relative minimum at the axis. Further, a quantitative check can be made on the value of the specific internal energy at the center of impact (target front surface at the axis of symmetry): the shock heating is given by the energy on the Hugoniot (calculated as 1.01×10^9 ergs/g in the preceding paragraph) minus the loss in energy $\int pdV$ due to the adiabatic expansion. The latter integral has been evaluated using a special equation-of-state program, giving 0.88×10^9 ergs/g. Thus the net shock heating is 1.3×10^8 ergs/g. The work per unit volume against the plastic forces (Fig. 83) is seen to be $W = 4.5 \times 10^{-3}$ megabars $= 4.5 \times 10^9$ ergs/cm^3; the work per gram is therefore $E_p = W/\rho = (4.5 \times 10^9/7.85)$ ergs/g $= 5.7 \times 10^8$ ergs/g. The sum of the irreversible shock heating and this plastic work is therefore $E = (1.3 + 5.7) 10^8$ ergs/g $= 7.0 \times 10^8$ ergs/g. This value of the specific internal energy at late times is in very good agreement with the result 7.5×10^8 ergs/g seen

18

in Fig. 63, and which was obtained by integrating the hydro-dynamic equations of motion. From this discussion we see then that (a) the computed value of the specific internal energy at the impact center is reasonable, and (b) the increase of specific internal energy with radial distance, along the target front surface, is attributable to the large amount of work against plastic forces in the region of maximum target shear.

(e) Instantaneous Plastic Strain Rate Versus Radial Distance at Five Target Levels

These results are seen as Figs. 64 through 73.

The plastic strain rates data represent the least smooth of the results to be presented because these data are intensive quantities obtained by differentiation of other intensive quantities (the velocities) with respect to the space variables. Small oscillations, e.g., those at the 1/4 level at 1.0 µsec, are apparently spurious, but the data are reliable in regard to general trend and the time-averaged (or integrated) results.

Very high strain rates are evident at early times in the vicinity (r = 0.375 cm) of the projectile edge, corresponding to the maximum shear region. By the later times this region of maximum shear occurs at larger radii (e.g., at r = 6 cm in the 5 µsec plot, Fig. 73). Of the various levels in the target the highest strain rates are always for the material which was originally near the front target surface.

(f) Plastic Work Versus Radial Distance at Various Levels in the Target

Plots of the total plastic work per unit volume of material are presented as Figs. 74-83. The results are essentially self-explanatory and show, as was indicated by the

19

strain-rate results described in (d) above, that most of the plastic work is concentrated in the impact region near the target front surface. Further, as was pointed out above, the plastic work is somewhat higher at the projectile radius distance than at $r = 0$, causing a relative minimum in the specific internal energy at the axis. At 5.0 µsec the integrated values of the total plastic work for the entire problem (from a separate calculation) is 4.2×10^9 ergs. This compares with a total internal energy of 6.8×10^9 ergs. Thus, work against the plastic forces has accounted for some 62 percent of the gain in internal energy.

2. Problem No. 2

    (a) Total Stress (Axial Direction)
        Versus Y Along Axis of Symmetry

    These plots of total stress are seen as Figs. 84 through 89. At the earliest time, 0.5 µsec, 125 kbar shocks are seen to propagate in both directions from the impact surface. As a result of rarefactions and shock divergence, these shocks attenuate to 75 kbar by 1.0 µsec. Subsequent plots show continuing shock attenuation, accompanied by oscillations near the interface (Fig. 86, time 1.5 µsec) and near the back surface of the target (Fig. 87, time 2.0 µsec). These fluctuations in the stresses correlate with material failure in tension (see Figs. 12-22) which begins at the interface and back surface just before the times of 1.5 and 2.0 µsec respectively. This sudden release of tension, occurring when the material satisfies the prescribed failure conditions (see Section II-D) gives rise to local disturbances.

    (b) Velocity Versus Y Along Axis of Symmetry

    These plots for Problem No. 2 are seen as Figs. 90 through 95. Two effects will be noted. At 2.0 µsec, Fig. 93,

20

the projectile material in the vicinity of the interface
actually has a velocity which is slightly greater than the
initial velocity of impact, by a few percent. Whether this
apparent slight acceleration is real is not quite clear.

Also, at the latest times, spallation is evident near
the back surface of the target, where the material near the
back surface is seen to have a greater velocity than the tar-
get material nearer to the projectile. This evidence of
spallation correlates well with spallation results presented
in Figs. 12-22.

(c) Relative Volume Versus Radial Distance at Various Levels in the Target

These plots, for the six requested times, are shown as
Figs. 96 through 101. At the earliest time (.5 μsec, Fig. 96)
the maximum compressions $\left(\frac{V}{V_0} = \frac{\rho_0}{\rho} = .9\right)$ are seen to occur
near the target front face, i.e., at the front surface level
and the one-fourth level. At 1.0 μsec (Fig. 97) maximum
compression occurs in the middle of the target, as seen by
comparing the third plot with the other four. At still later
times (e.g., 1.5 μsec, Fig. 98) the compression pulse has
advanced further, so that maximum compression occurs at the
three-quarter station. The behavior is indicative of a pressure
pulse which propagates at the aluminum shock wave velocity.

The occasional irregularities in the plots at the
target front surface level (vicinity of fourth or fifth point
in Fig. 97, vicinity of fifth or sixth point in Fig. 101)
reflect the fact that these points are in the (small) region
of the highly deformed crater lip, where the material
characteristics are rapidly changing.

(d) Specific Internal Energy Versus
     Radial Distance at Various Target Levels

These results, for the various times, are seen as
Figs. 102 through 107 inclusive. As might be expected, specific
internal energies are highest near the target front surface
and, also, tend to be somewhat higher at the projectile radius
distance than at the axis or at greater radii.

(e) Instantaneous Plastic Strain Rate Versus
     Radial Distance at Five Target Levels

These data for Test Problem No. 2 are displayed as
Figs. 108 through 113 inclusive.

(f) Plastic Work Versus Radial Distance at
     Various Levels in the Target

Plots of the total plastic work are shown in Figs. 114
through 119. The earliest plots exhibit a concentration of
plastic work in the high shear region, near the target front
face at the projectile radius. Eventually, this effect is
over-ridden (see 3.0 μsec, Fig. 119) as much more plastic work
is performed within the target. In this impact the softer and
lighter aluminum appears to be flowing around the iron projectile,
causing an associated build-up within the aluminum of work done
against plastic forces. This process continues long past
3 μsec, at which time separate edits of kinetic, internal
and plastic-work energies show that the energy in the problem
is still 82% kinetic, with only 11% of the energy having
been expended against plastic forces. At the later time of
10.0 μsec (Fig. 22 shows the configuration at this time) the
energy is 53% kinetic, with nearly all of the remaining energy
being lost due to work against plastic forces.

22

IV. CONCLUDING REMARKS

The preceding pages consist of the information requested by the JTCG/ME. The results given are complete and have been presented in such a form (at locations of moving tracer points) that comparisons can be made directly with the corresponding Lagrangian code results.

Much related work has been described in previous reports. This includes the SLUG and DORF code calculations mentioned in the Introduction, and those times in the HELP calculations that are later than those requested. Also, a number of exploratory calculations were made to evaluate the effects of smaller time steps or slight modifications in the transport from mixed cells. These latter calculations did not differ significantly from those presented here.

Much additional information pertaining to the above calculations can be obtained from the printed numerical solutions. S^3 will be happy to supply such information in response to queries or can loan the printed results to responsible parties.

In regard to the ongoing program, it is expected that Item (2) of the Introduction, the application of Eulerian methods to give the most realistic possible descriptions of armor penetration processes, will receive primary attention in the months immediately ahead.

23

REFERENCES

1. See for example, T. Y. Thomas, "Plastic Flow and Fracture in Solids," Academic Press (1961).

2. Fisher, R. H., and R. A. Kruger, "Summary of S^3 Presentation at Fifth PREDIX Meeting," Systems, Science and Software Document 3SR-129 (1969).

3. Tuler, F. R., and B. M. Butcher, "A Criterion for the Time Dependence of Dynamic Fracture," International Journal of Fracture Mechanics," December 1968.

TEST PROBLEM NO. 1

Projectile-Target Configuration with Spalled Cells Shaded

For T = 0.0, 0.5, 1.0, 1.5, 2.0, 2.5, 3.0, 3.5, 4.0,
       4.5, and 5.0 μsec.

(In target interior tracers plotted as points)

(In projectile interior tracers connected by straight
line segments)

(Interior tracers originally located at bottom left corner
of every block of four cells)

Figure 1.

Figure 2.

Figure 3.

Figure 4.

Figure 5.

Figure 6.

Figure 7.

32

Figure 8.

Figure 9.

Figure 10.

Figure 11.

36

TEST PROBLEM NO. 2

Projectile-Target Configuration Superimposed
on Eulerian Grid with Spalled Cells Shaded

For T = 0.0, 0.5, 1.0, 1.5, 2.0, 2.5, 3.0, 5.0,
      7.5, and 10.0 μsec.

Figure 12.

Figure 13.

Figure 14.

Figure 15.

Figure 16.

42
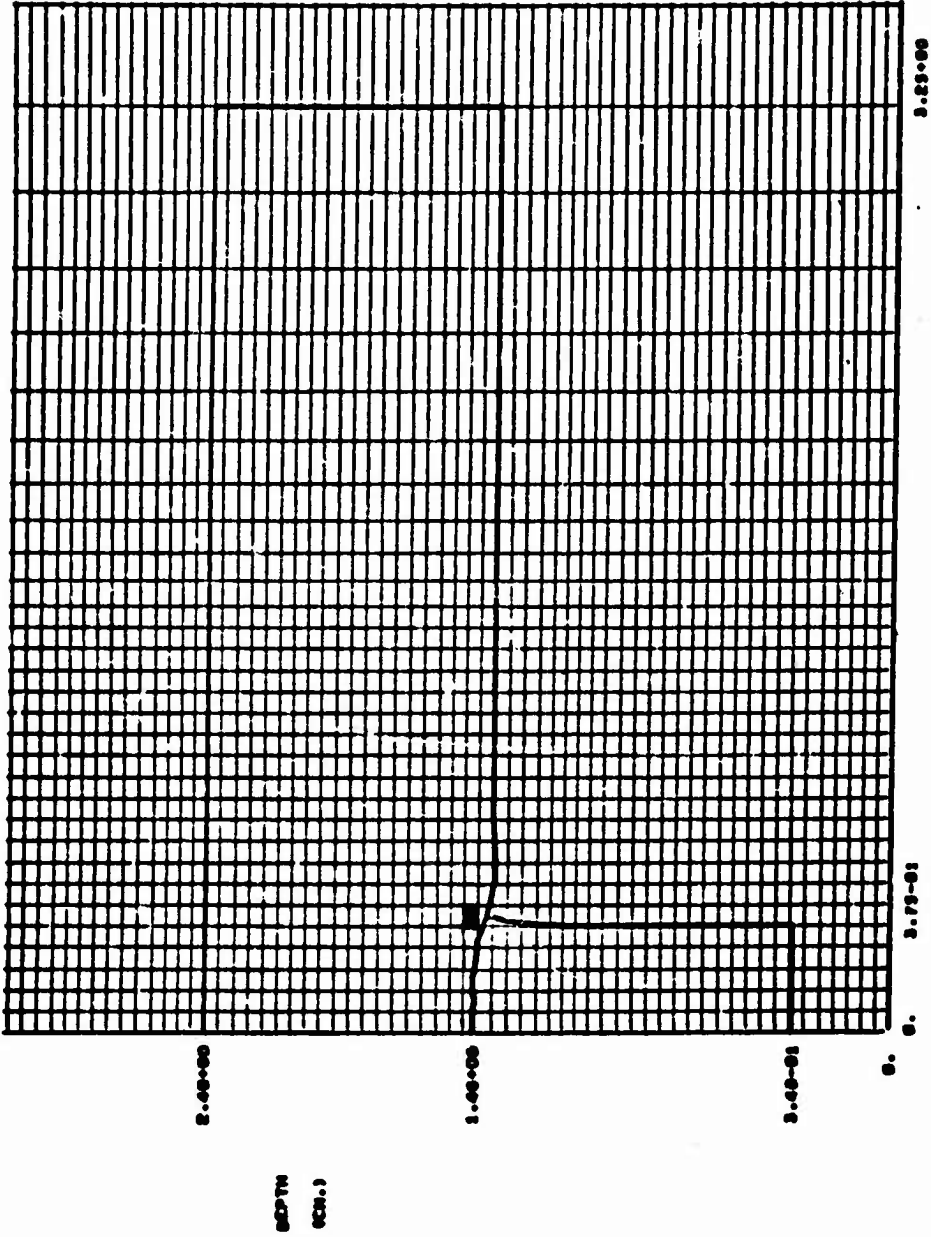
Figure 17.

Figure 18.

Figure 19.
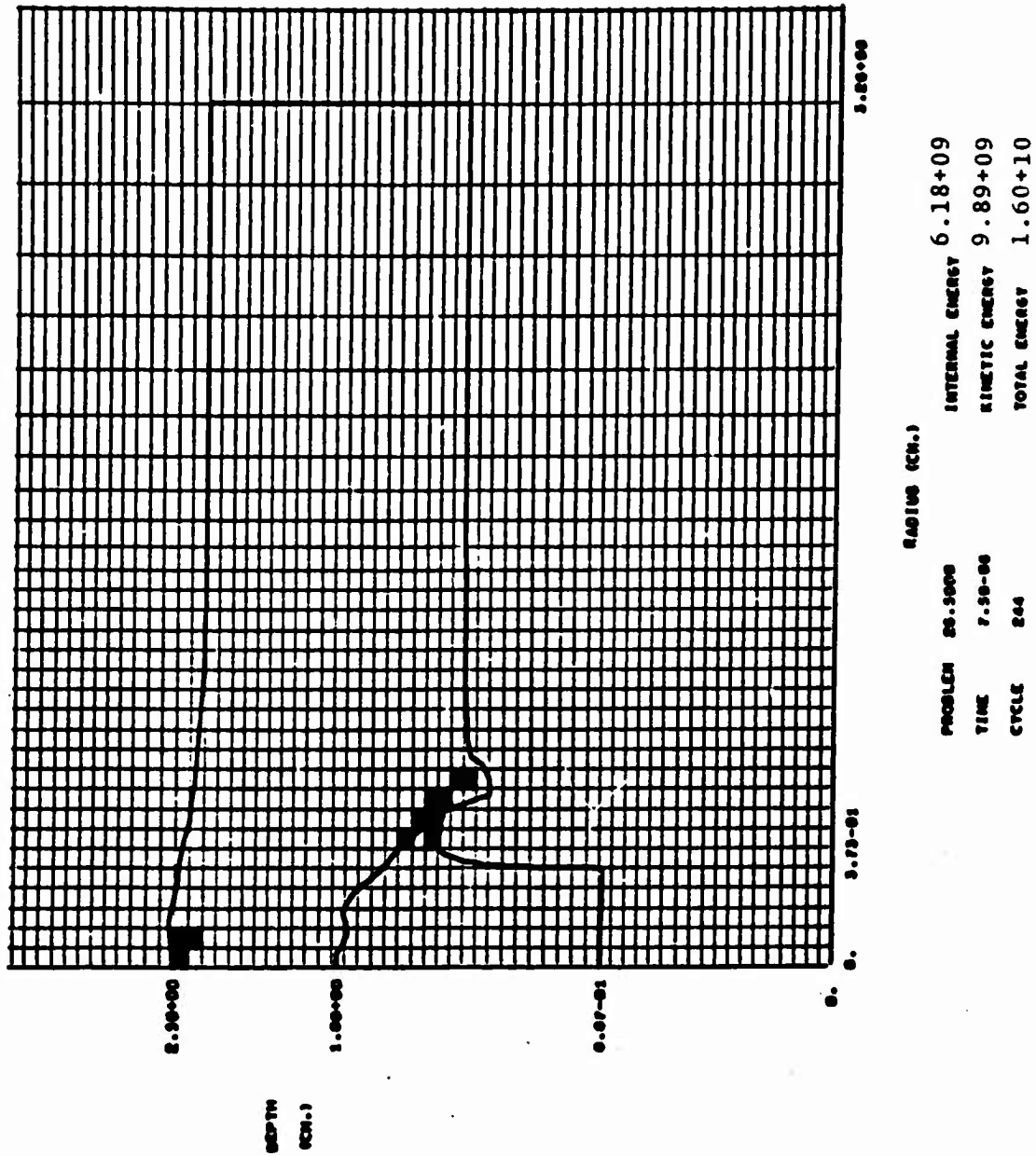
Figure 20.
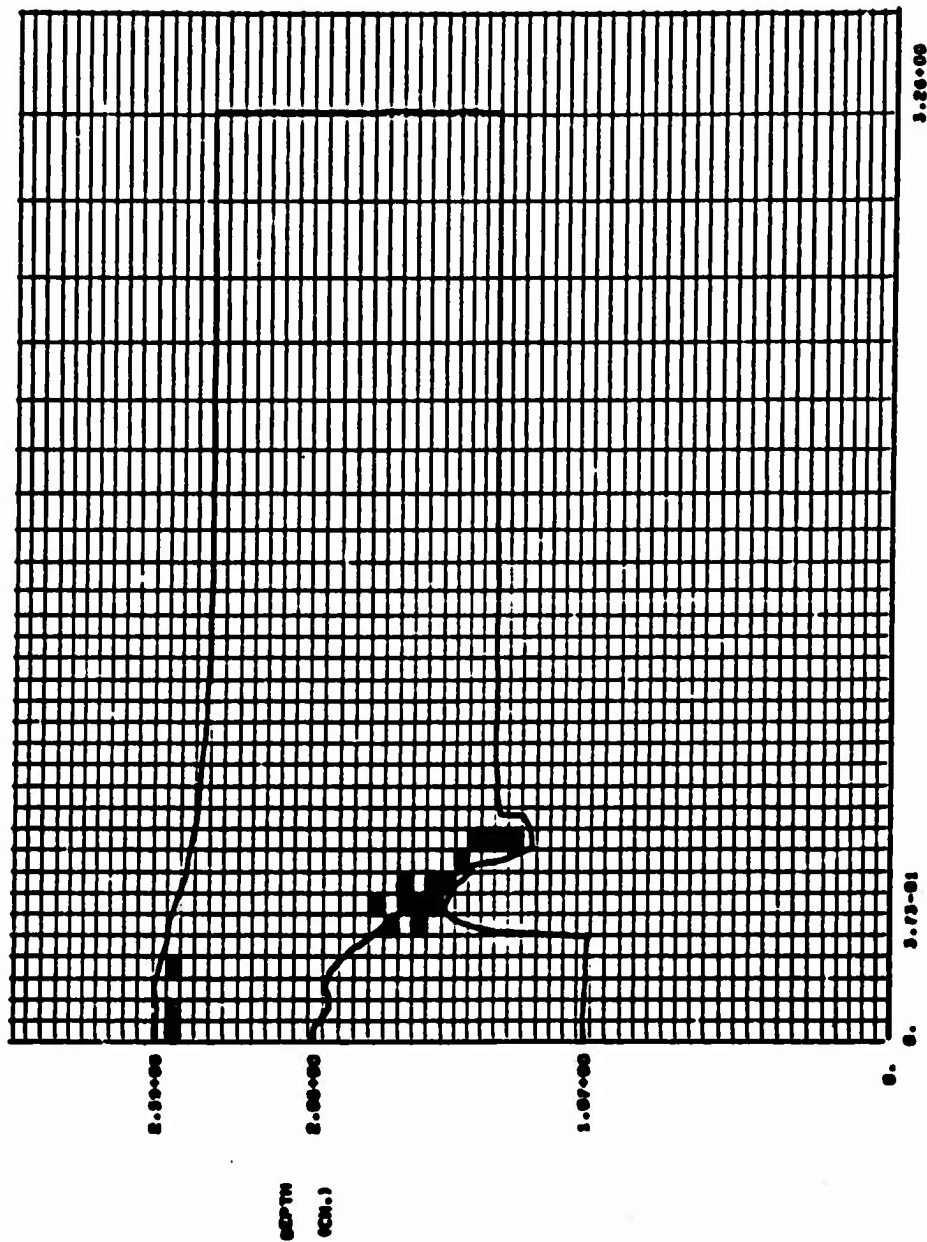
Figure 21.

TEST PROBLEM NO. 2

Projectile-Target Configuration Depicting Position of
Interior Tracers Originally Located at Cell Centers

For T = 10.0 μsec.
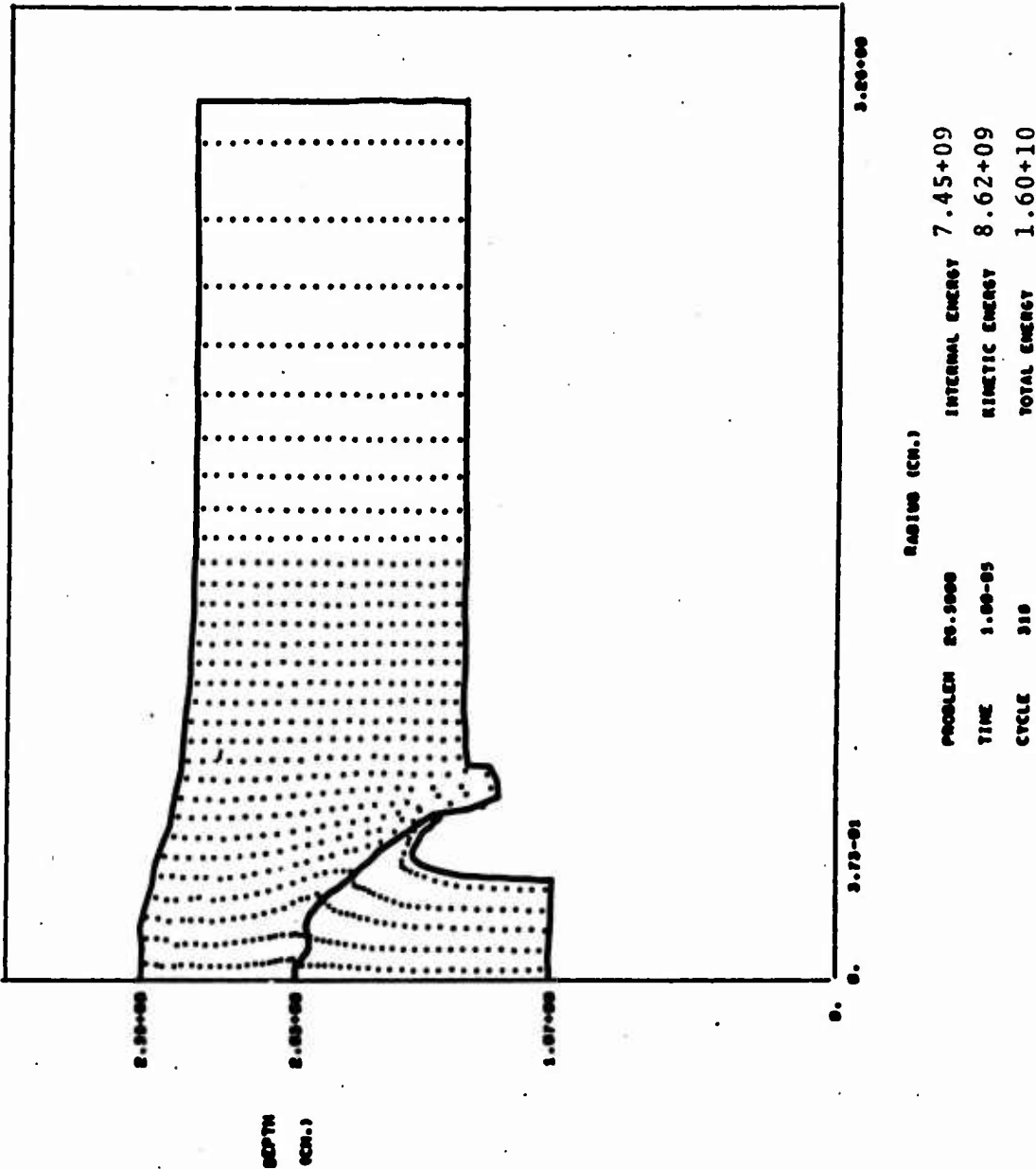
Figure 22.

TEST PROBLEM NO. 1

Total Stress (Axial Direction) Versus Y
Along Axis of Symmetry

For T = 0.0, 0.5, 1.0, 1.5, 2.0, 2.5, 3.0, 3.5, 4.0,
4.5, and 5.0 μsec.

PB = Projectile Back

PTI = Projectile Target Interface

TB ᴝ Target Back
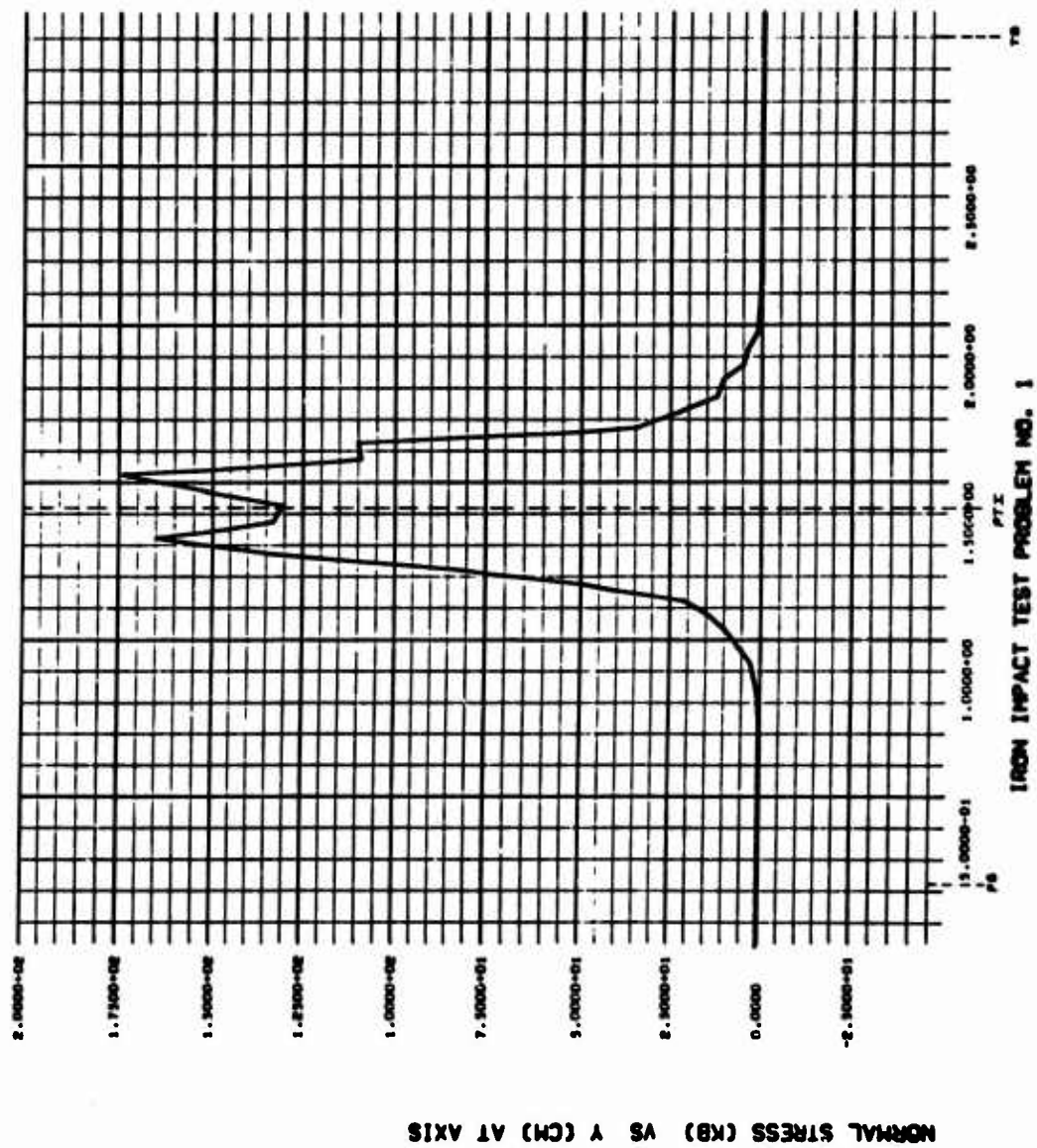
Figure 23.

TIME= 1.0000-06 PROB= 2.69144+01 CYCLE NO 41

NORMAL STRESS (KB) VS Y (CM) AT AXIS
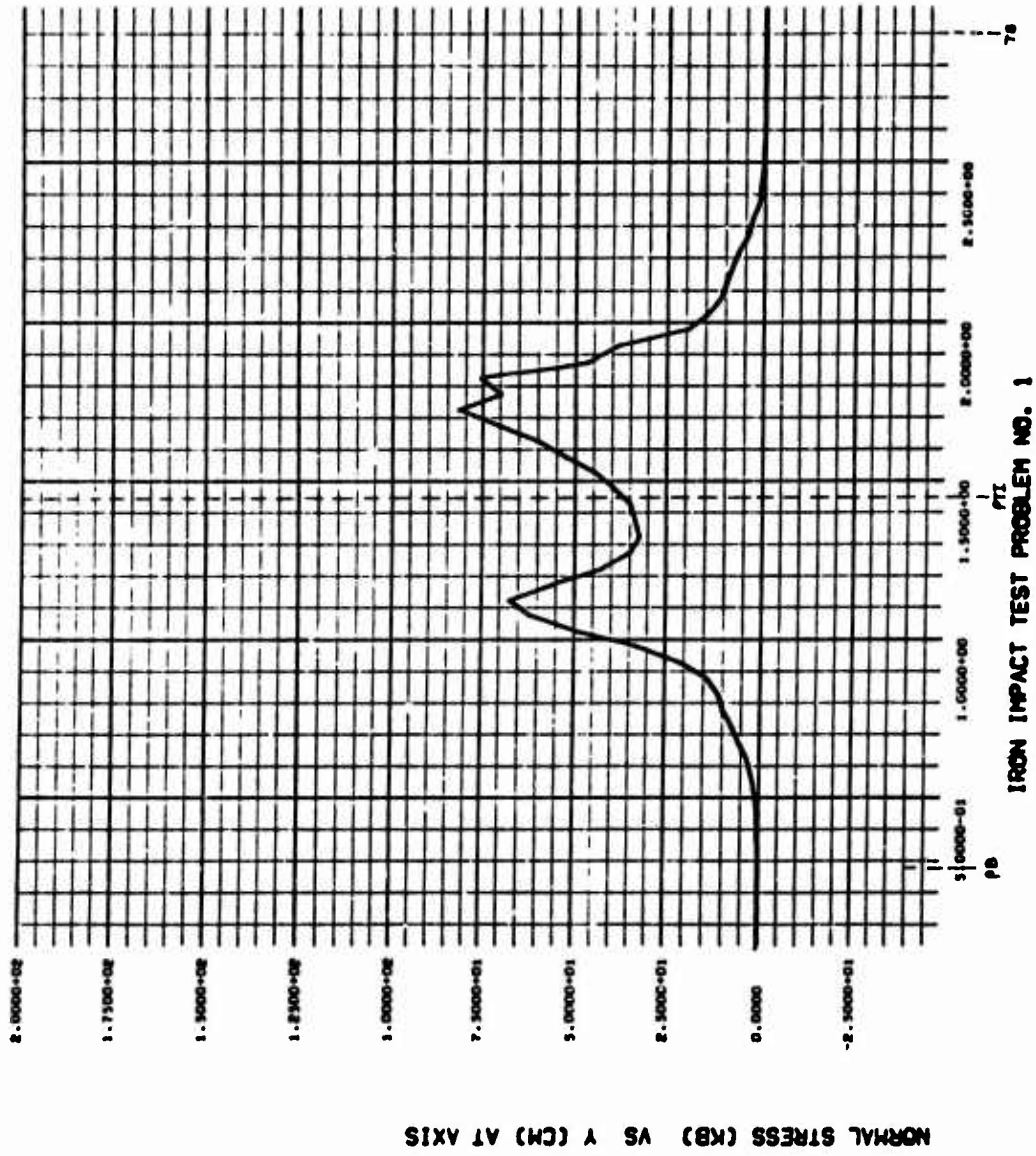
IRON IMPACT TEST PROBLEM NO. 1
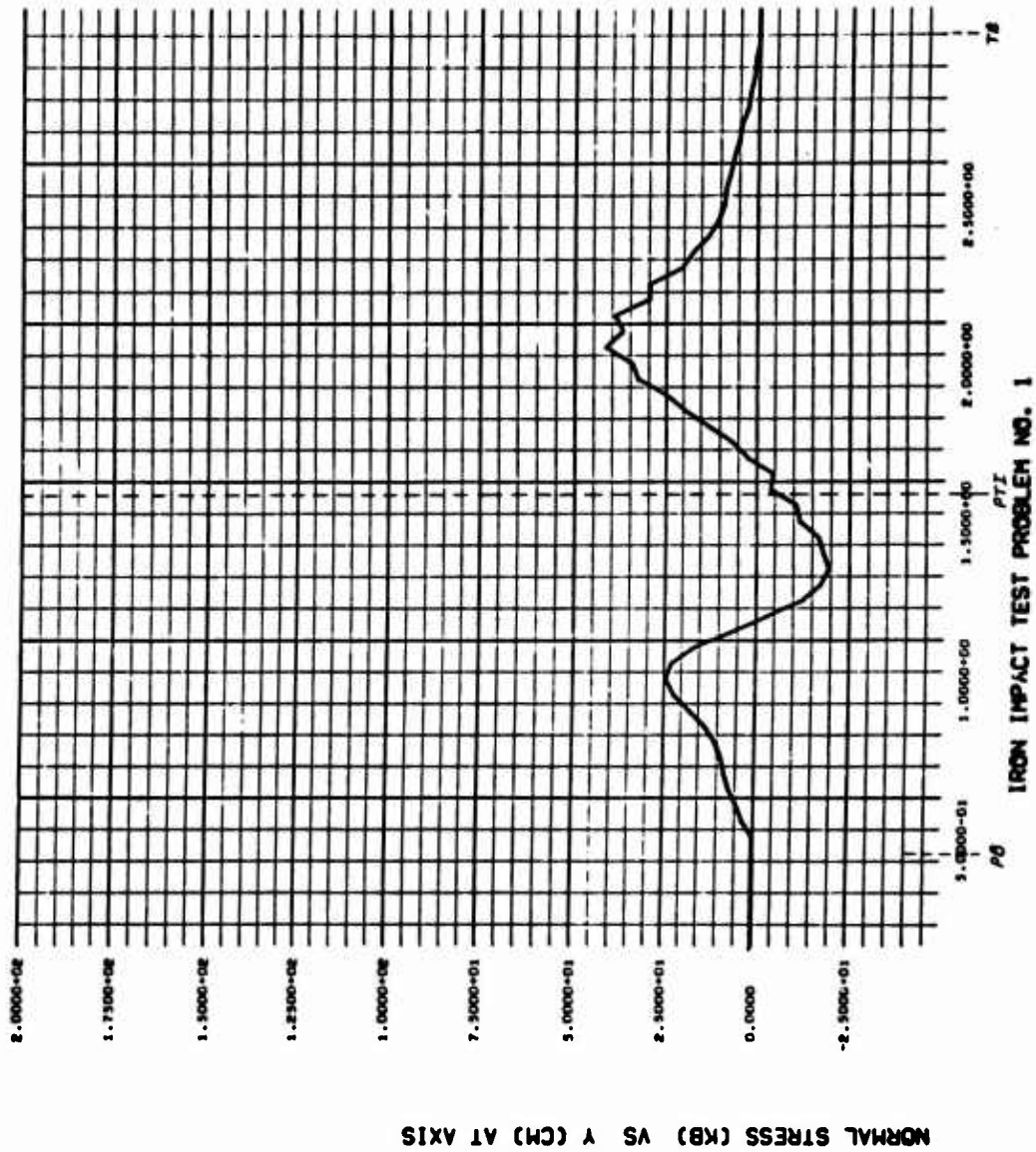
Figure 24.

Figure 25.

TIME= 2.0000-06 PROB= 2.69144+01 CYCLE NO 70
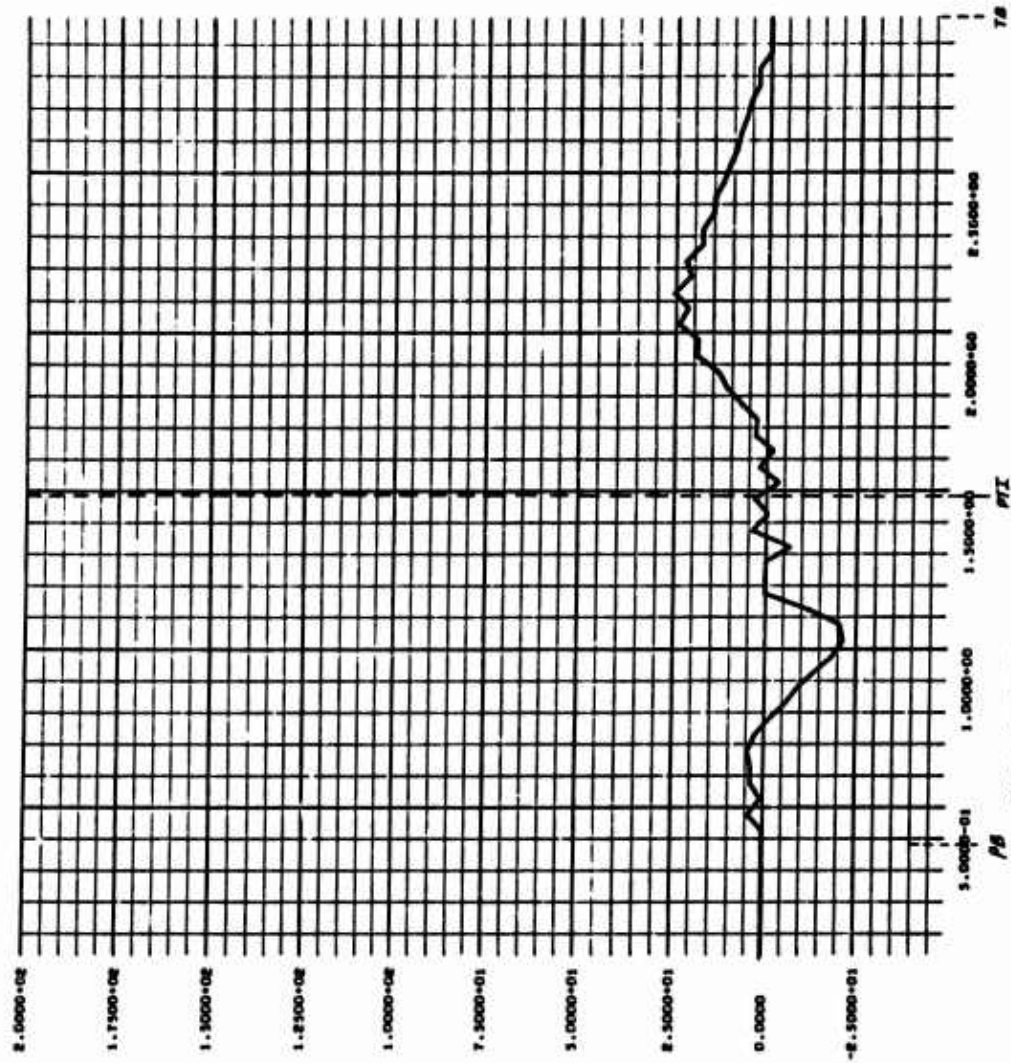
IRON IMPACT TEST PROBLEM NO. 1

Figure 26.
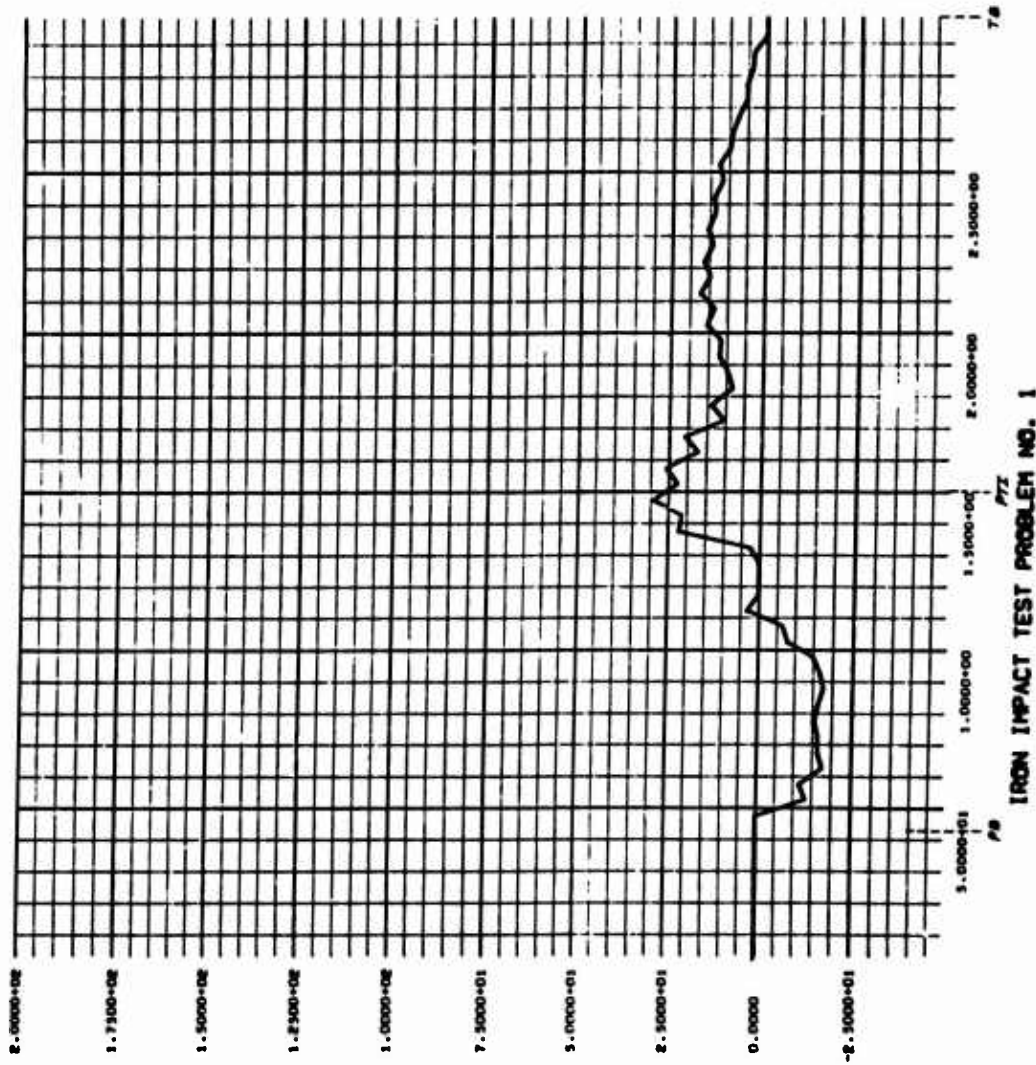
NORMAL STRESS (KB) VS Y (CM) AT AXIS
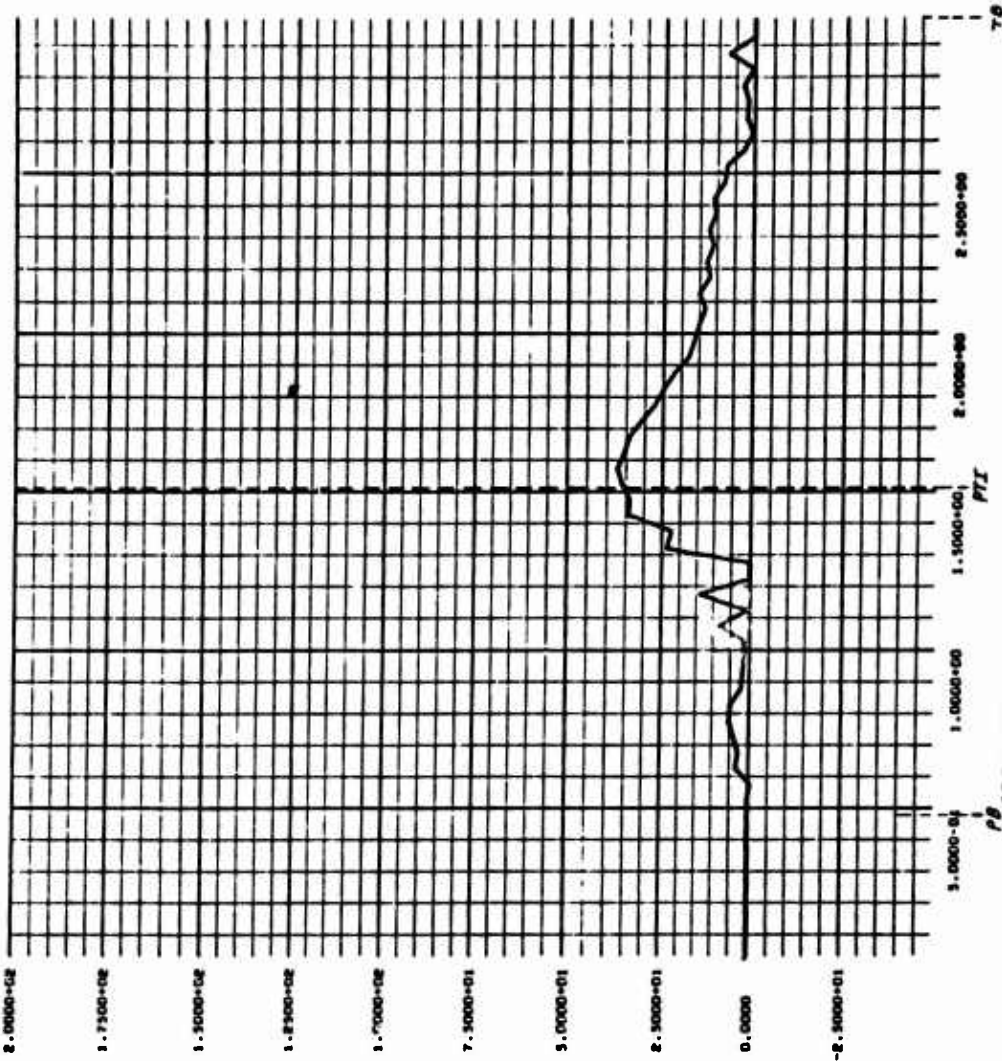
Figure 27.

Figure 28.

TIME= 3.5000-06 PROB= 2.69144+01 CYCLE NO 115

IRON IMPACT TEST PROBLEM NO. 1

Figure 29.

NORMAL STRESS (KB) VS Y (CM) AT AXIS

2.0000+02 1.7500+02 1.5000+02 1.2500+02 1.0000+02 7.5000+01 5.0000+01 2.5000+01 0.0000 -2.5000+01

5.0000-01 1.0000+00 1.5000+00 2.0000+00 2.5000+00
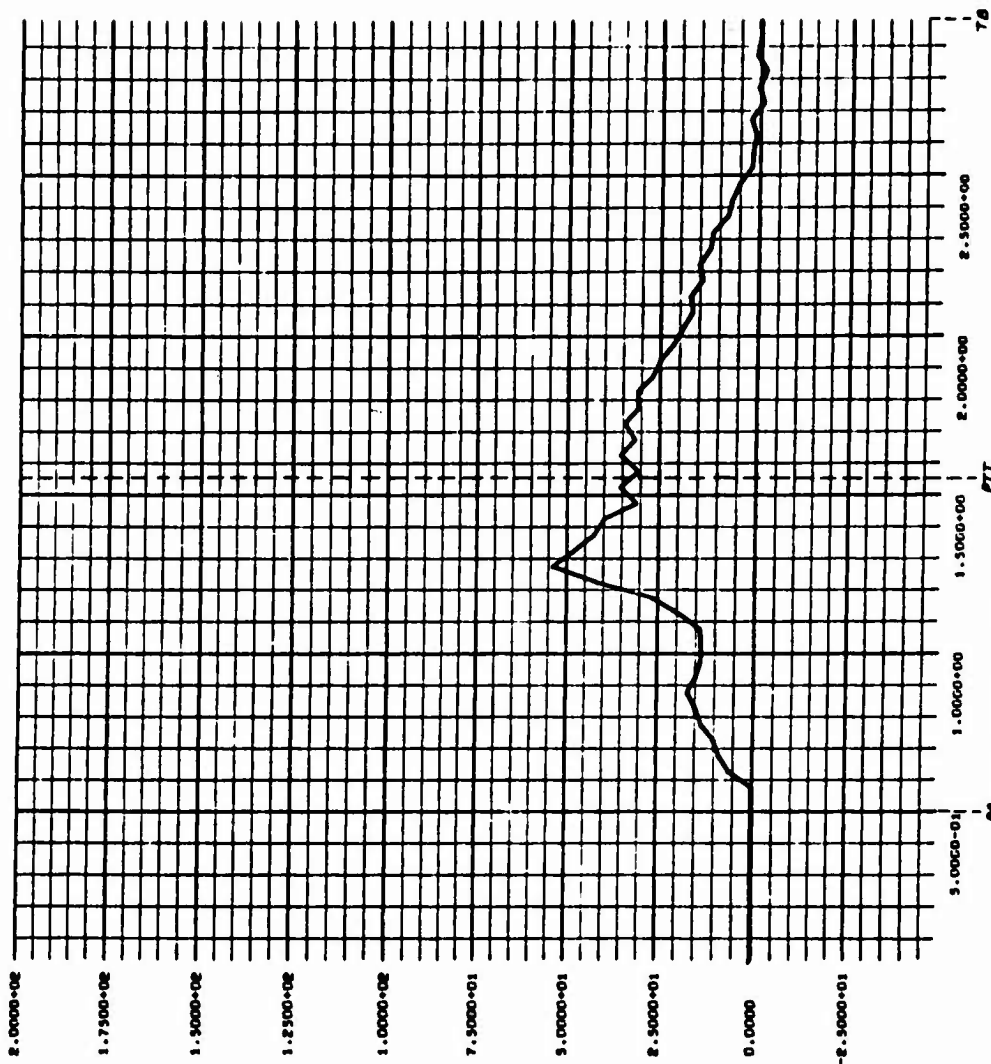
TIME= 4.0000-06 PROB= 2.69144+01 CYCLE NO 130

IRON IMPACT TEST PROBLEM NO. 1

Figure 30.

NORMAL STRESS (KB) VS Y (CM) AT AXIS

Figure 31.

Figure 32.

TEST PROBLEM NO. 1

Axial Velocity Versus Y Along Axis of Symmetry

For T = 0.0, 0.5, 1.0, 1.5, 2.0, 2.5, 3.0, 3.5, 4.0,
4.5, and 5.0 usec.

 PB = Projectile Back

PTI = Projectile Target Interface

 TB = Target Back

Figure 33.

Figure 34.

Figure 35.

IRON IMPACT TEST PROBLEM NO. 1

AXIAL VELOCITY (CM/MICROSEC)   VS   Y (CM) AT AXIS

Figure 36.

Figure 37.

Figure 38.

TIME= 3.5000-06 PROB= 2.69144+01 CYCLE NO 115

IRON IMPACT TEST PROBLEM NO. 1

AXIAL VELOCITY (CM/MICROSEC) VS Y (CM) AT AXIS

Figure 39.

68

Figure 40.

69

Figure 41.

TIME= 5.0000-06 PROB= 2.69144+01 CYCLE NO 158

AXIAL VELOCITY (CM/MICROSEC) VS Y (CM) AT AXIS
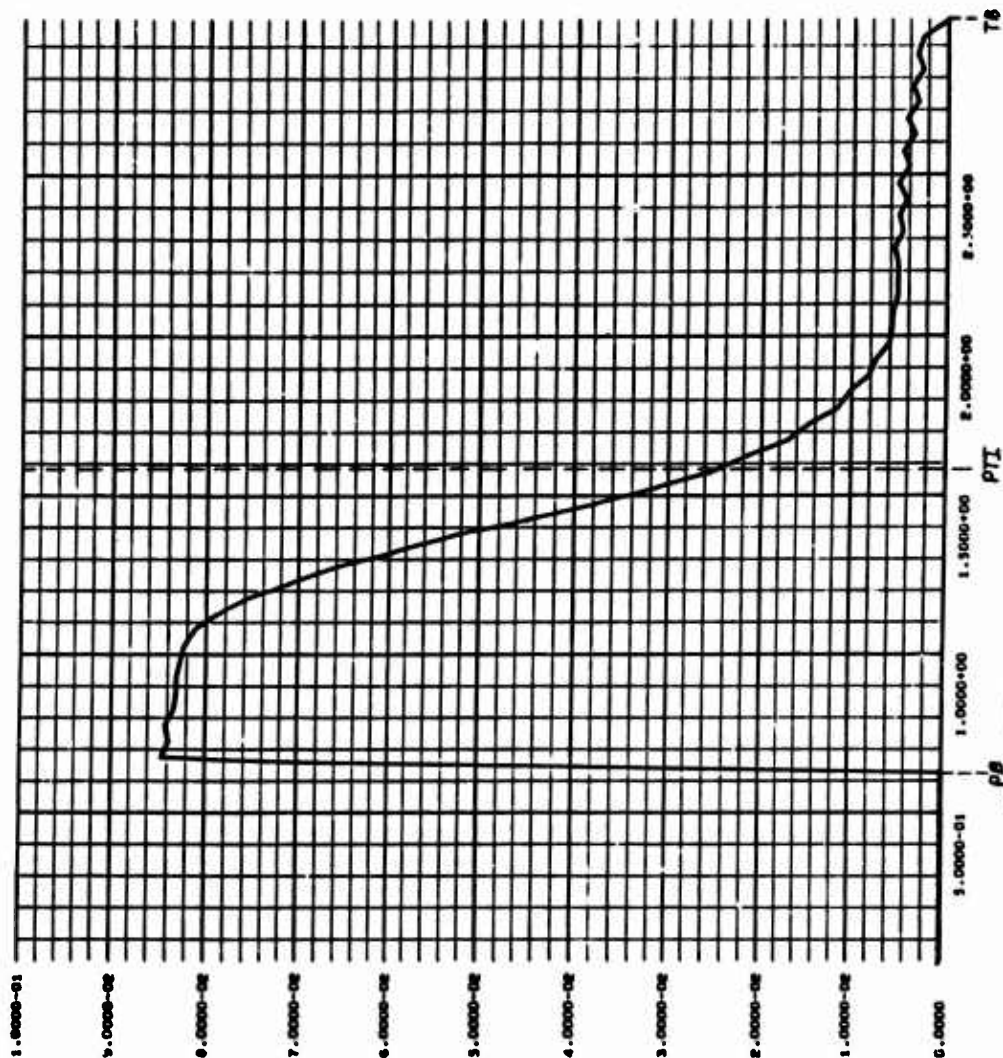
IRON IMPACT TEST PROBLEM NO. 1

Figure 43.

TEST PROBLEM NO. 1

Relative Volume Versus Radial Distance at Five Locations in the Target

For T = 0.0, 0.5, 1.0, 1.5, 2.0, 2.5, 3.0, 3.5, 4.0,
   4.5, and 5.0 μsec.

A = Target Front Surface

B = One-Quarter Distance into Target

C = One-Half Distance into Target

D = Three-Quarters Distance into Target

E = Back Surface
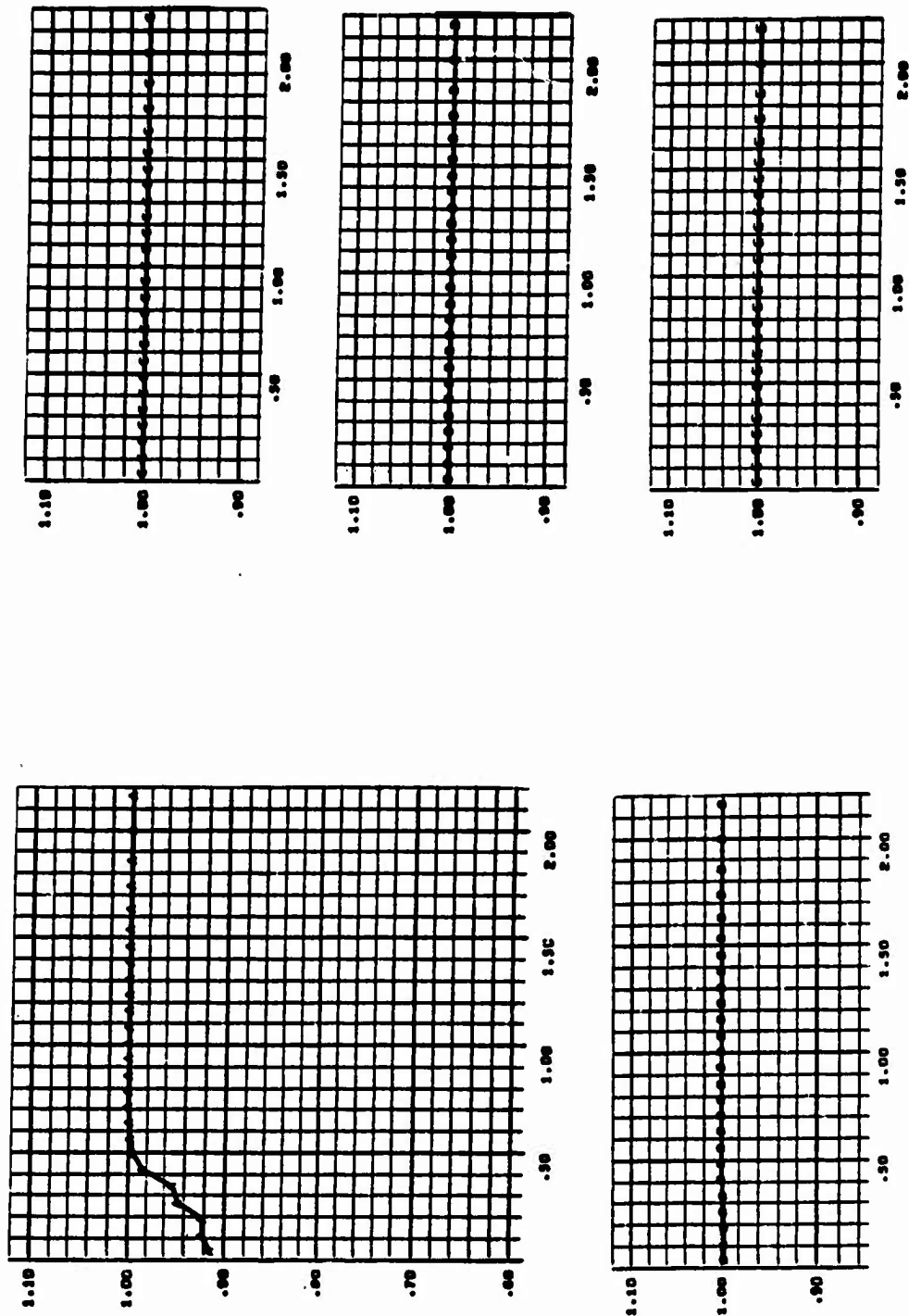
IRON - IRON IMPACT

RHOZ/RHO VS X (CM)   TIME= 5.0000-07

Figure 44.

73

IRON - IRON IMPACT

RHOZ/RHO VS X (CM)   TIME= 1.0000-06

Figure 45.

74
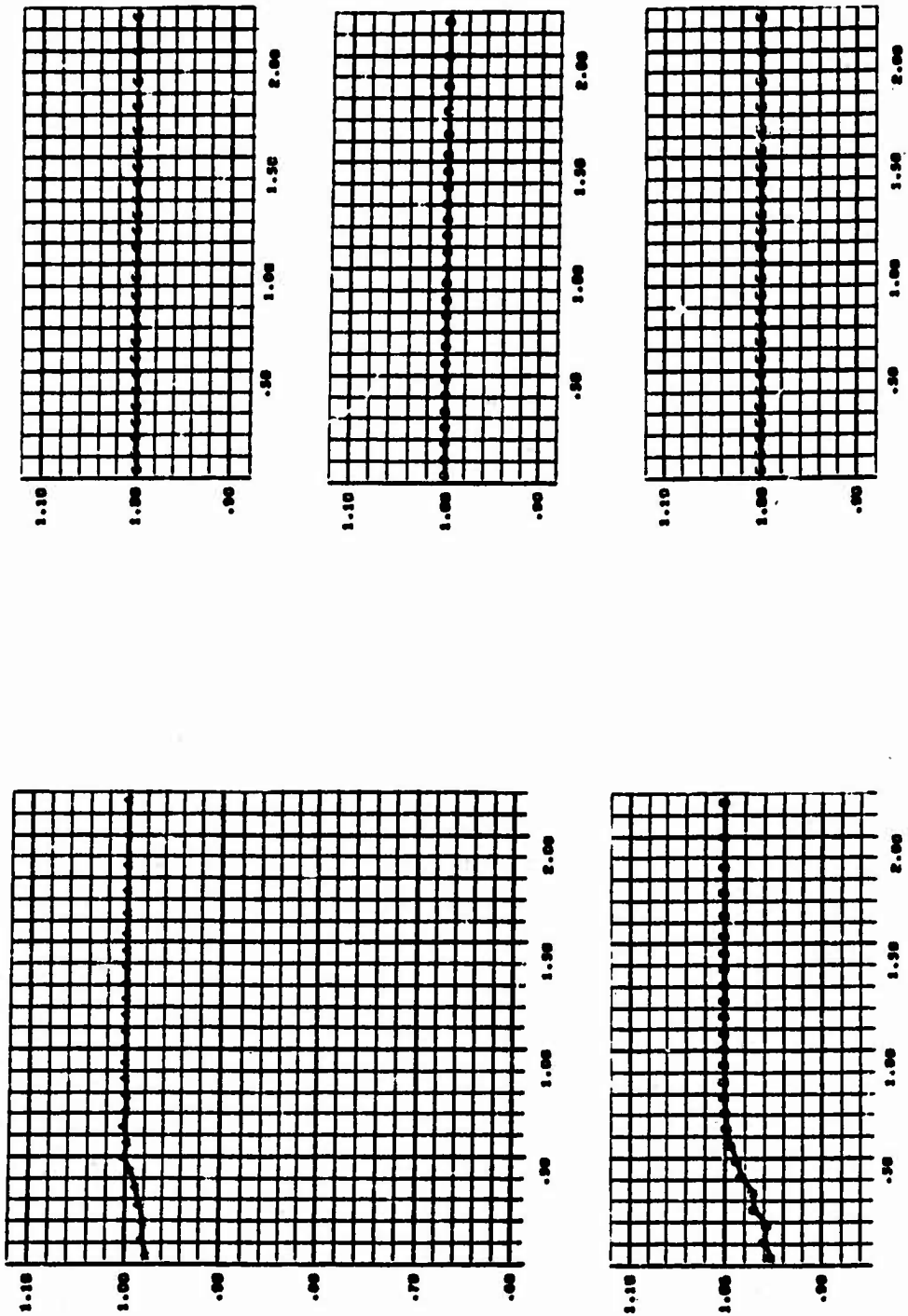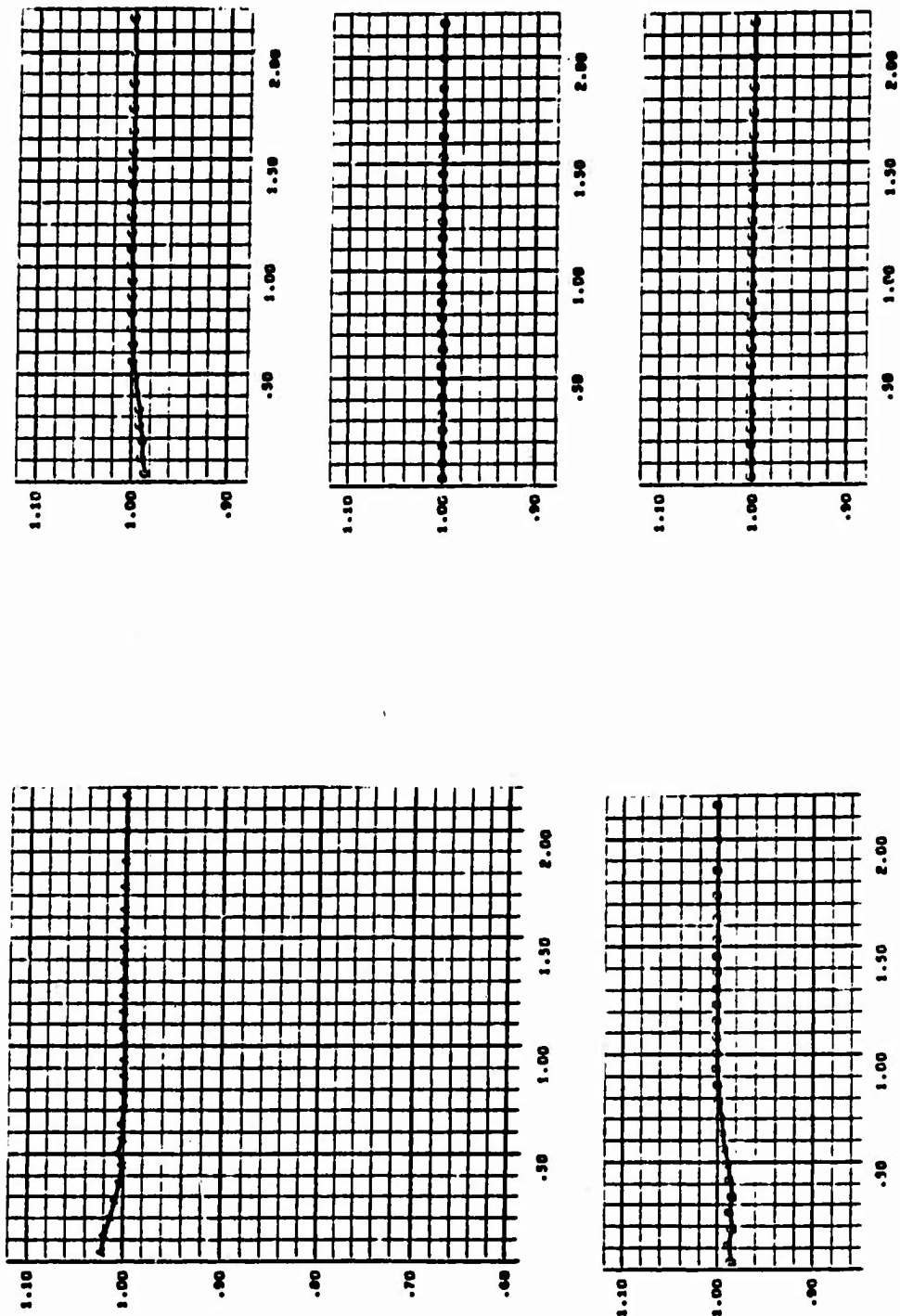
IRON - IRON IMPACT

RHOZ/RHO VS X (CM)   TIME= 1.5000-06

Figure 46.

IRON - IRON IMPACT
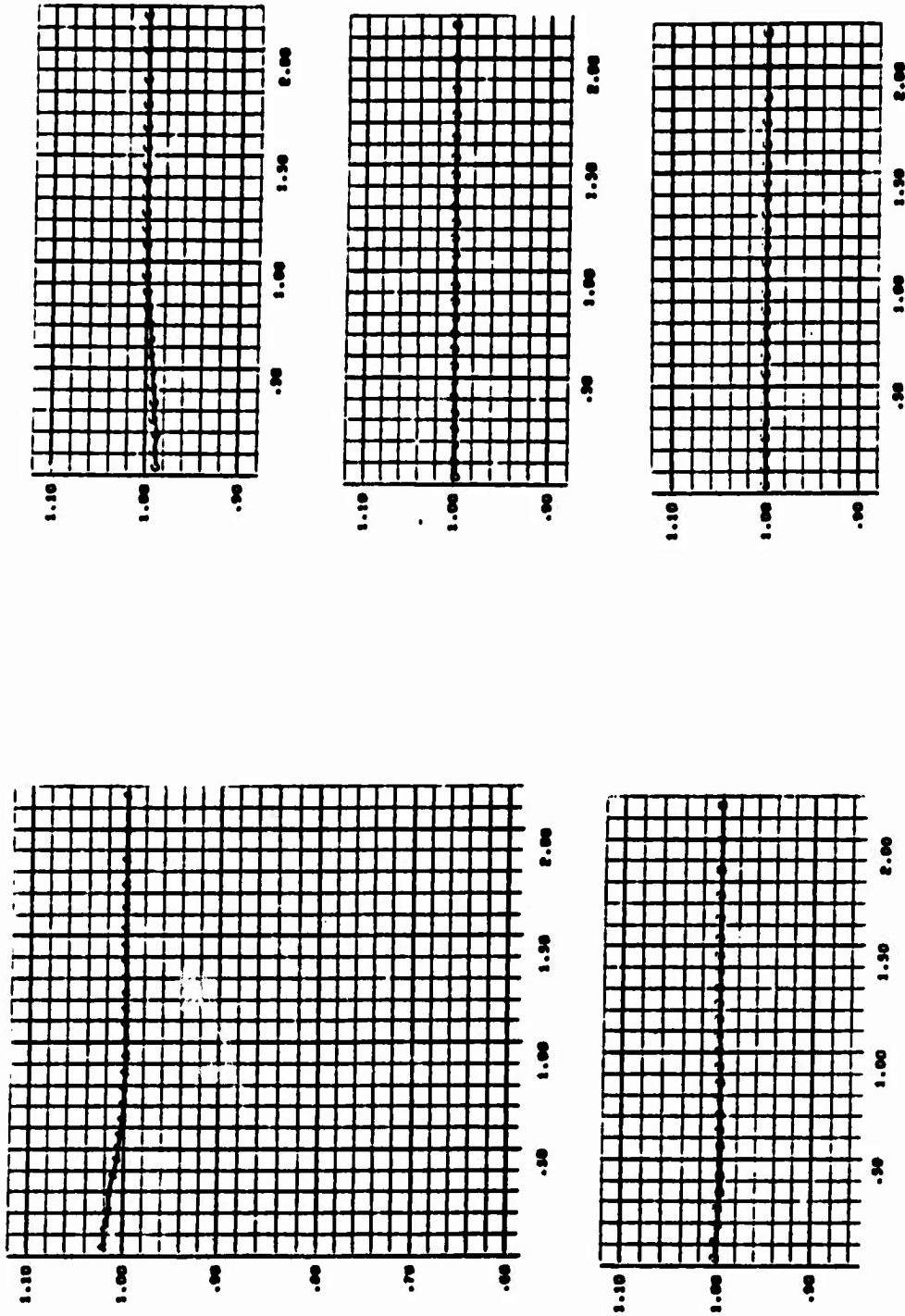
RHOZ/RHO VS X (CM)   TIME= 2.0000-06

Figure 47.

IRON - IRON IMPACT

RHOZ/RHO VS X (CM)   TIME= 2.5000-06
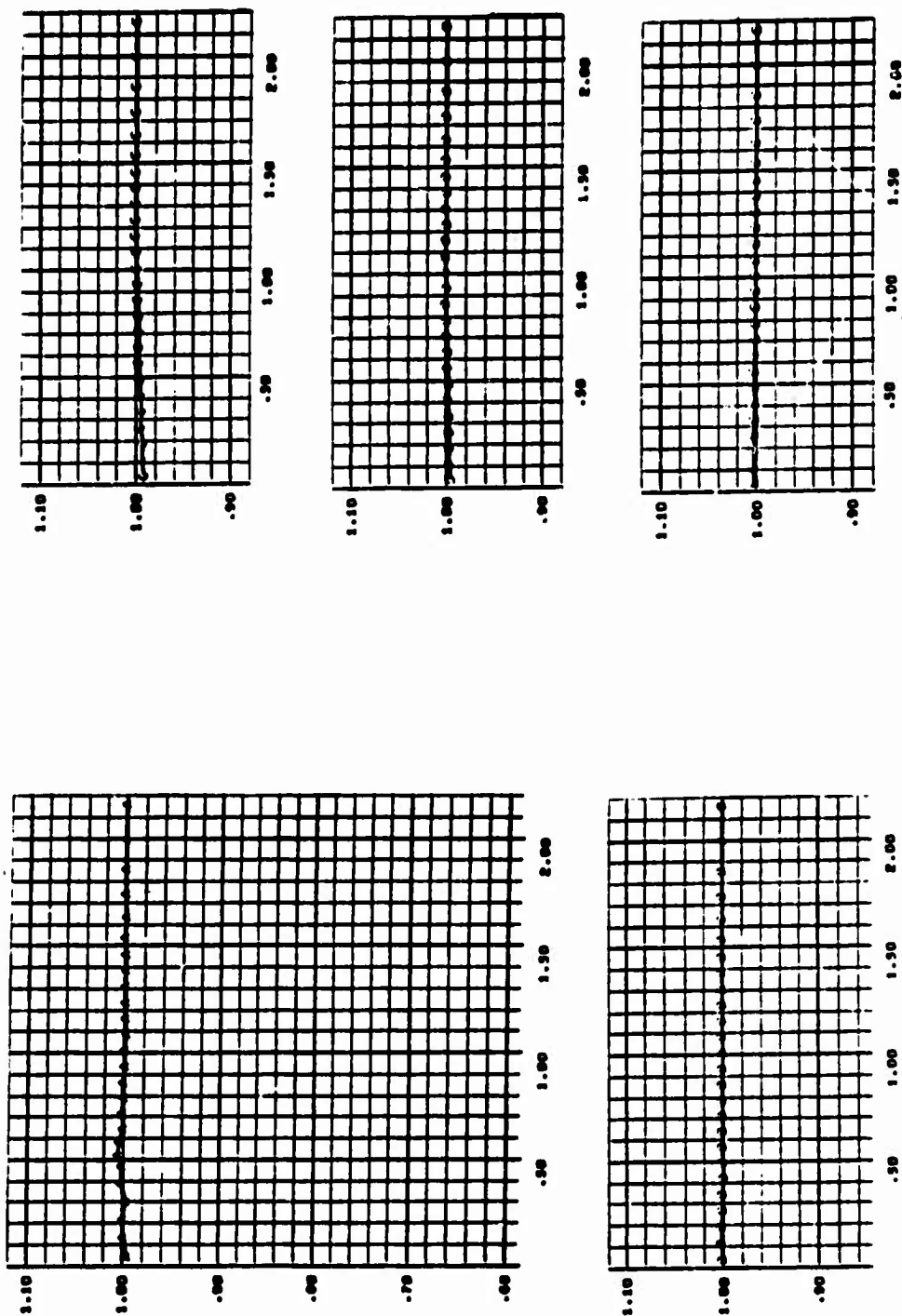
Figure 48.

IRON - IRON IMPACT
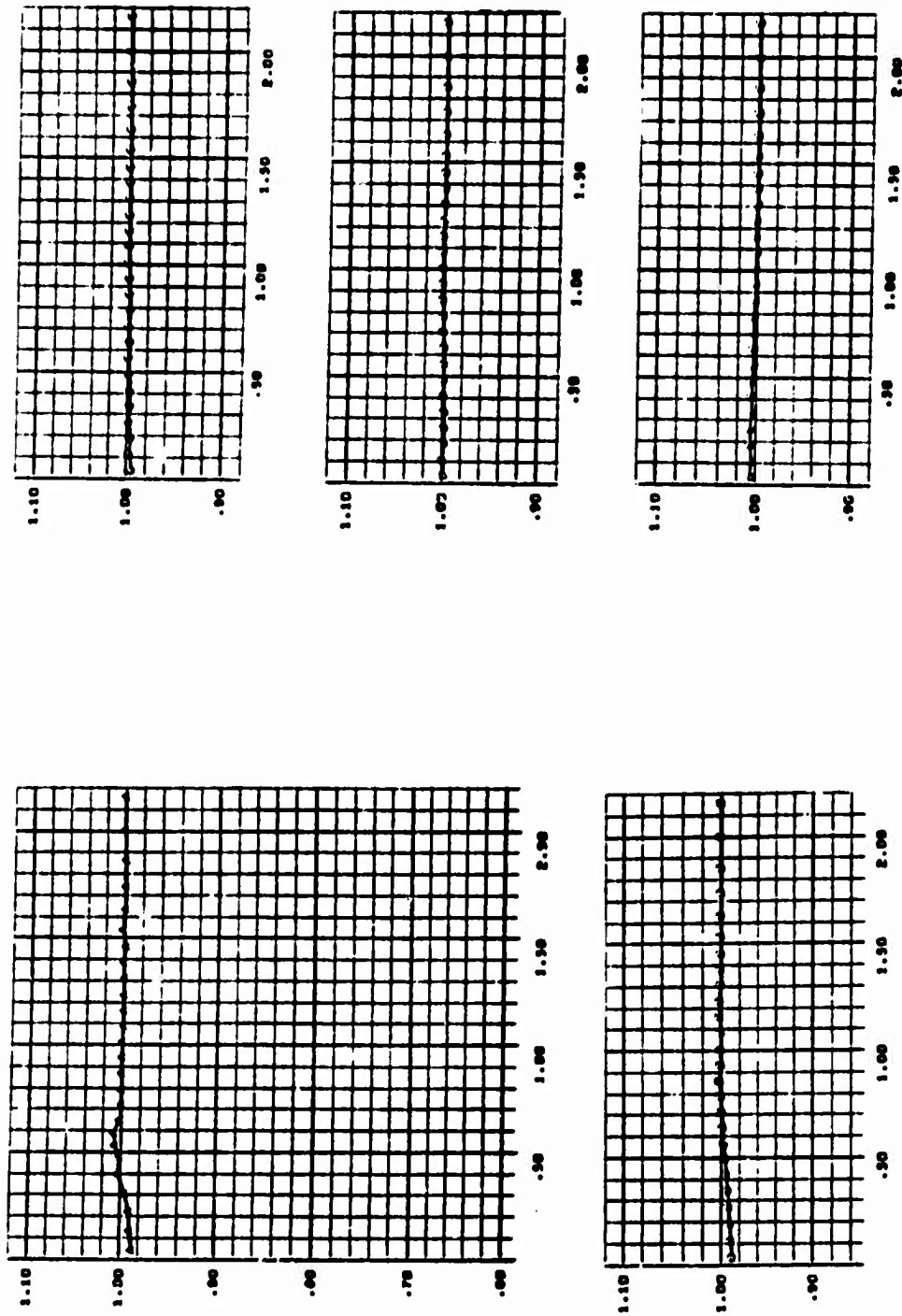
RHOZ/RHO VS X (CM)   TIME= 3.0000-06

Figure 49.

IRON - IRON IMPACT
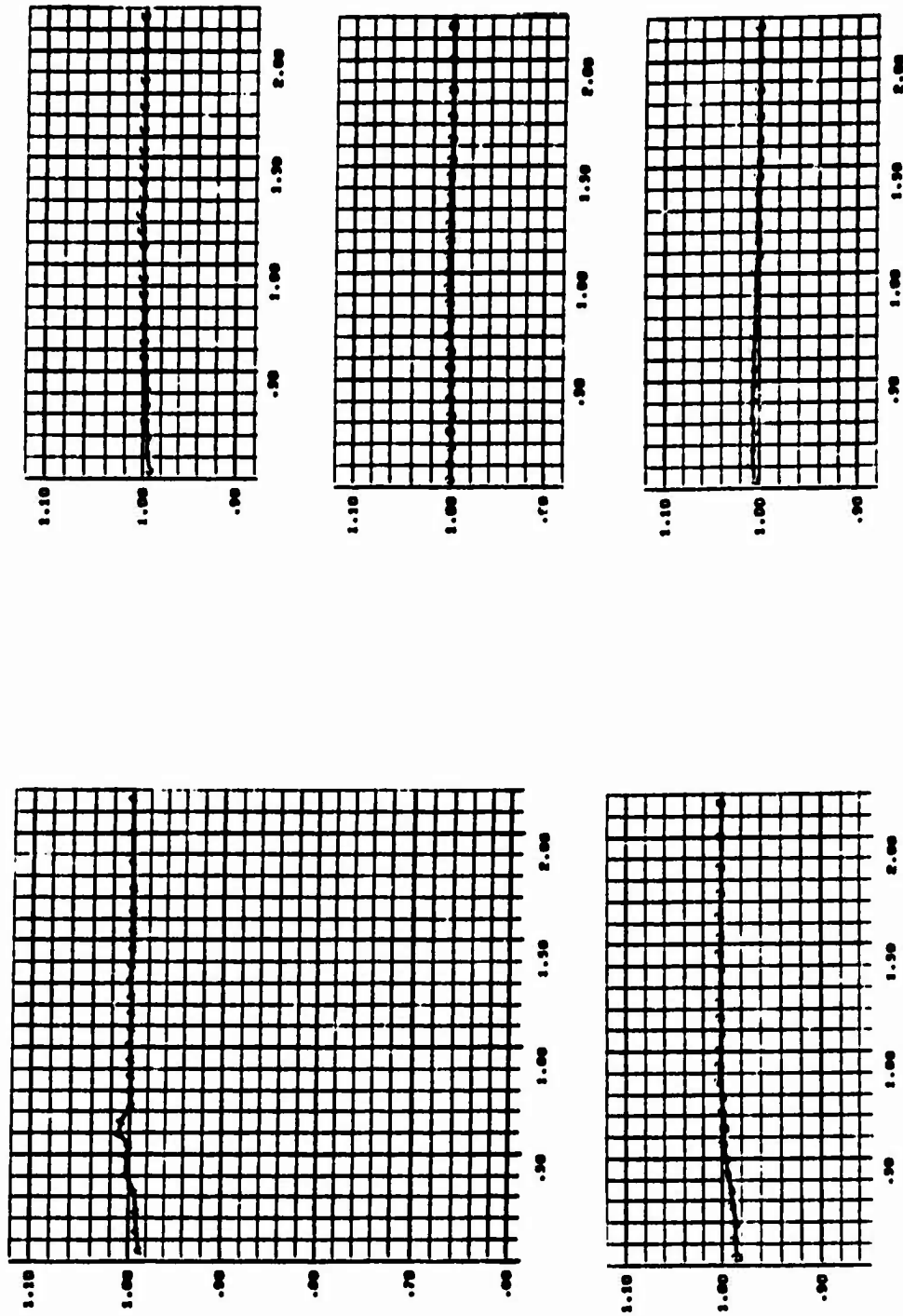
RHOZ/RHO VS X (CM)   TIME= 3.5000-06

Figure 50.

79

IRON - IRON IMPACT

RHOZ/RHO VS X (CM)   TIME= 4.0000-06

Figure 51.

80
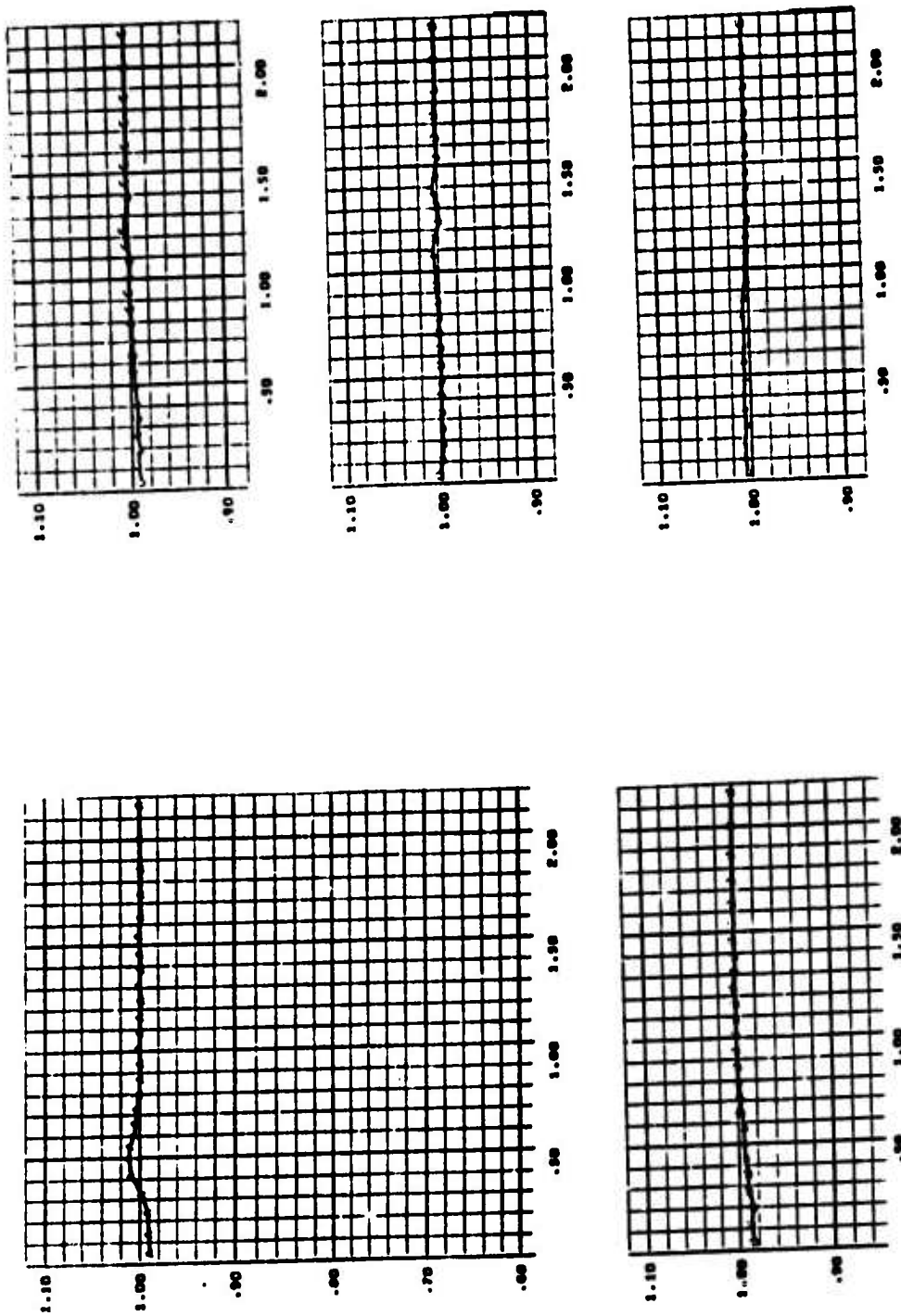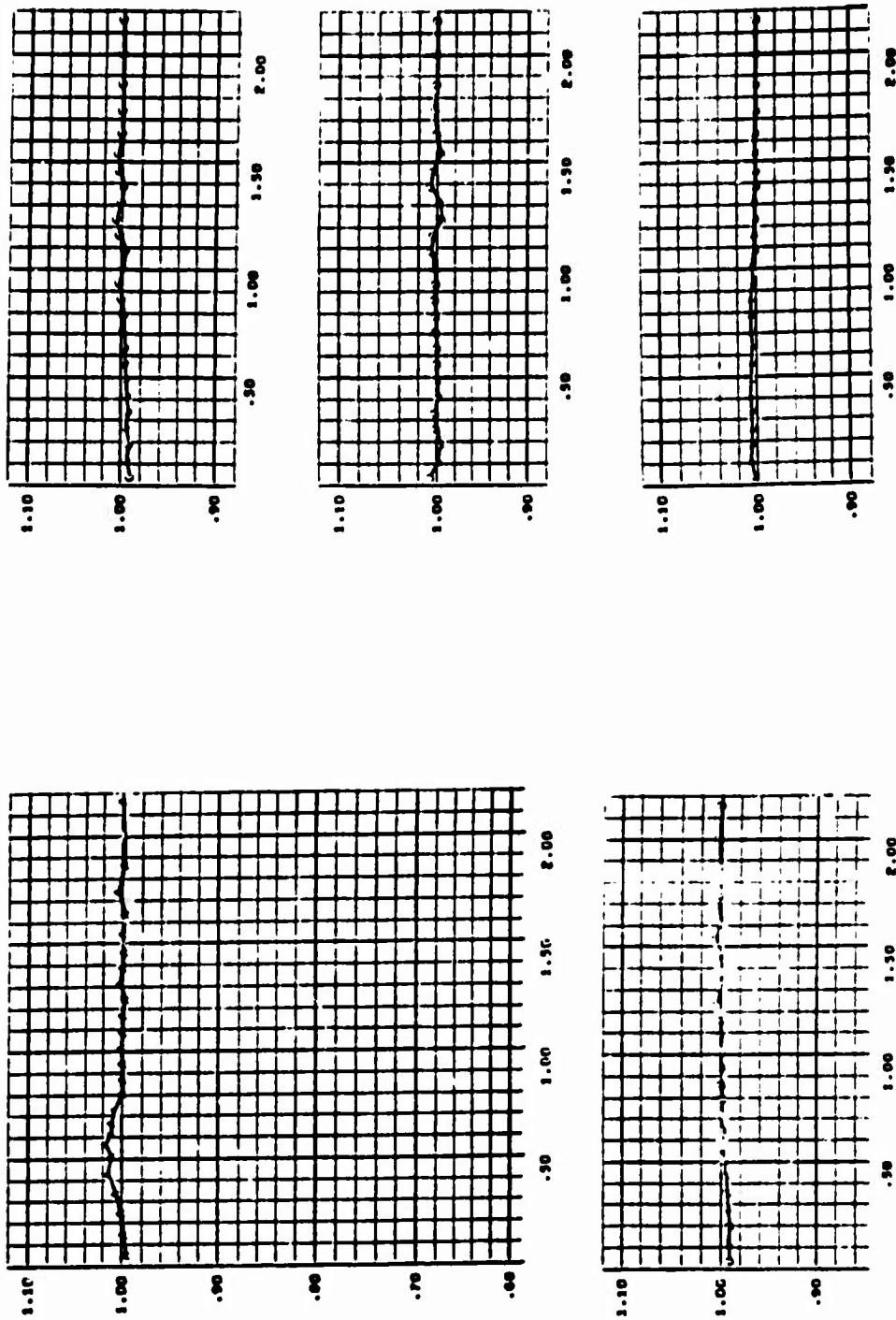
IRON - IRON IMPACT

RHOZ/CONS VS X (CM)   TIME= 4.5000-06

Figure 52.

81

IRON - IRON IMPACT
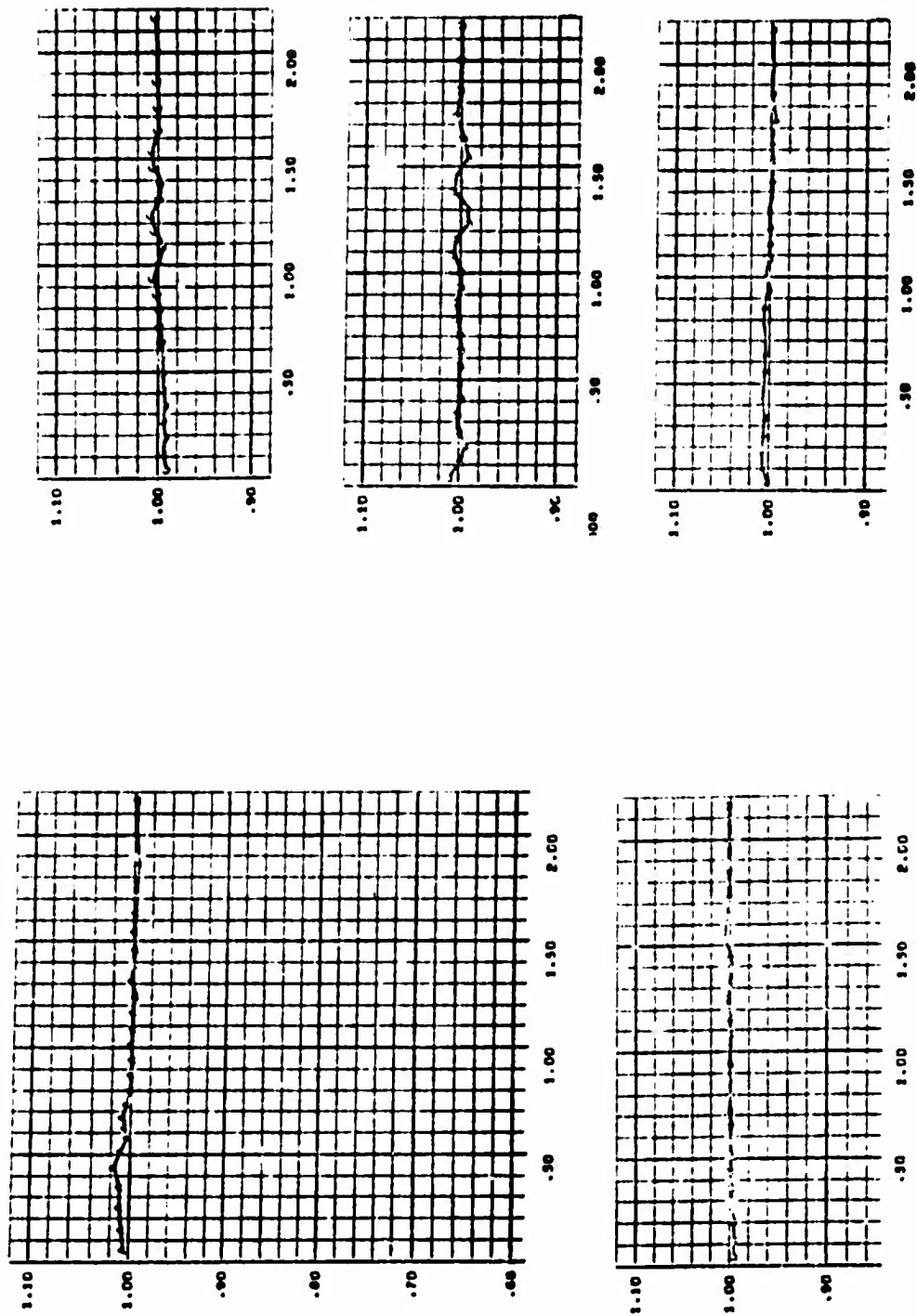
RHCZ/RHO   VS   X (CM)   TIME=   5.0000-06

Figure 53.

82

TEST PROBLEM NO. 1

Specific Internal Energy Versus Radial Distance
at Five Locations in the Target

For T = 0.0, 0.5, 1.0, 1.5, 2.0, 2.5, 3.0, 3.5, 4.0
        4.5, and 5.0 µsec.

A = Target Front Surface

B = One-Quarter Distance into Target

C = One Half Distance into Target

D = Three-Quarters Distance into Target

E = Back Surface

83
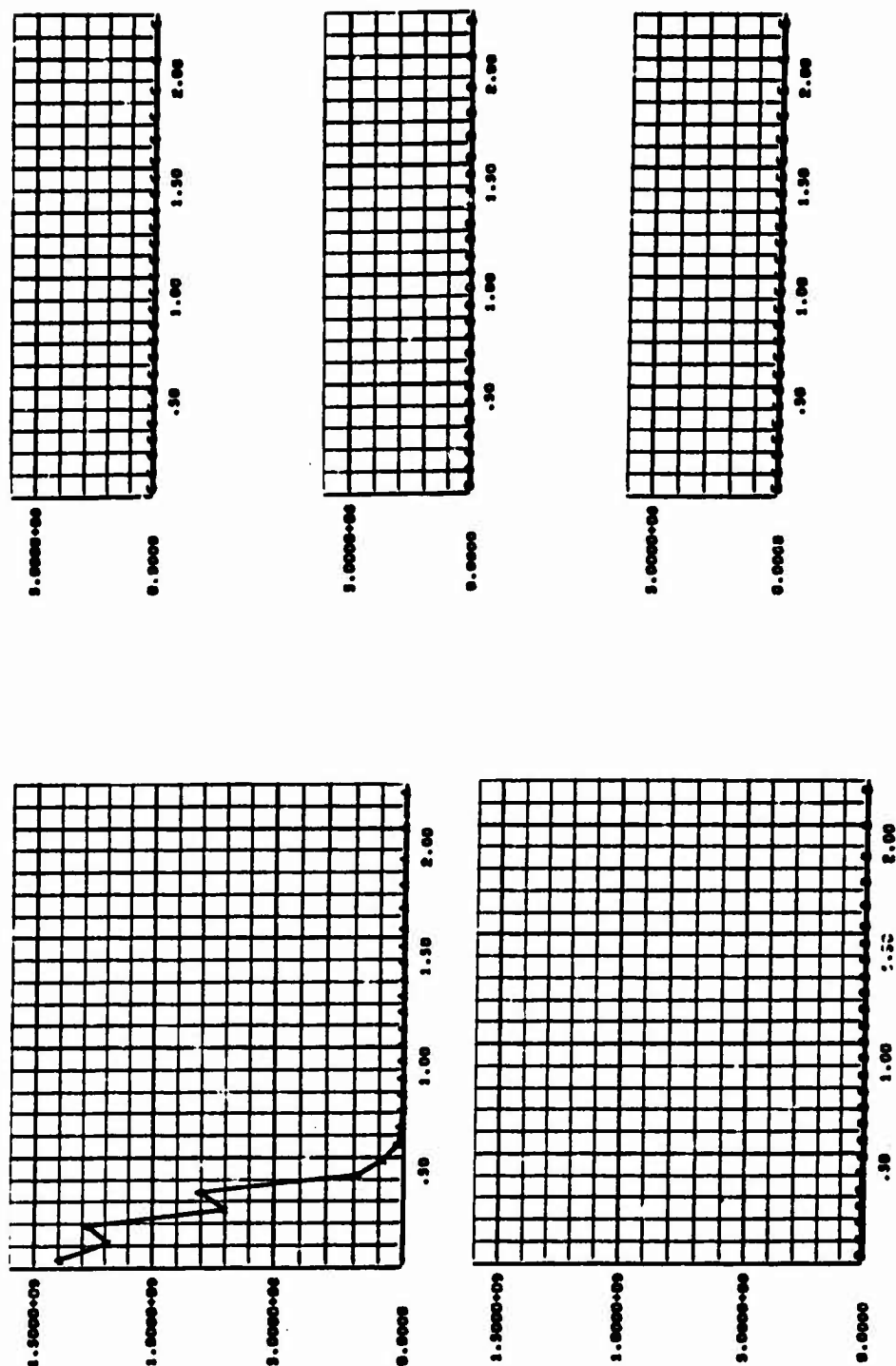
IRON - IRON IMPACT

SPECIFIC INTERNAL ENERGY (ERGS/G) VS X (CM)   TIME= 5.0000-07

Figure 54.

IRON - IRON IMPACT
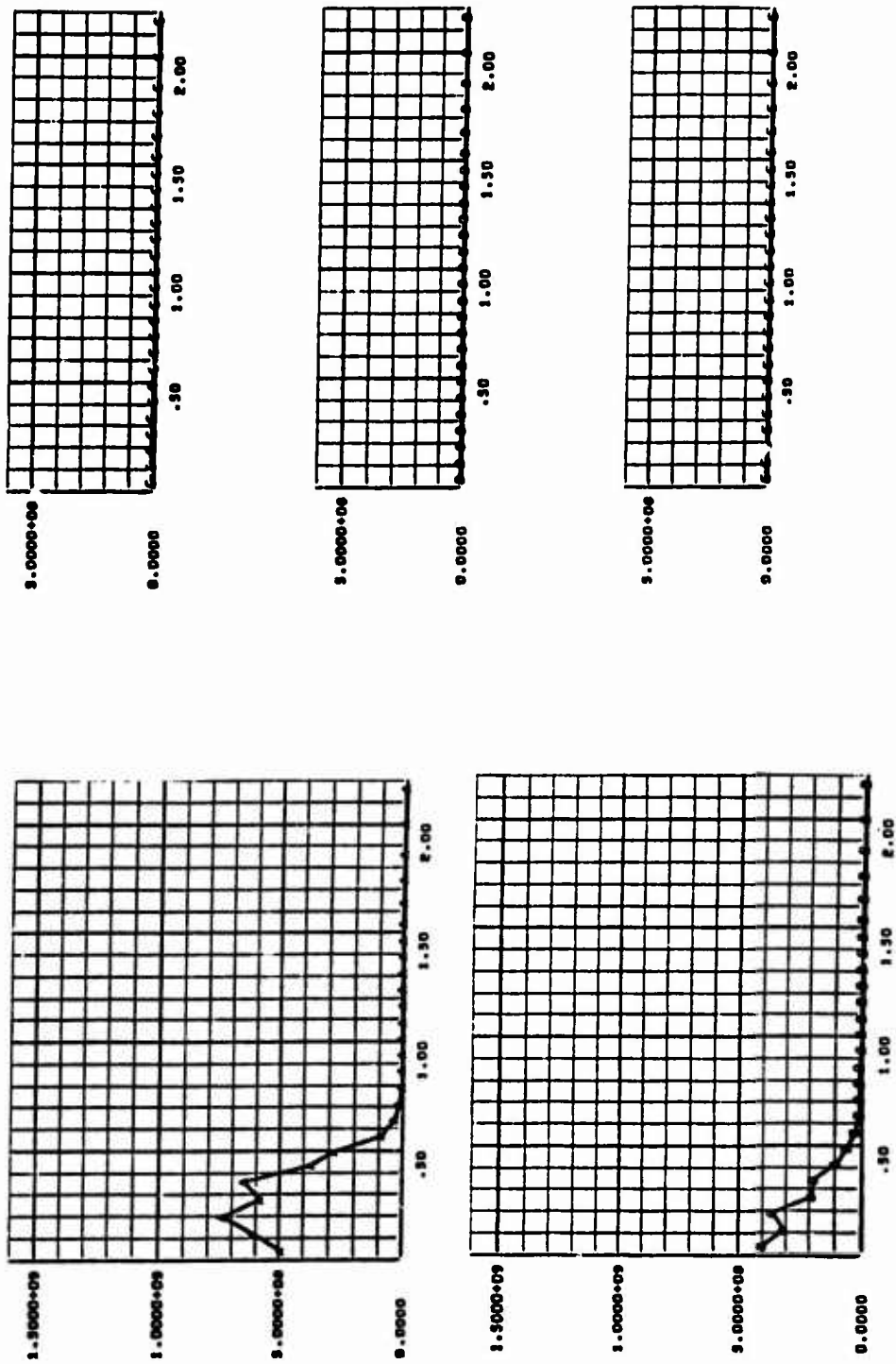
SPECIFIC INTERNAL ENERGY (ERGS/G)   VS   X (CM)   TIME= 1.0000-06

Figure 55.

85

IRGN - IRON IMPACT

SPECIFIC INTERNAL ENERGY (ERGS/G) VS X (CM)
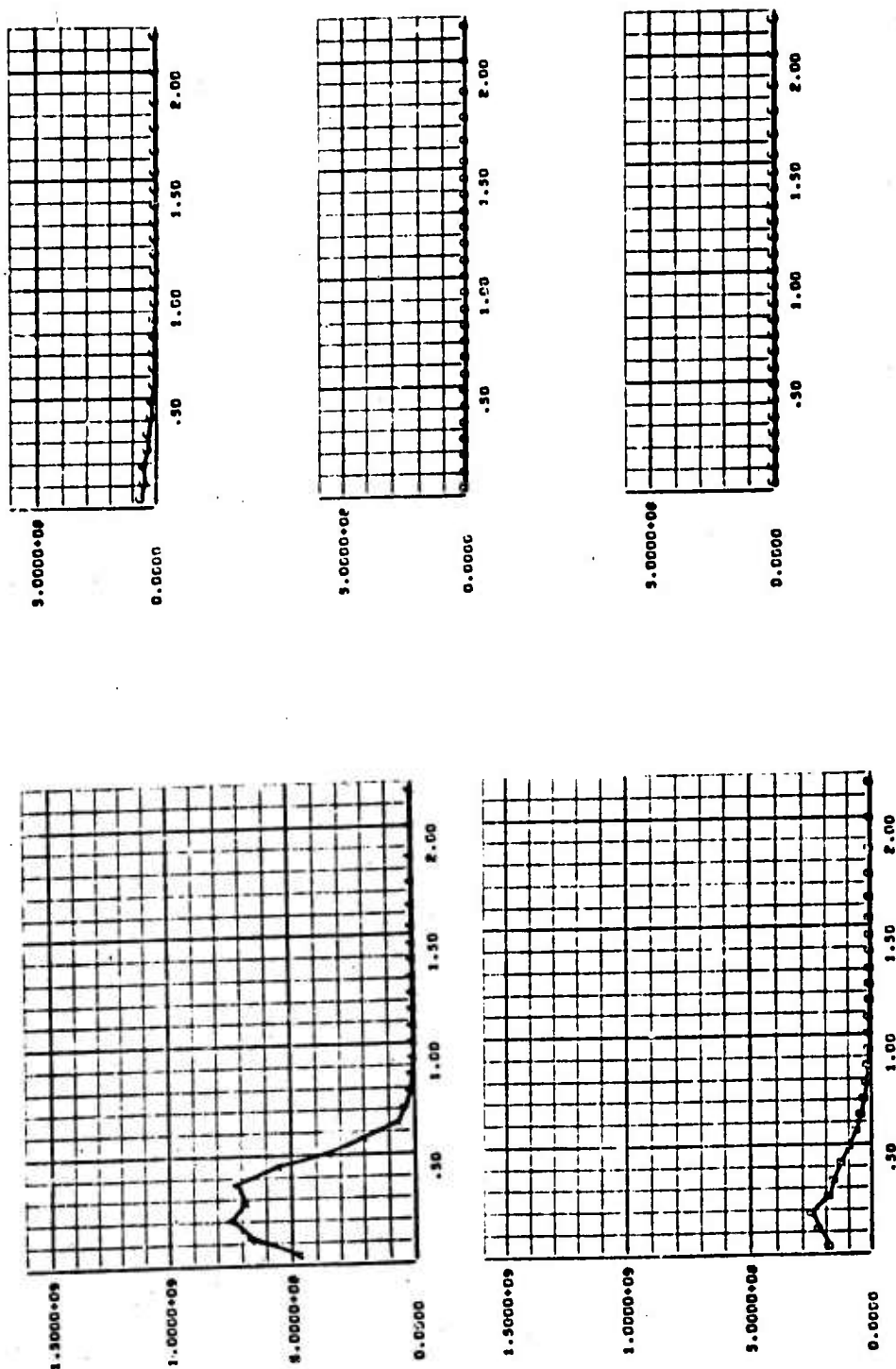
TIME = 1.5000-06

Figure 56
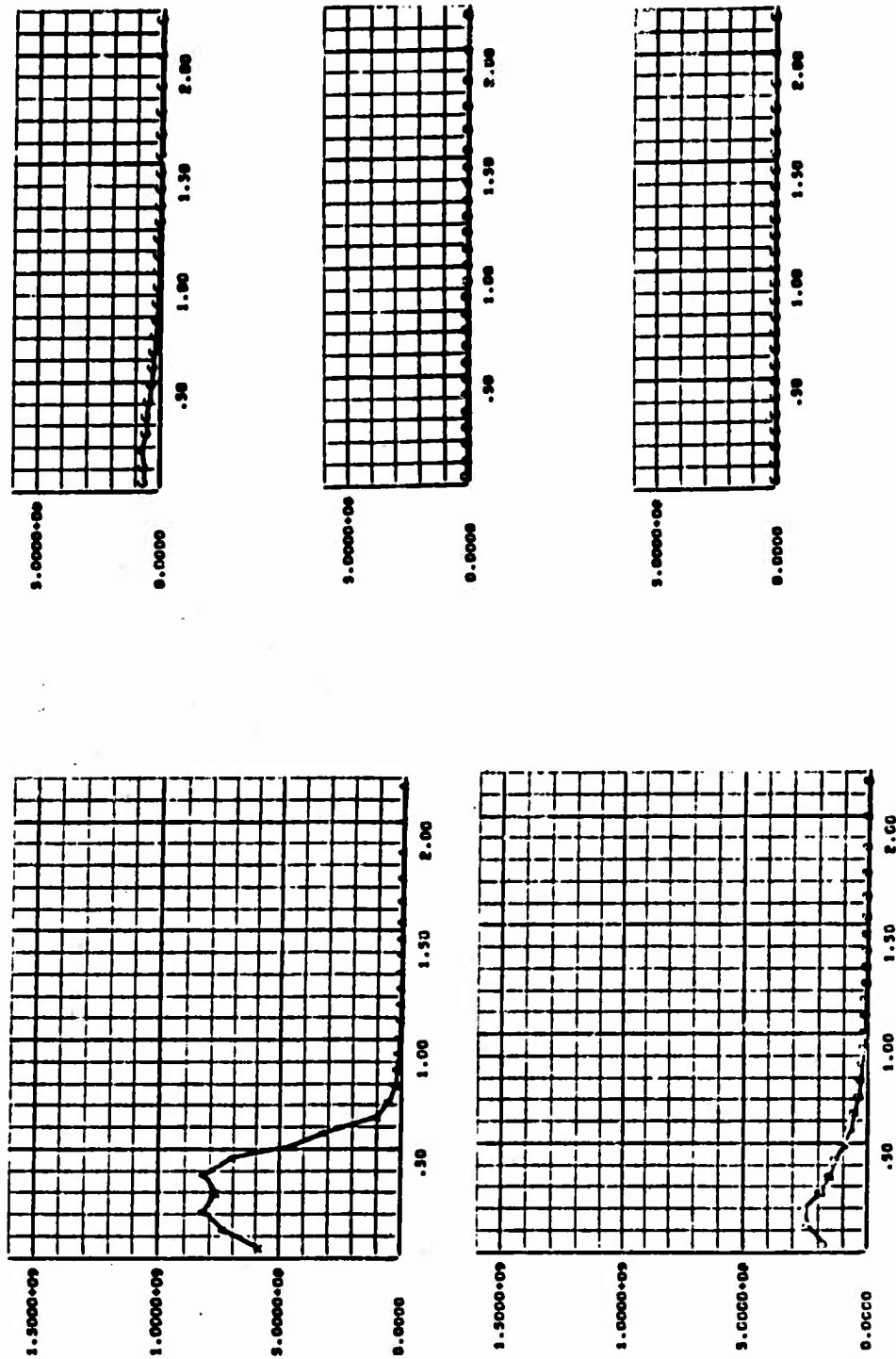
IRON - IRON IMPACT

SPECIFIC INTERNAL ENERGY (ERGS/G) VS X (CM)   TIME= 2.0000-05

Figure 57.

IRON - IRON IMPACT
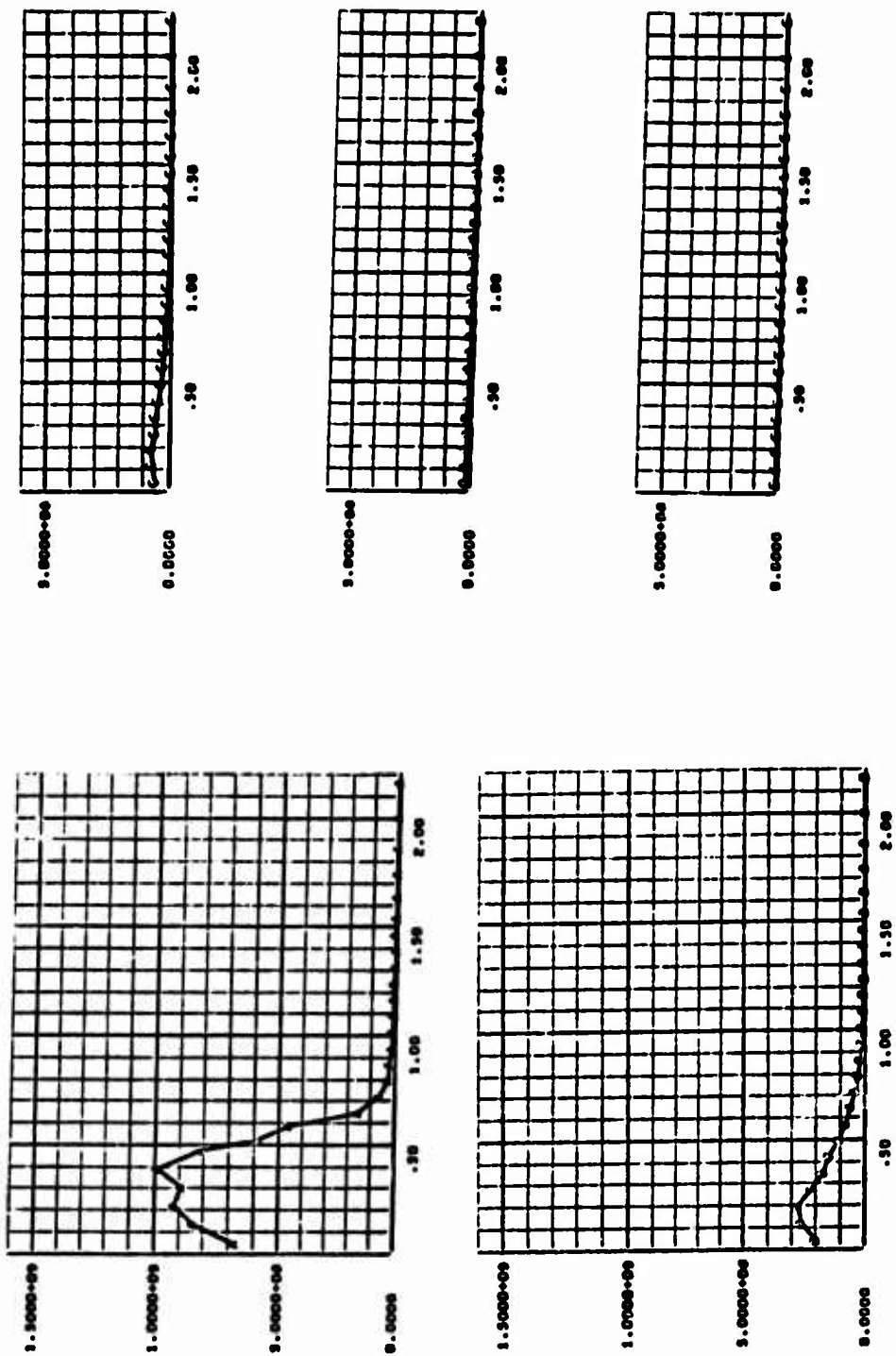
SPECIFIC INTERNAL ENERGY (ERGS/G) VS X (CM)   TIME= 2.5000-06

Figure 58.

IRON - IRON IMPACT
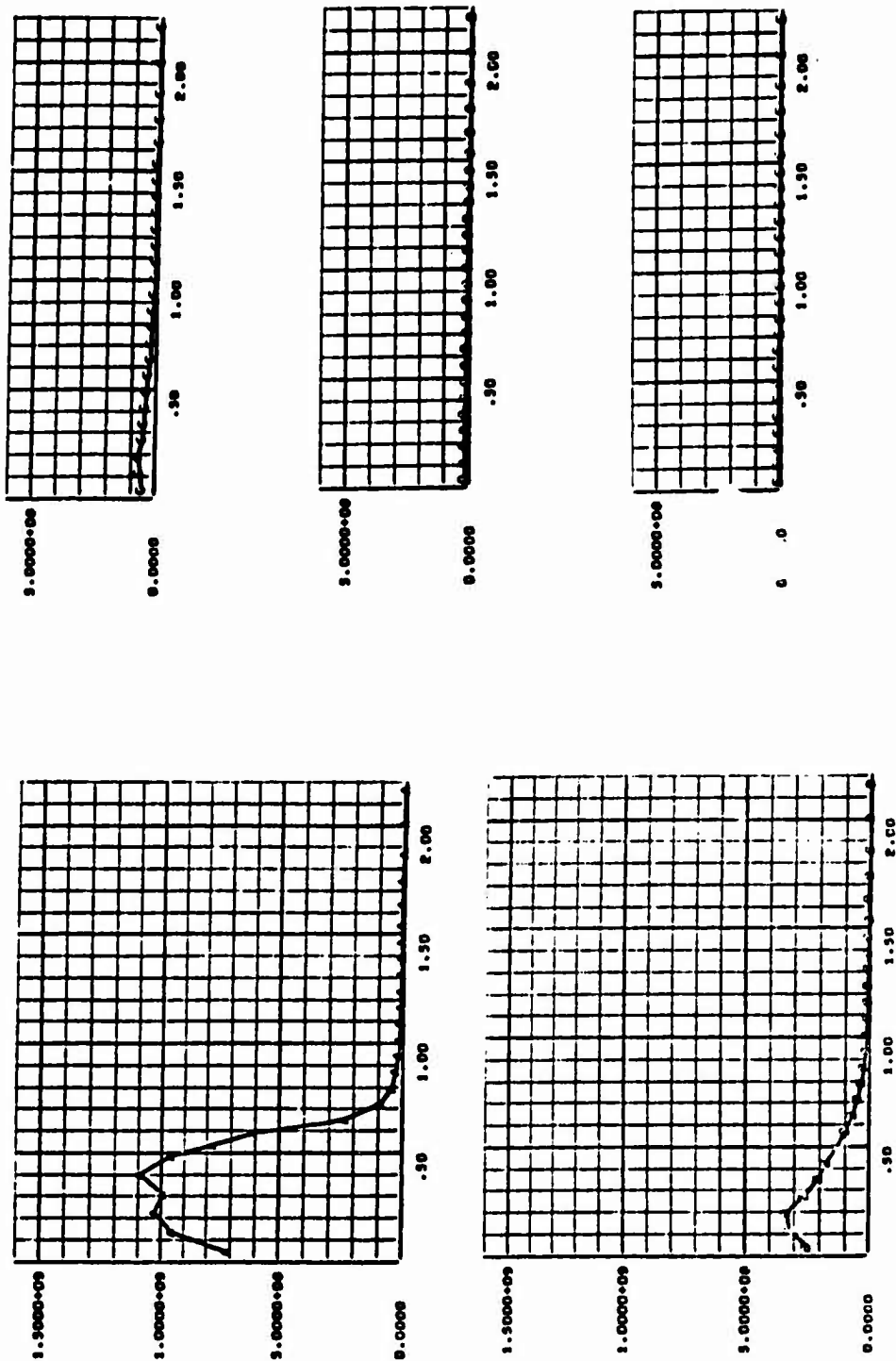
SPECIFIC INTERNAL ENERGY (ERGS/G) VS X (CM)   TIME= 3.0300-06

Figure 59.

IRON - IRON IMPACT
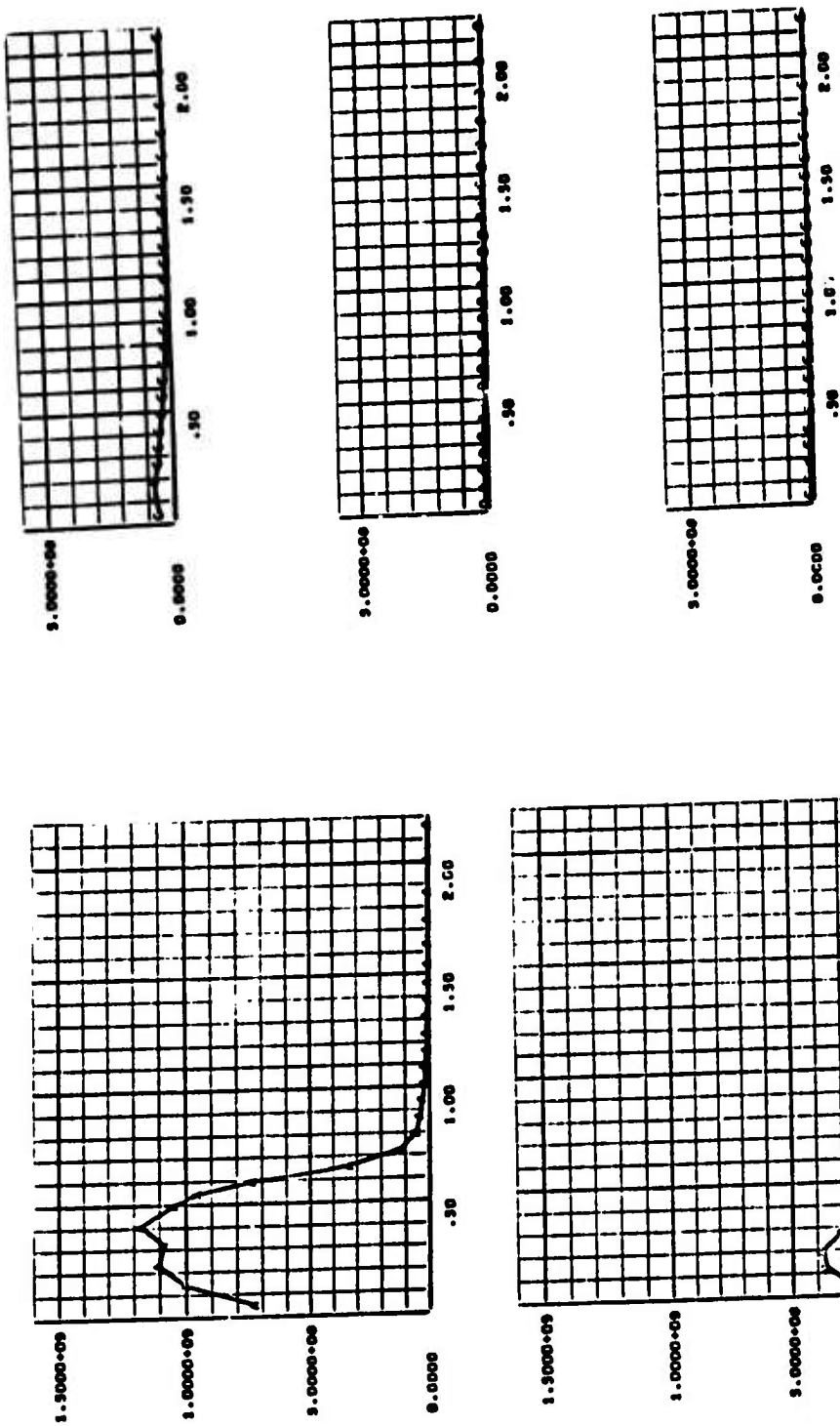
SPECIFIC INTERNAL ENERGY (ERGS/G) VS X (CM)   TIME=   3.5000-06

Figure 60.

90
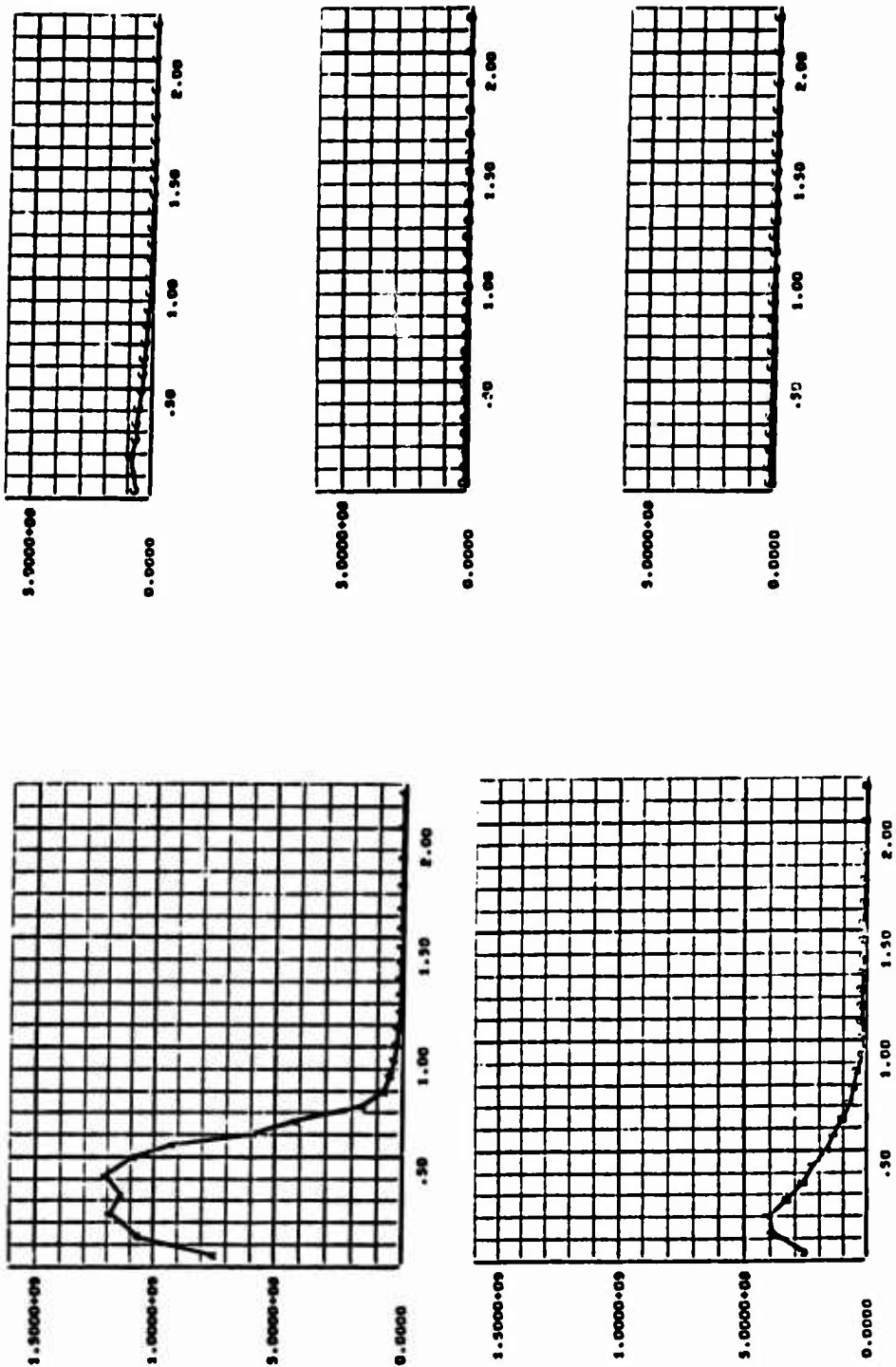
IRON - IRON IMPACT

SPECIFIC INTERNAL ENERGY (ERGS/G) VS X (CM)   TIME= 4.0000-06

Figure 61.

91
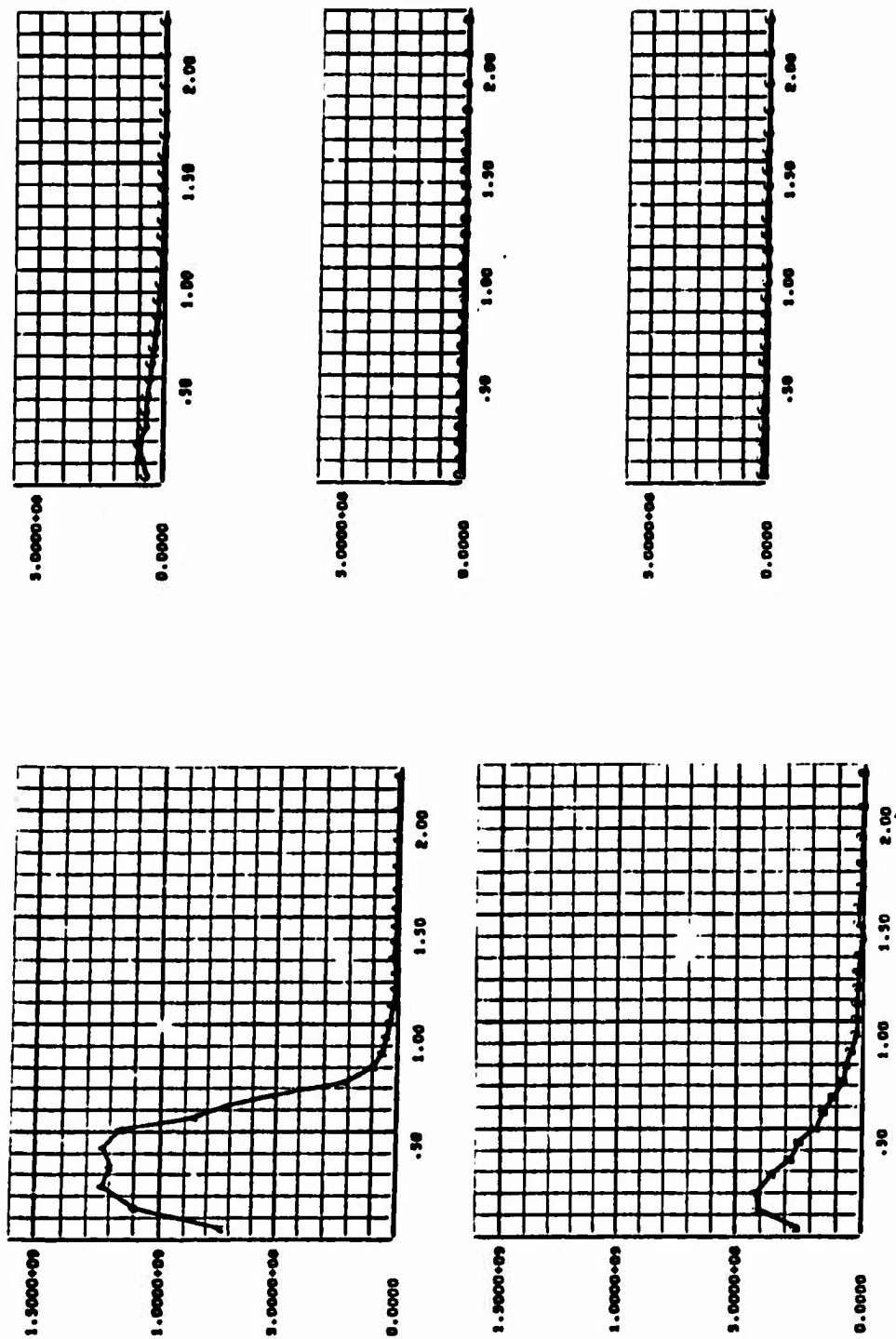
IRON - IRON IMPACT

SPECIFIC INTERNAL ENERGY (ERGS/G) VS X (CM)

TIME= 4.5000-06

Figure 62.

IRON - IRON IMPACT
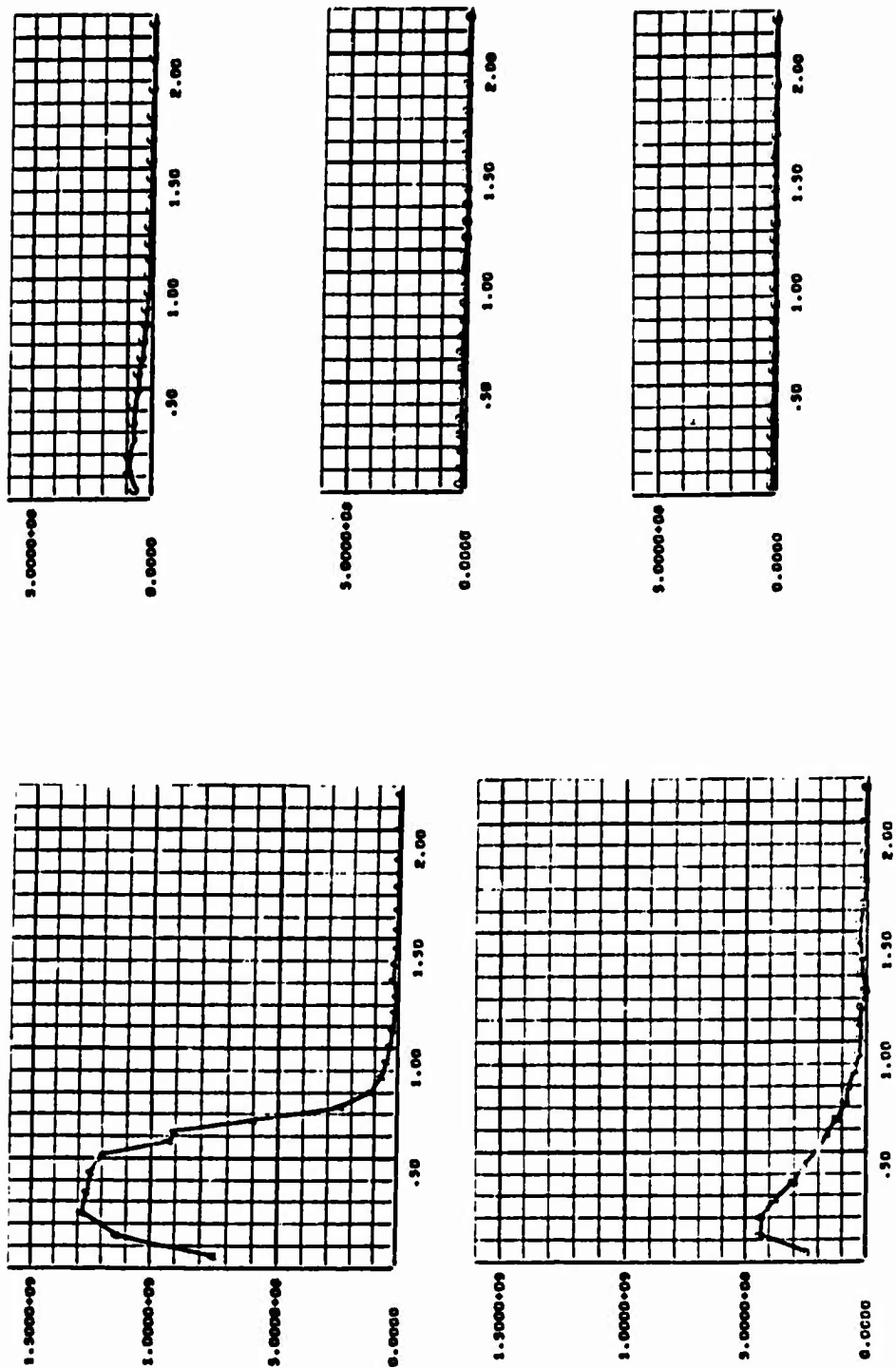
SPECIFIC INTERNAL ENERGY (ERGS/G) VS X (CM)   TIME= 5.0000-06

Figure 63.

93

TEST PROBLEM NO. 1

Instantaneous Plastic Strain Rate Versus Radial Distance at Five Locations in the Target

For T = 0.0, 0.5, 1.0, 1.5, 2.0, 2.5, 3.0, 3.5, 4.0,
         4.5, and 4.0 µsec.

A = Target Front Surface

B = One-Quarter Distance into Target

C = One-Half Distance into Target

D = Three-Quarters Distance into Target

E = Back Surface
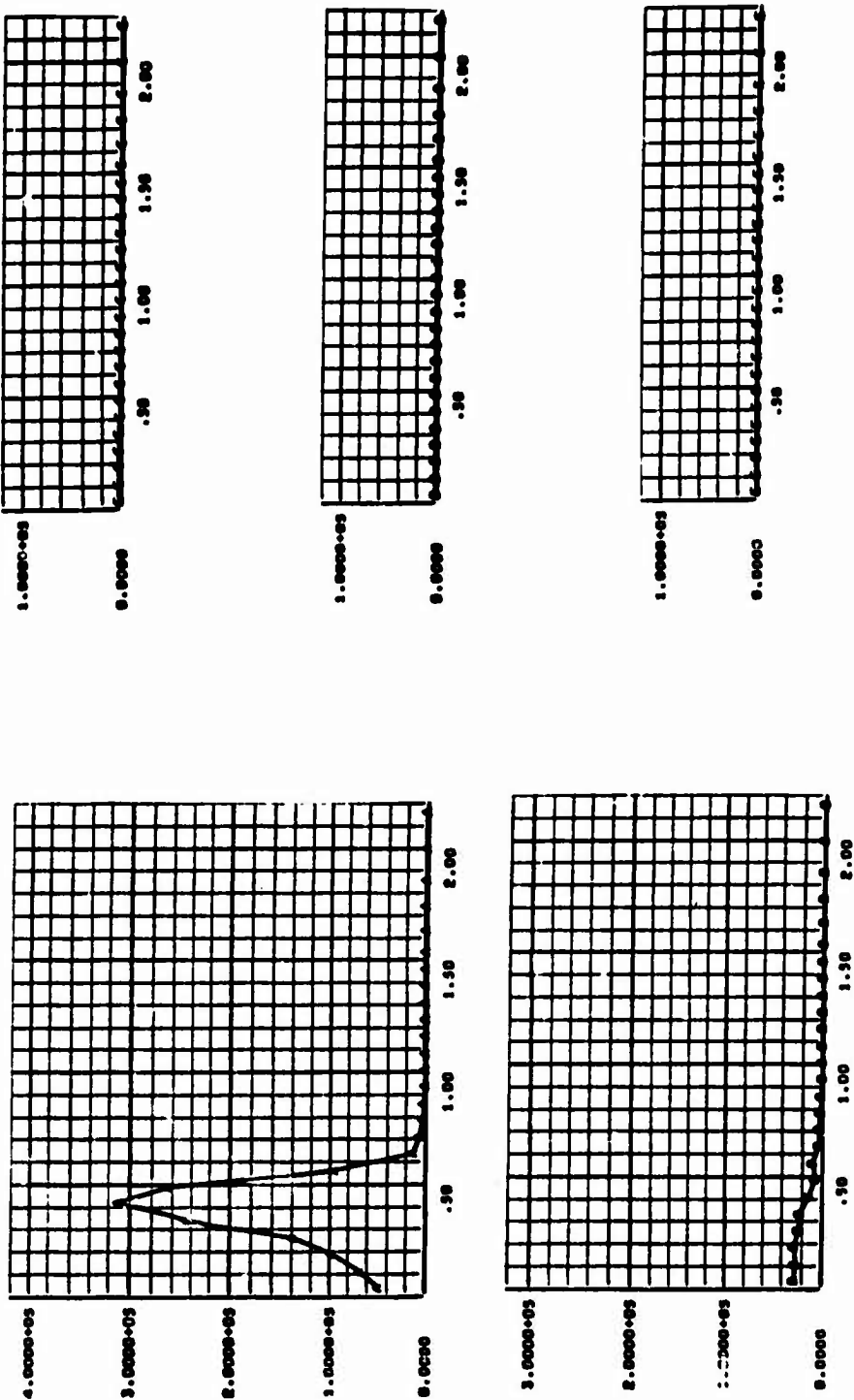
IRON - IRON IMPACT

PLASTIC STRAIN RATE (1/SEC) VS x (CM)   TIME= 5.0000-07

Figure 64.

IRON - IRON IMPACT
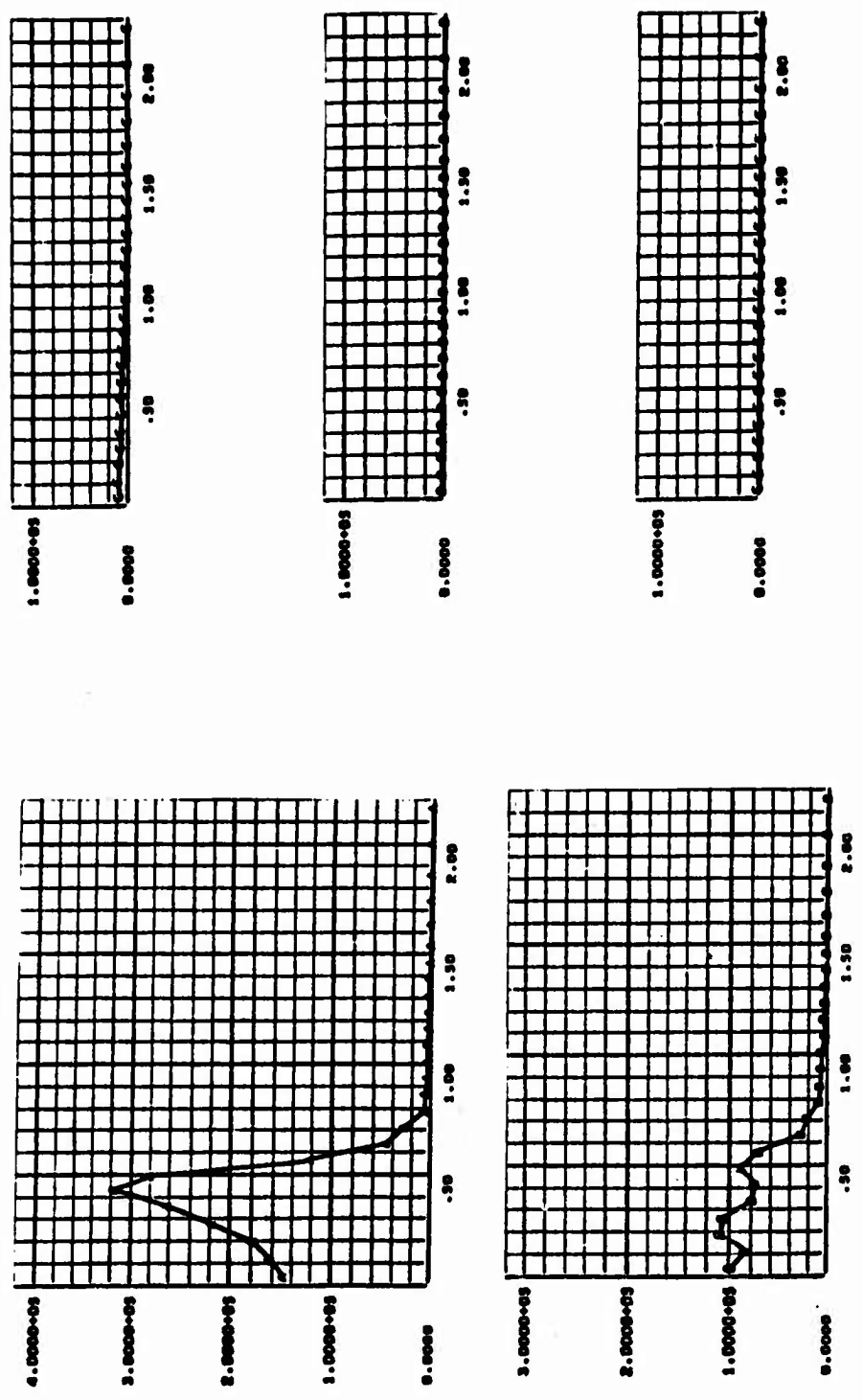
PLASTIC STRAIN RATE (1/SEC) VS X (CM)   TIME= 1.0000-06

Figure 65.

IRON - IRON IMPACT
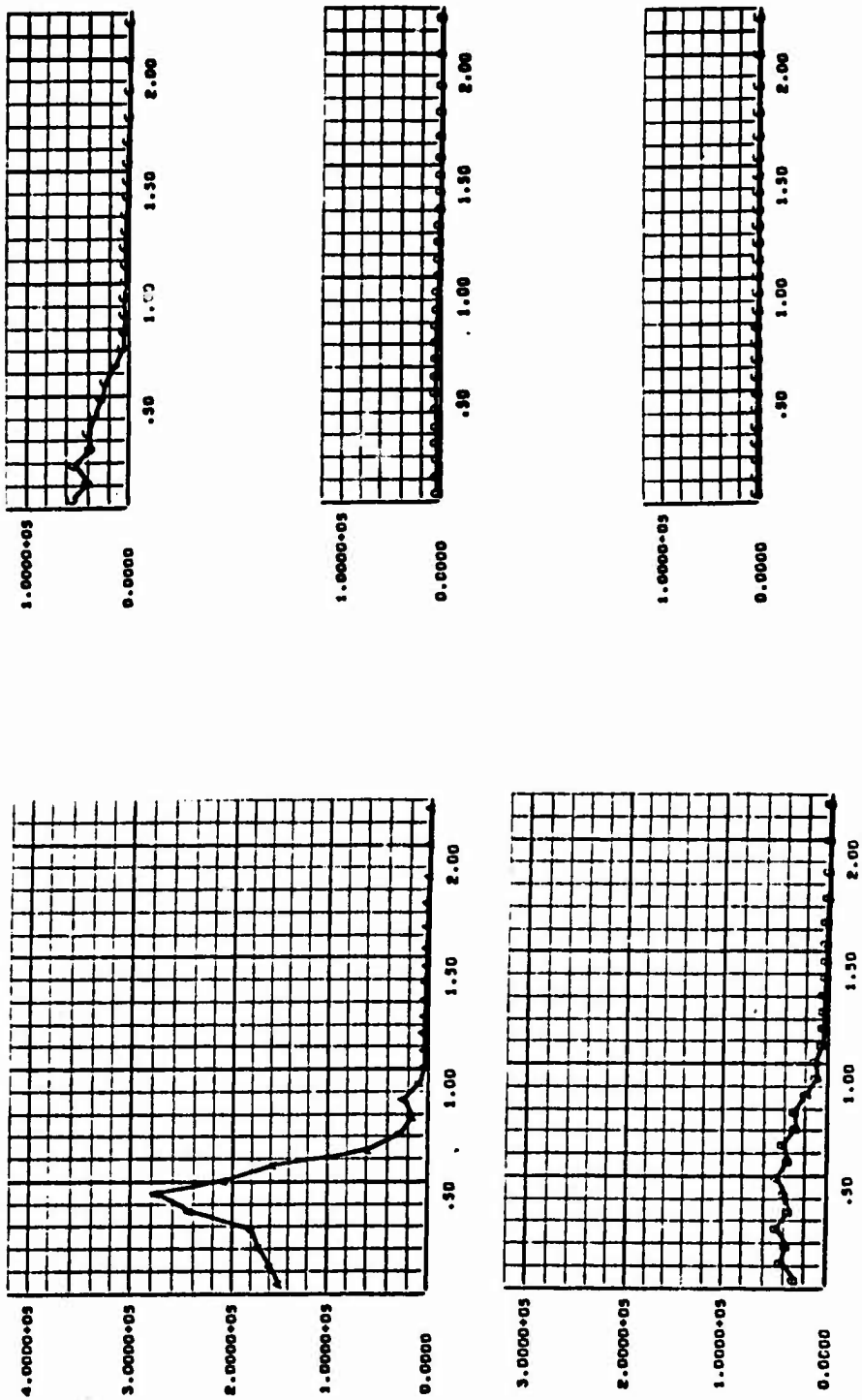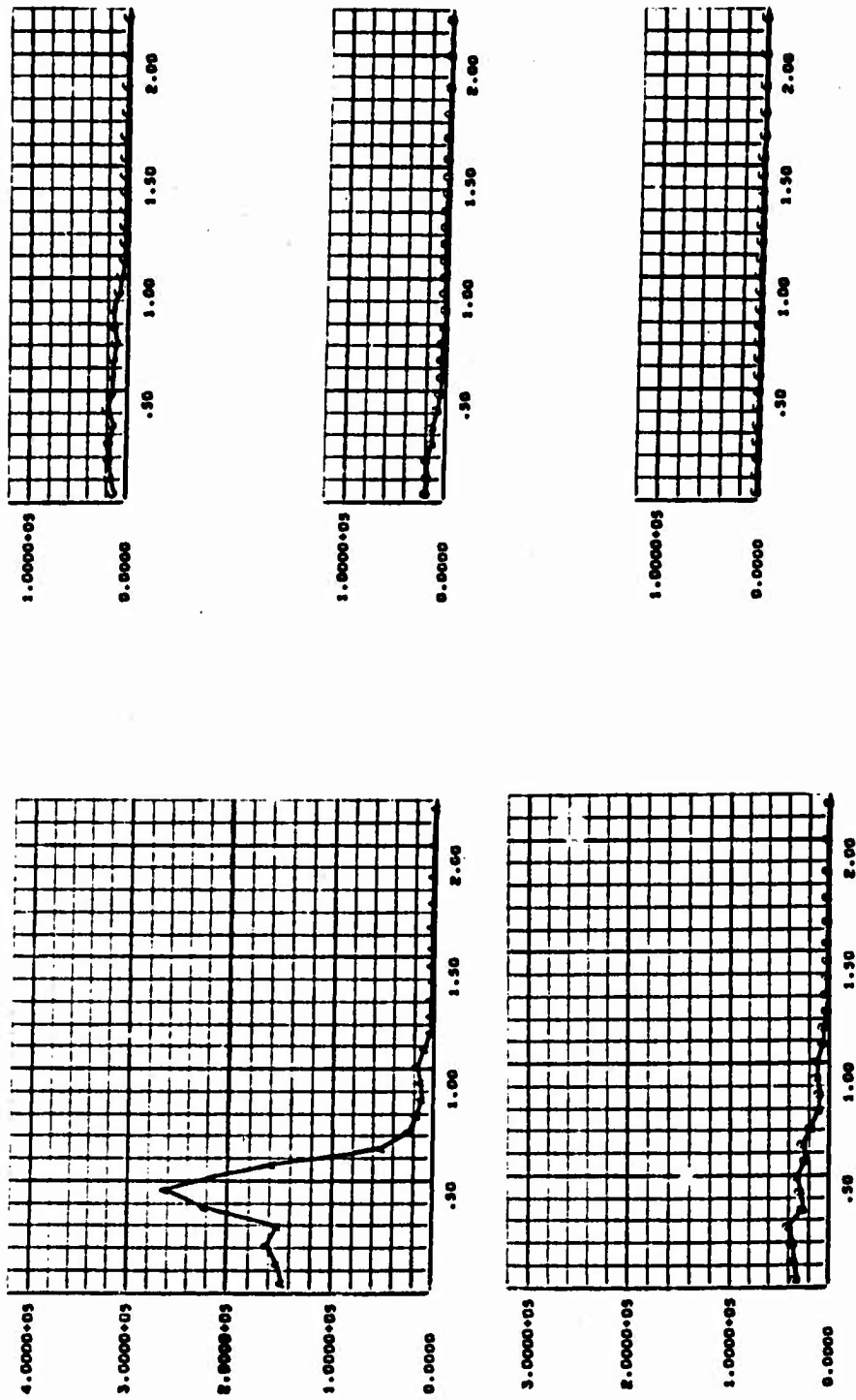
PLASTIC STRAIN RATE (1/SEC) VS X (CM)   TIME= 1.5000-06

Figure 66.

3SR-201

97

IRON - IRON IMPACT

PLASTIC STRAIN RATE (1/SEC) VS X (CM)   TIME=   2.0000-05

Figure 67.

98
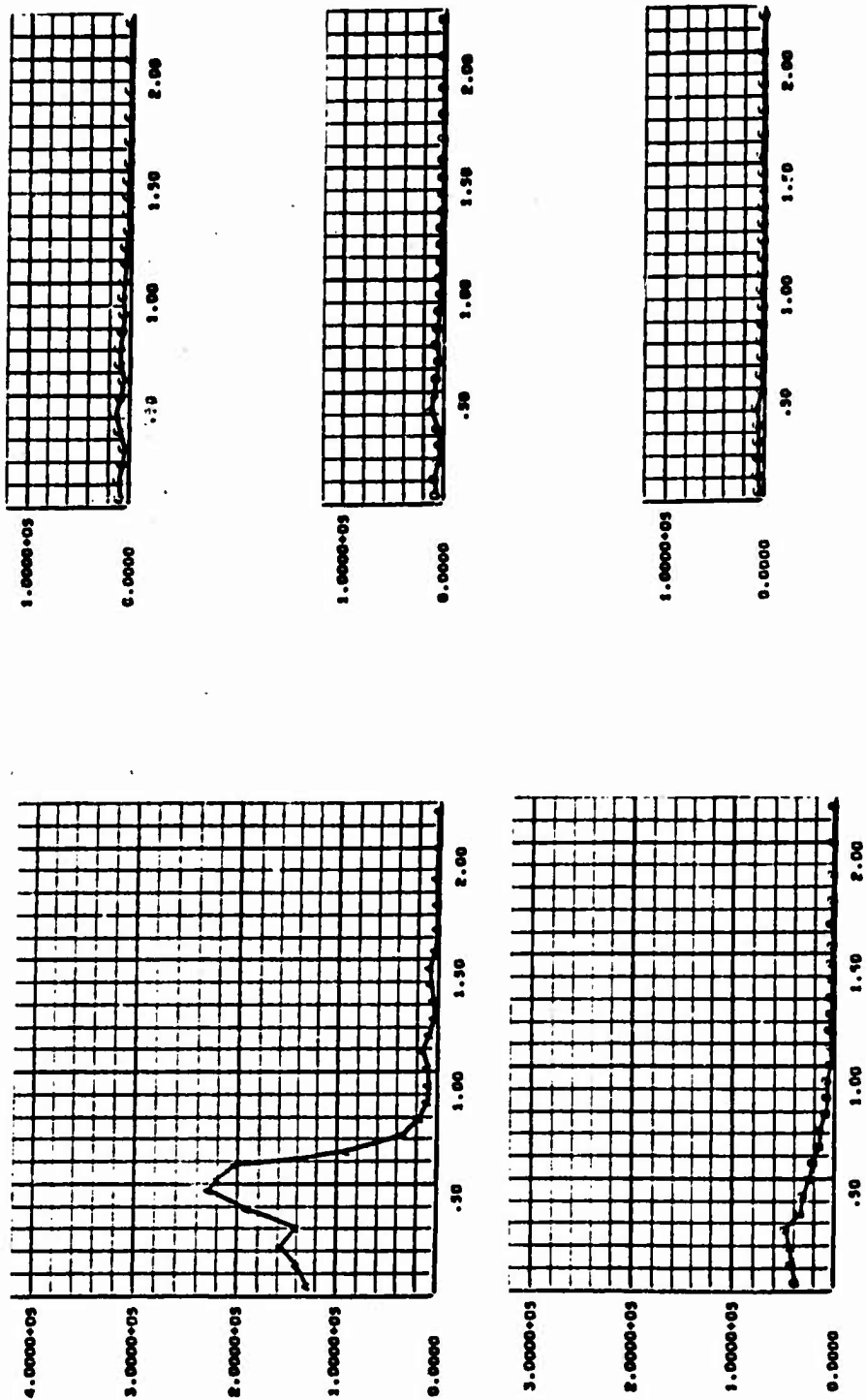
IRON - IRON IMPACT

PLASTIC STRAIN RATE (1/SEC) VS X (CM)   TIME=   2.5000-06

Figure 68.

IRON - IRON IMPACT
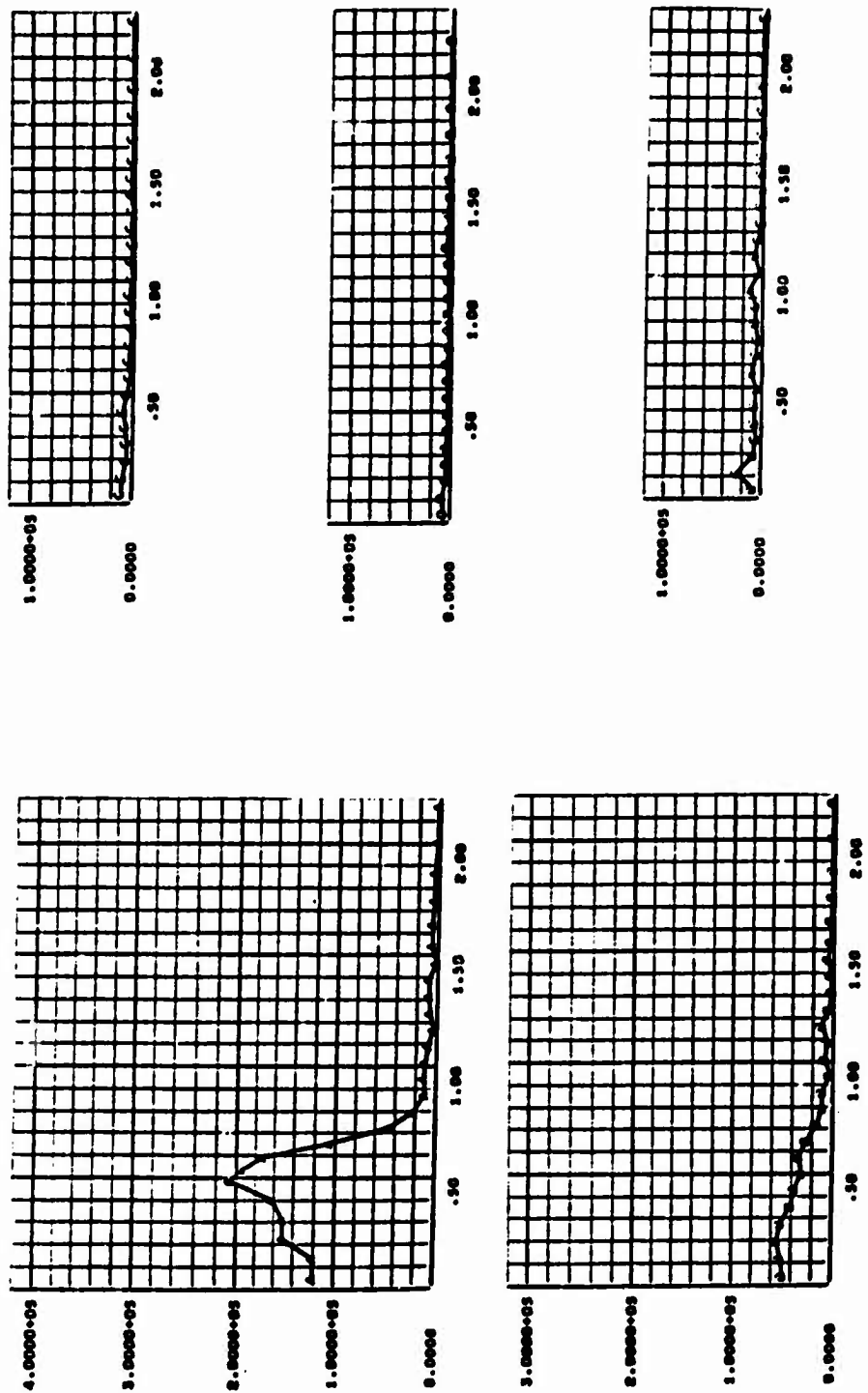
PLASTIC STRAIN RATE (1/SEC) VS X (CM)

TIME=   3.0000-06

Figure 69.

IRON - IRON IMPACT
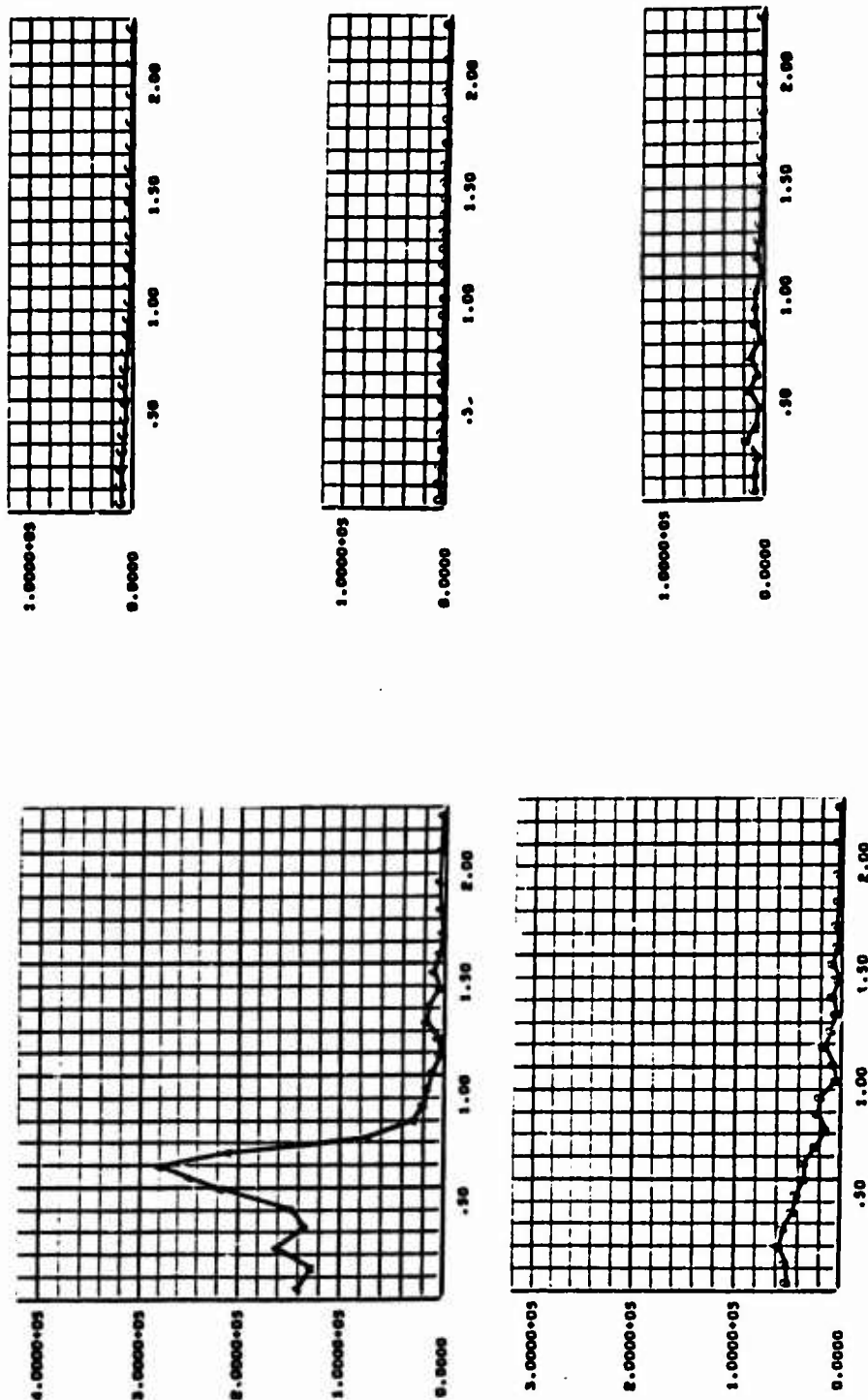
PLASTIC STRAIN RATE (1/SEC) VS X (CM)   TIME=   3.5000-06

Figure 70.

IRON - IRON IMPACT
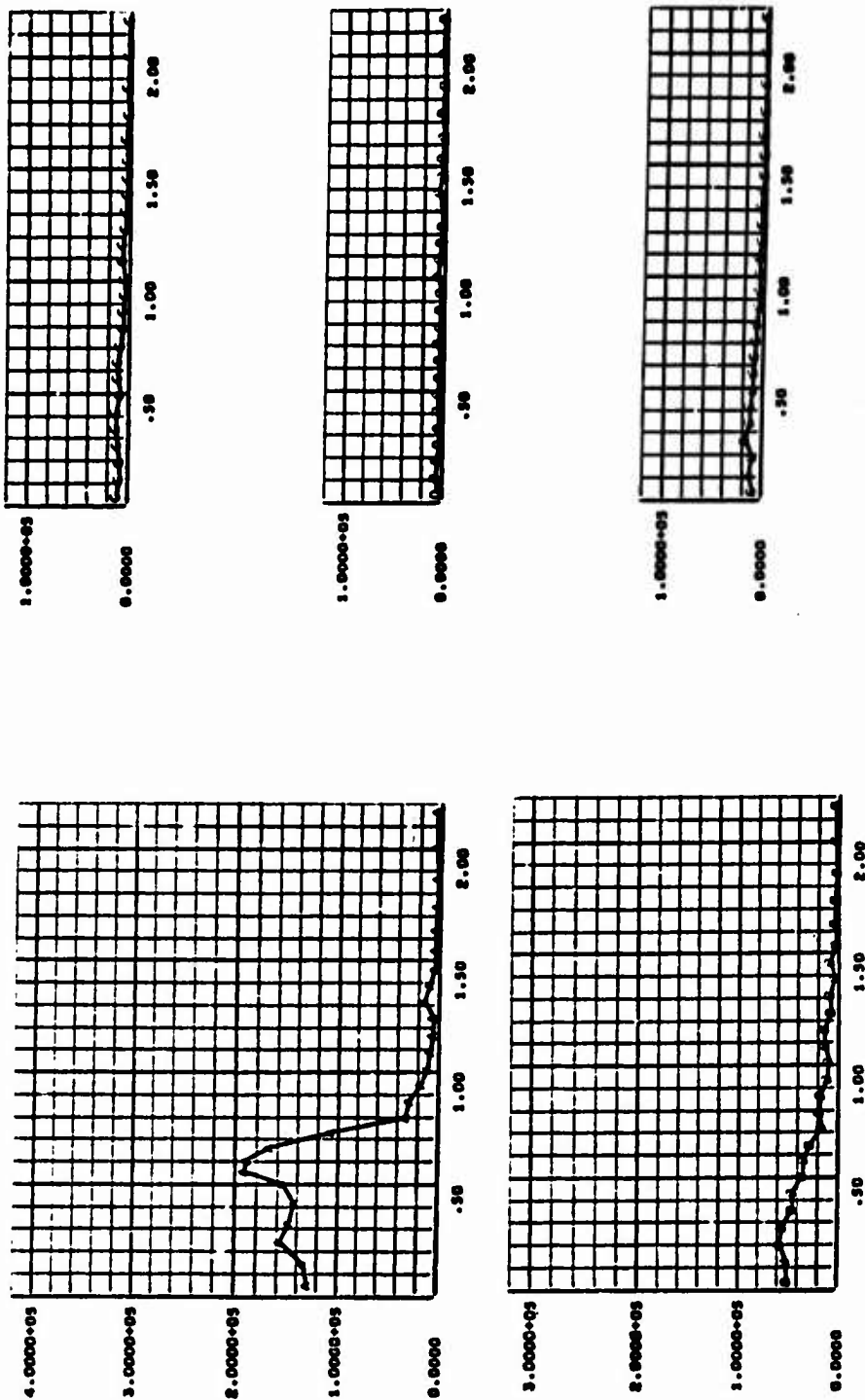
PLASTIC STRAIN RATE (1/SEC) VS X (CM)

TIME=   4.0000-06

Figure 71.

IRON - IRON IMPACT

PLASTIC STRAIN RATE (1/SEC) VS X (CM)

TIME= 4.5000-06

Figure 72.

IRON - IRON IMPACT
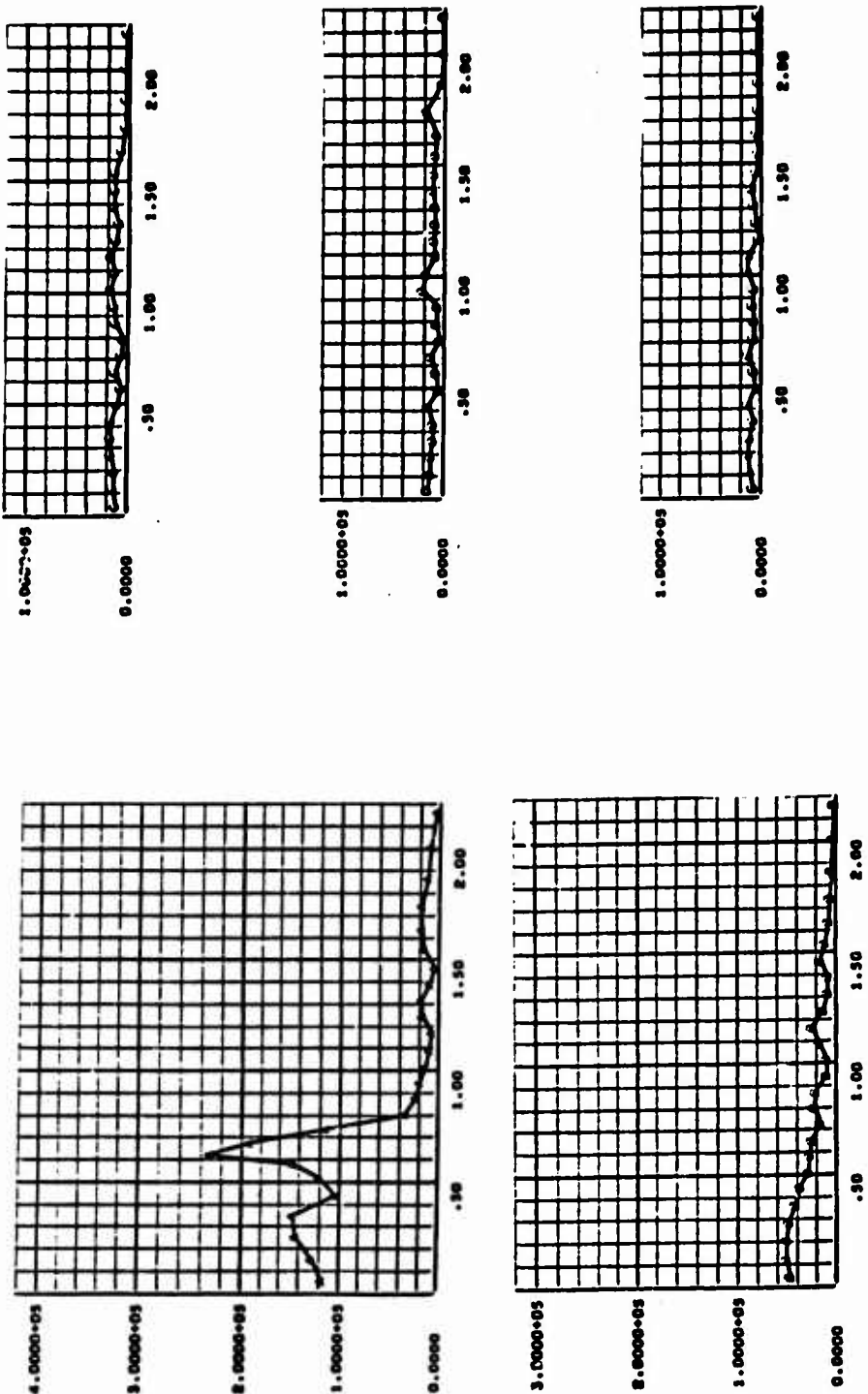
PLASTIC STRAIN RATE (1/SEC) VS X (CM)

TIME= 5.0000-06

Figure 73.

TEST PROBLEM NO. 1

Plastic Work Versus Radial Distance at Five Locations in the Target

For T = 0.0, 0.5, 1.0, 1.5, 2.0, 2.5, 3.0, 3.5, 4.0, 4.5, and 5.0 μsec.

A = Target Front Surface

B = One-Quarter Distance into Target

C = One-Half Distance into Target

D = Three-Quarters Distance into Target

E = Back Surface
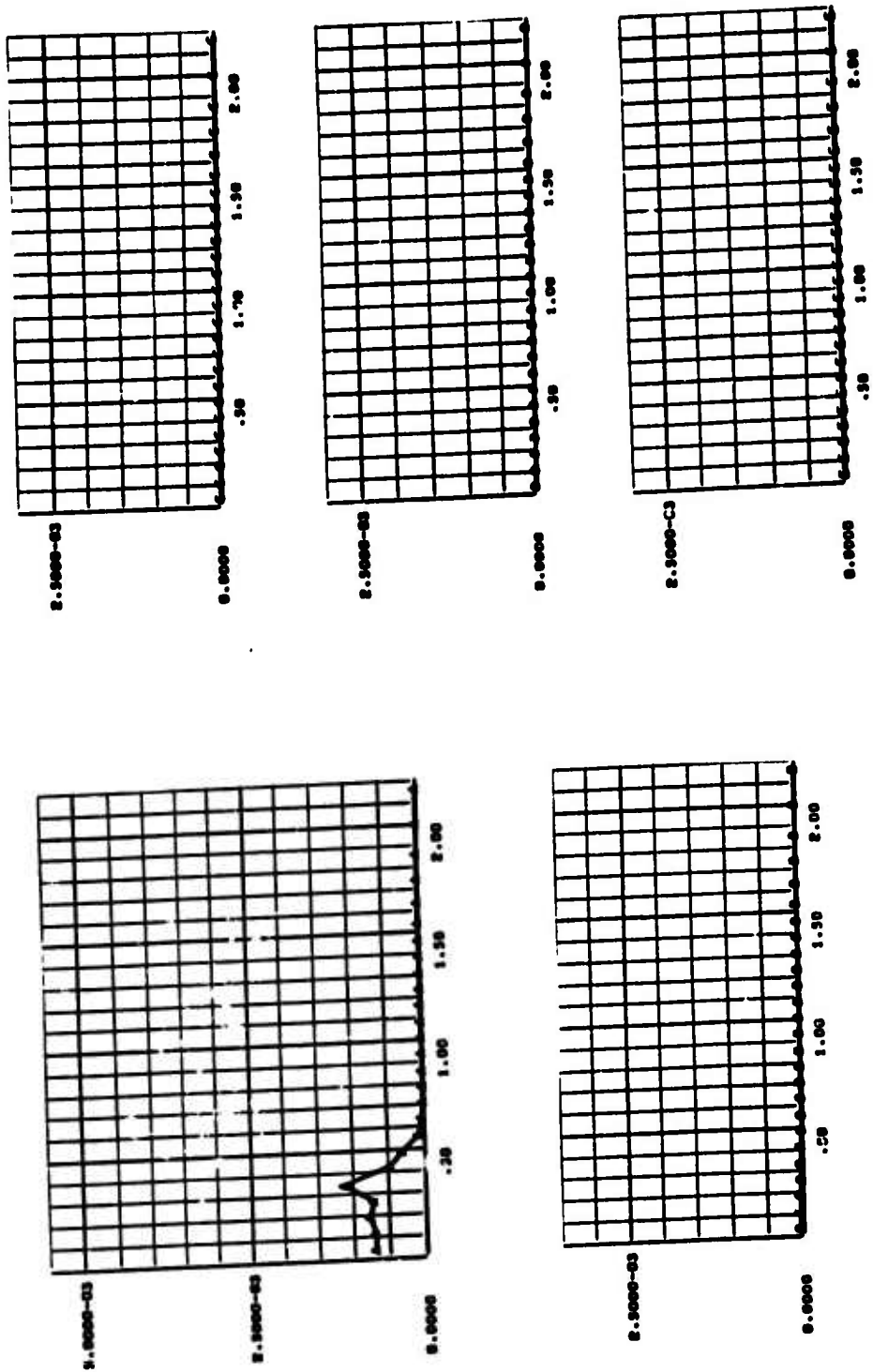
IRON — IRON IMPACT

TIME= 5.0000-07

PLASTIC WORK (MB)   VS   X (CM)

Figure 74.

IRON — IRON IMPACT
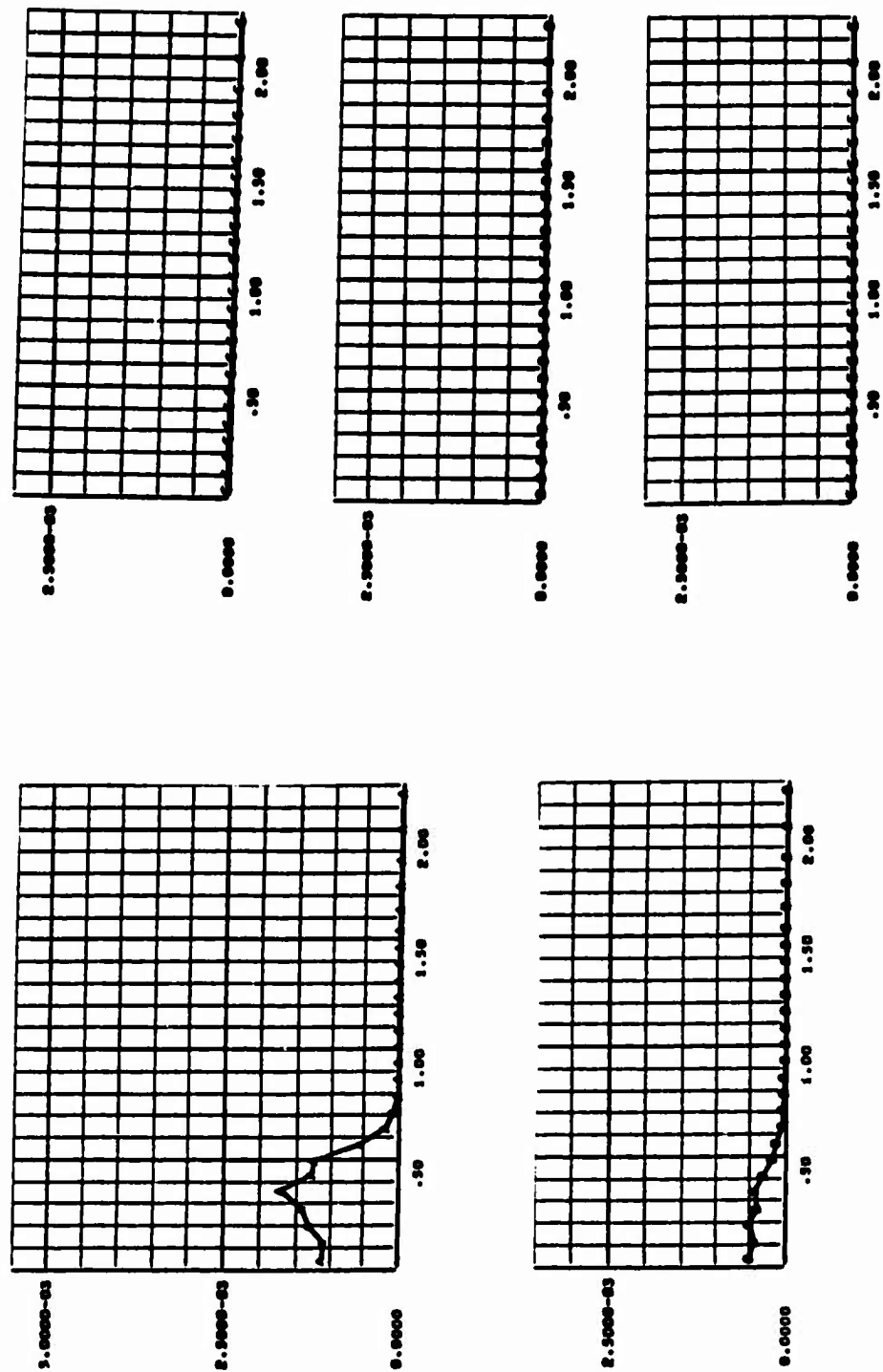
PLASTIC WORK (M3) VS X (CM)   TIME= 1.0000-06

Figure 75.

IRON - IRON IMPACT
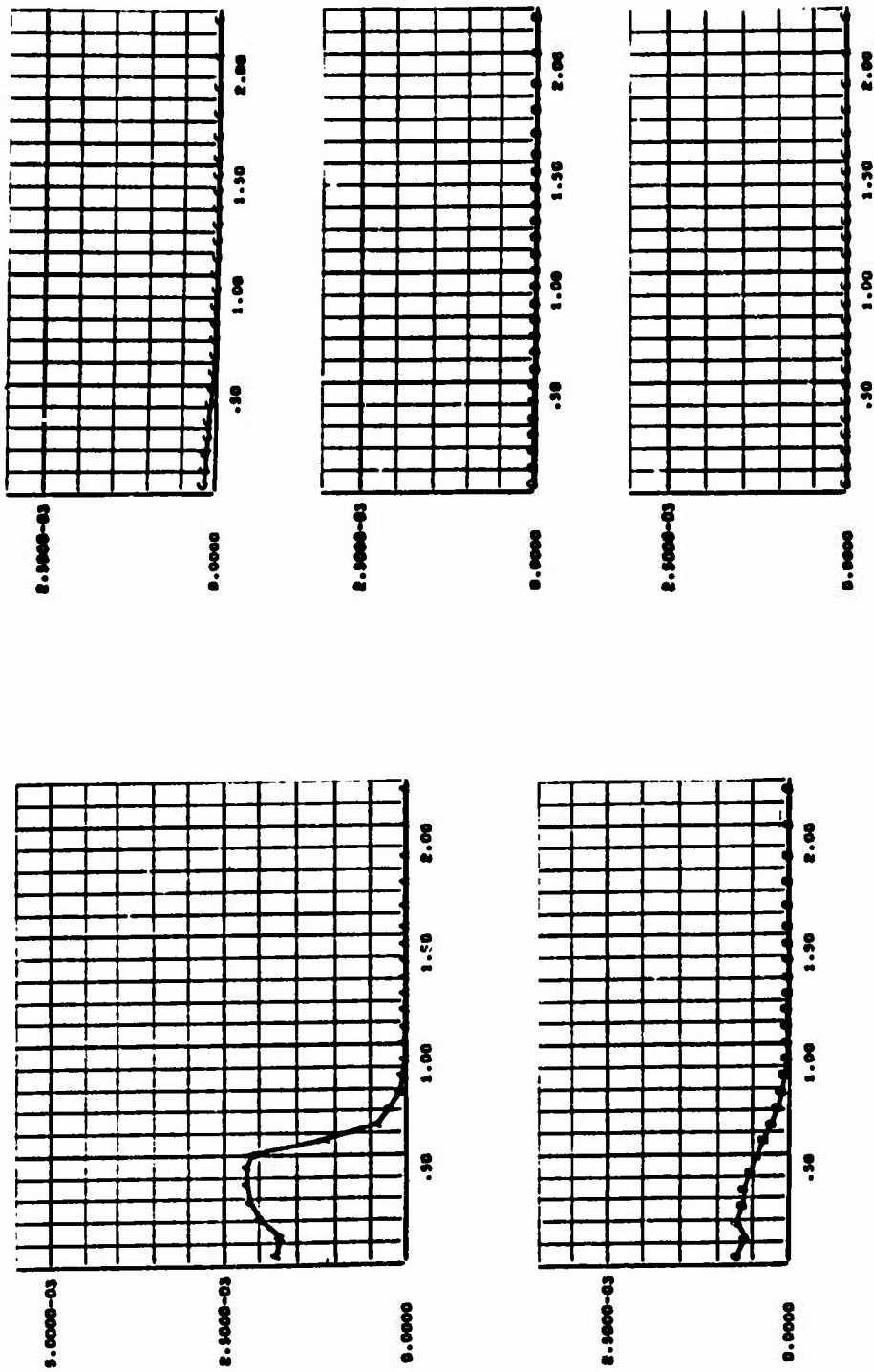
PLASTIC WORK (MB) VS X (CM)

TIME= 1.5000-06

Figure 76.

IRON - IRON IMPACT
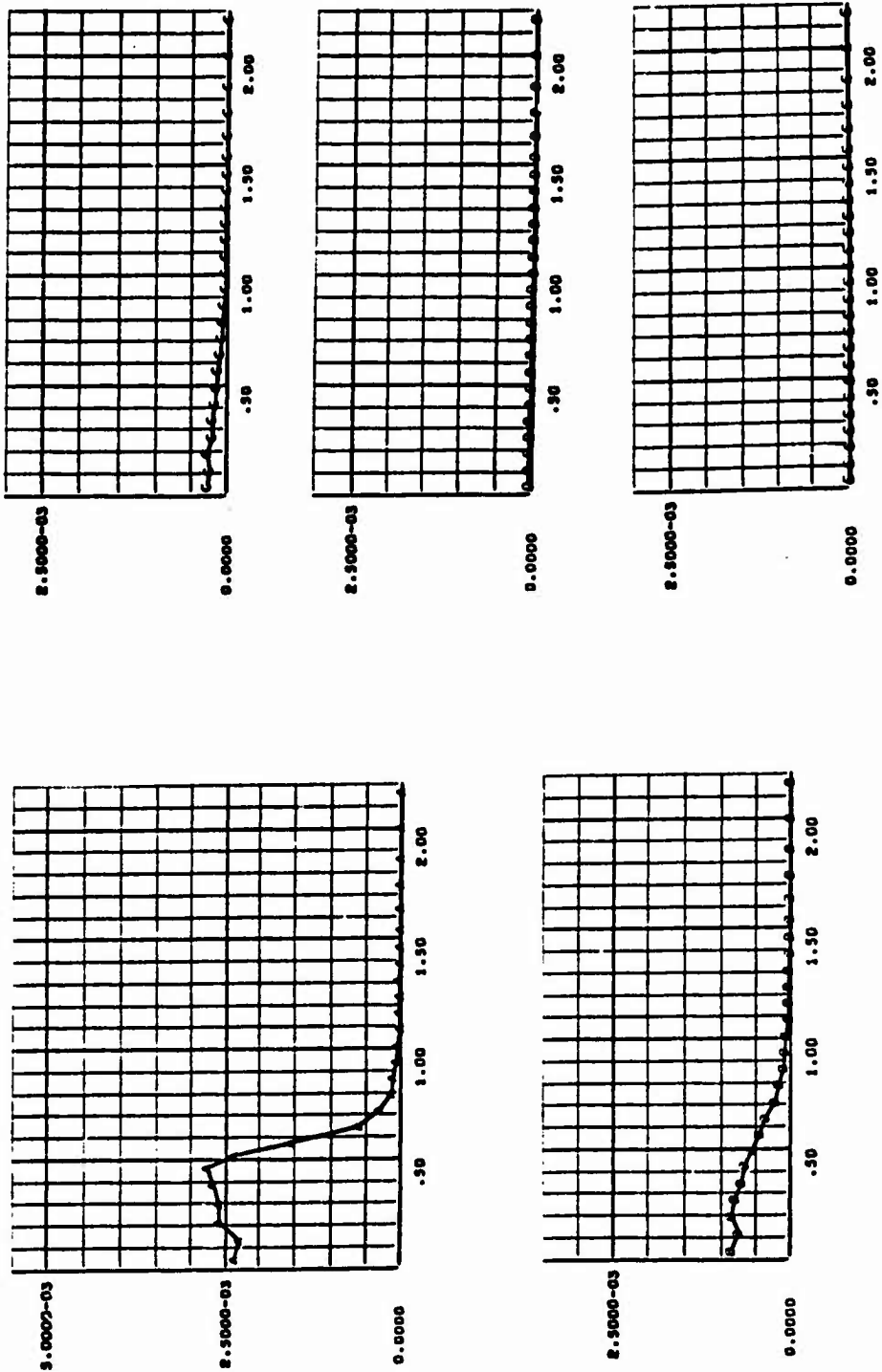
PLASTIC WORK (MB) VS x (CM)   TIME= 2.0000-06

Figure 77.

109
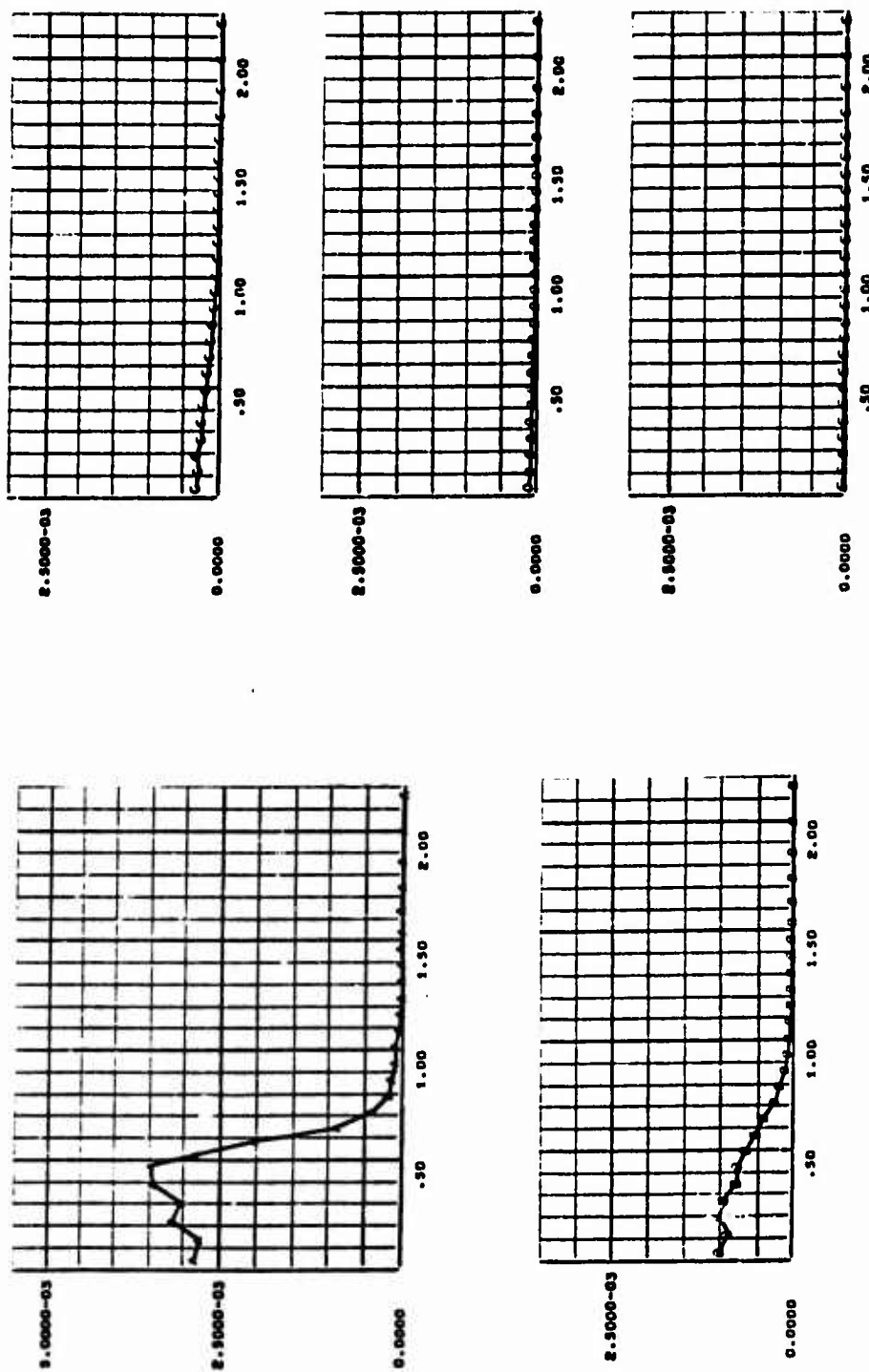
IRON - IRON IMPACT

PLASTIC WORK (MB) VS X (CM)

TIME= 2.5000-06

Figure 78.

IRON - IRON IMPACT
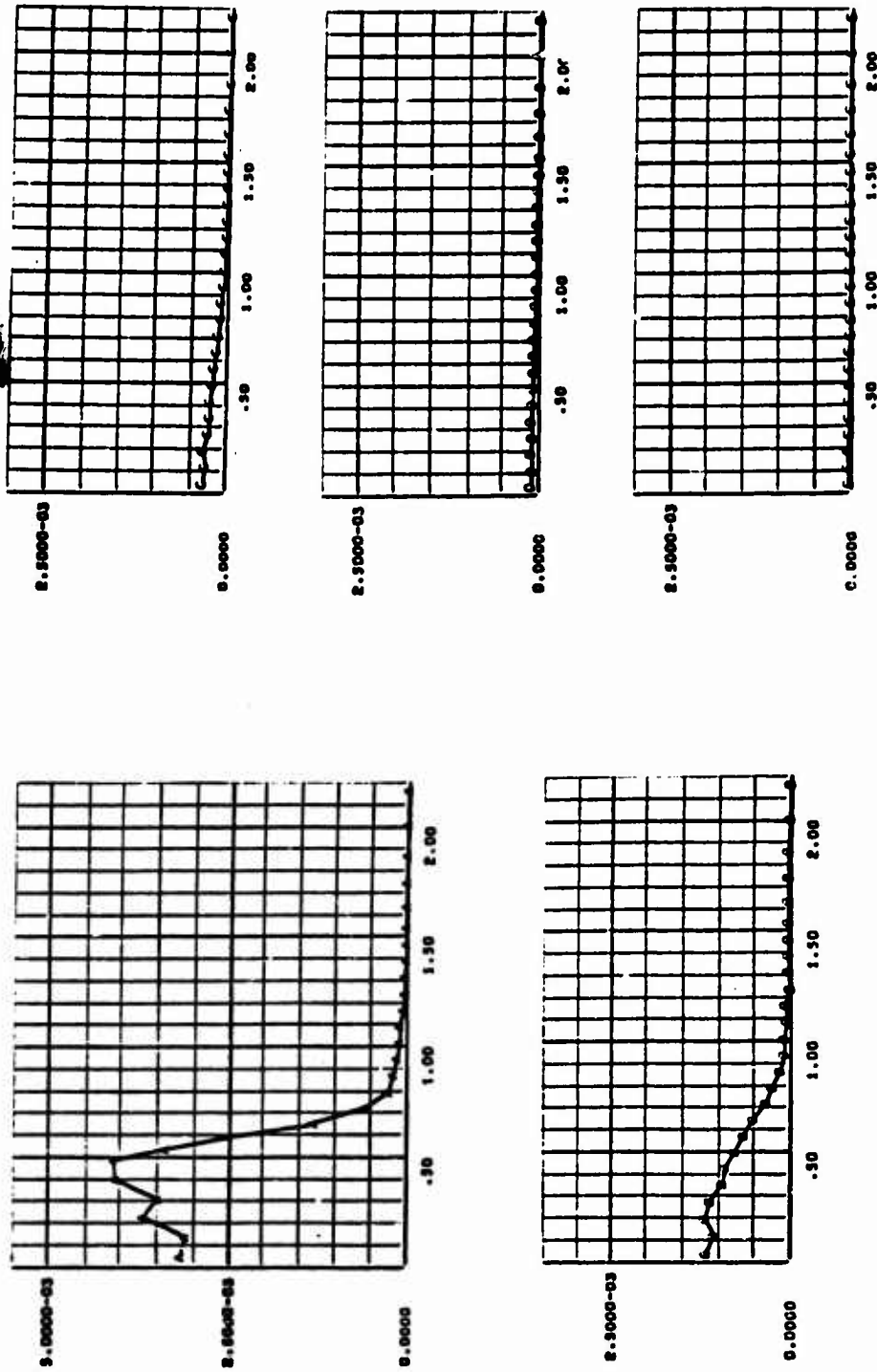
PLASTIC WORK (MB)   VS   X (CM)   TIME=   3.0000-06

Figure 79.

IRON - IRON IMPACT
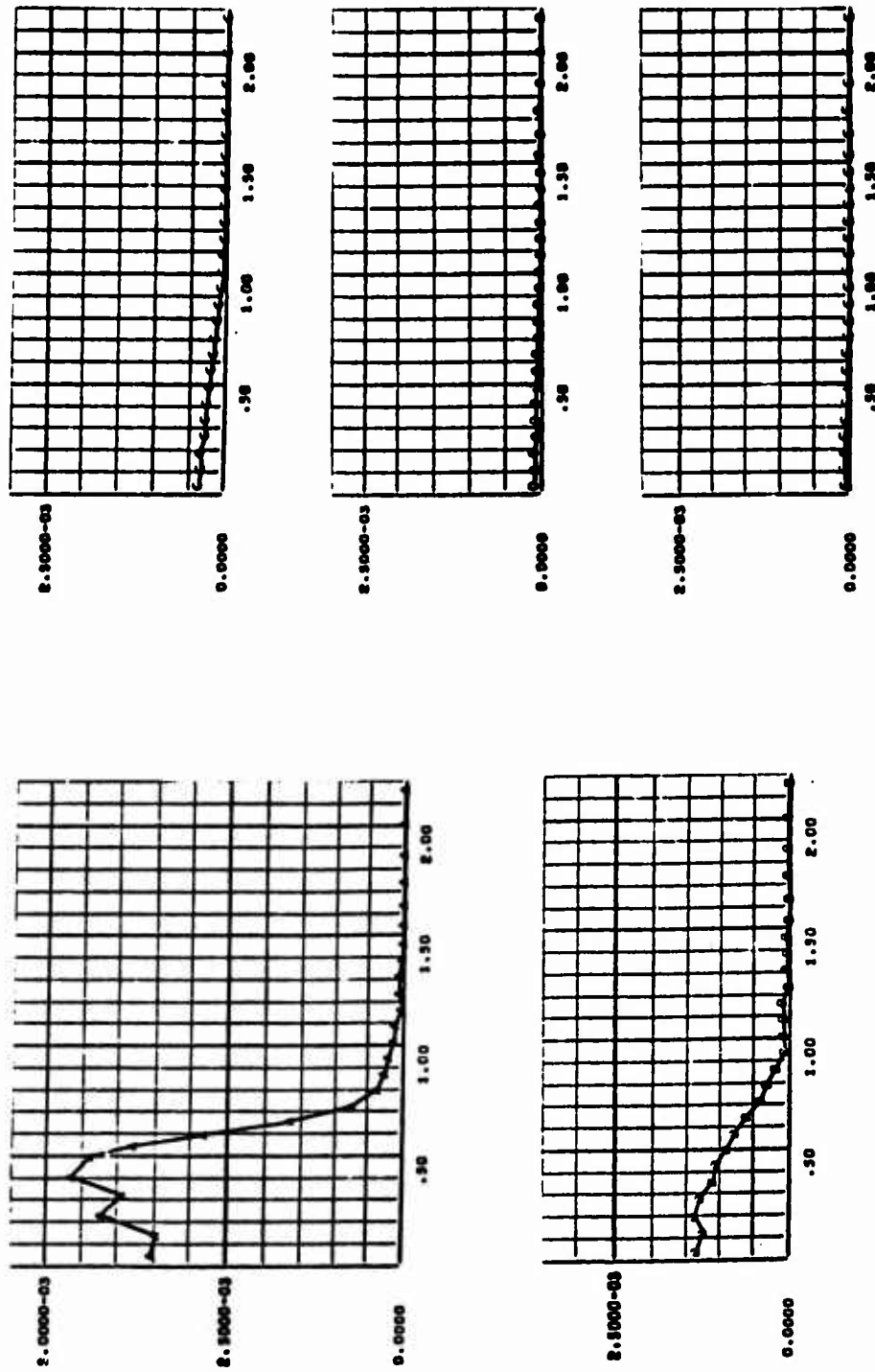
PLASTIC WORK (MB) VS X (CM)   TIME= 3.5000-06

Figure 80.

IRON - IRON IMPACT
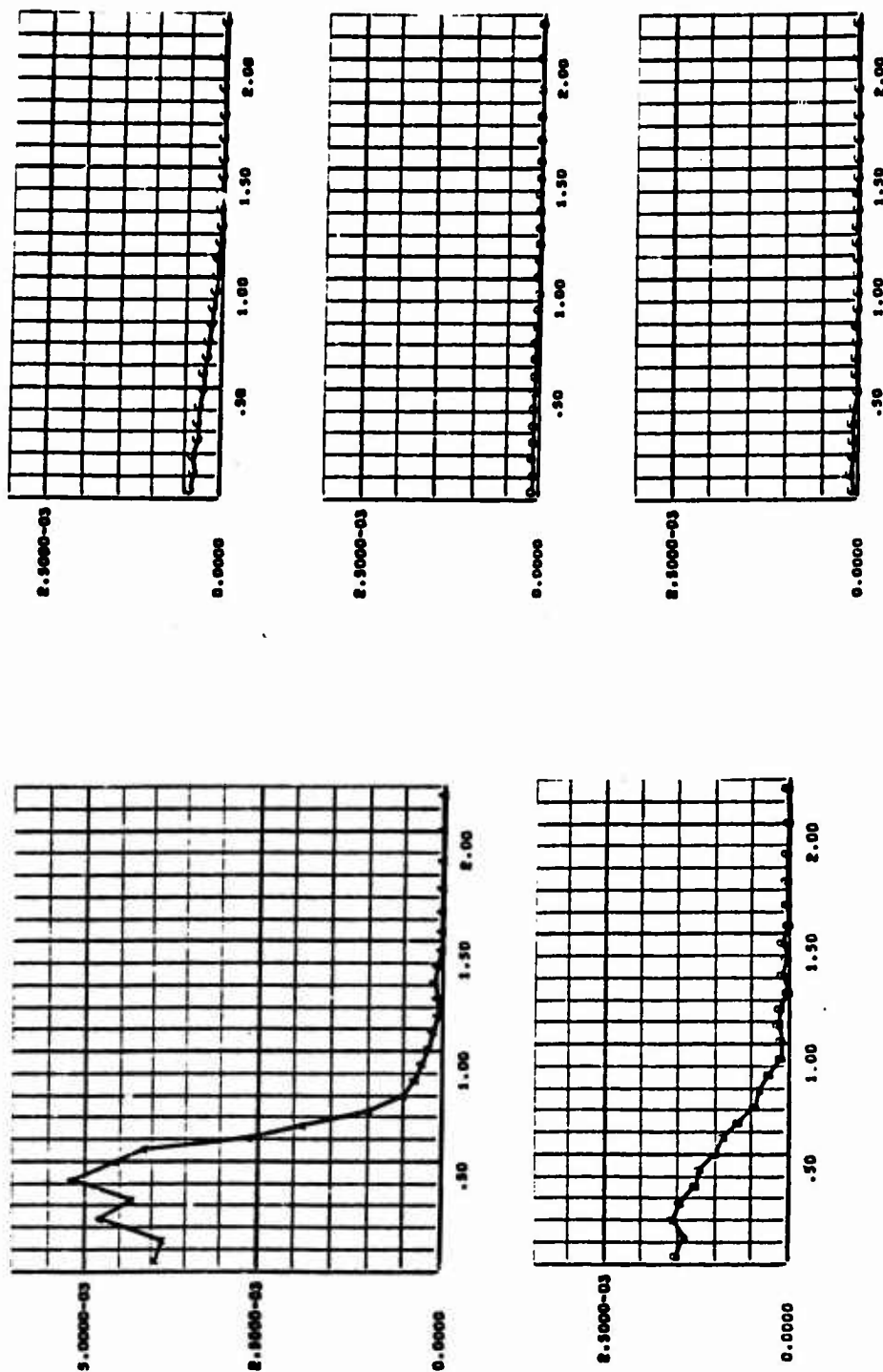
PLASTIC WORK (MB) VS X (CM)

TIME= 4.0000-06

Figure 81.

IRON – IRON IMPACT
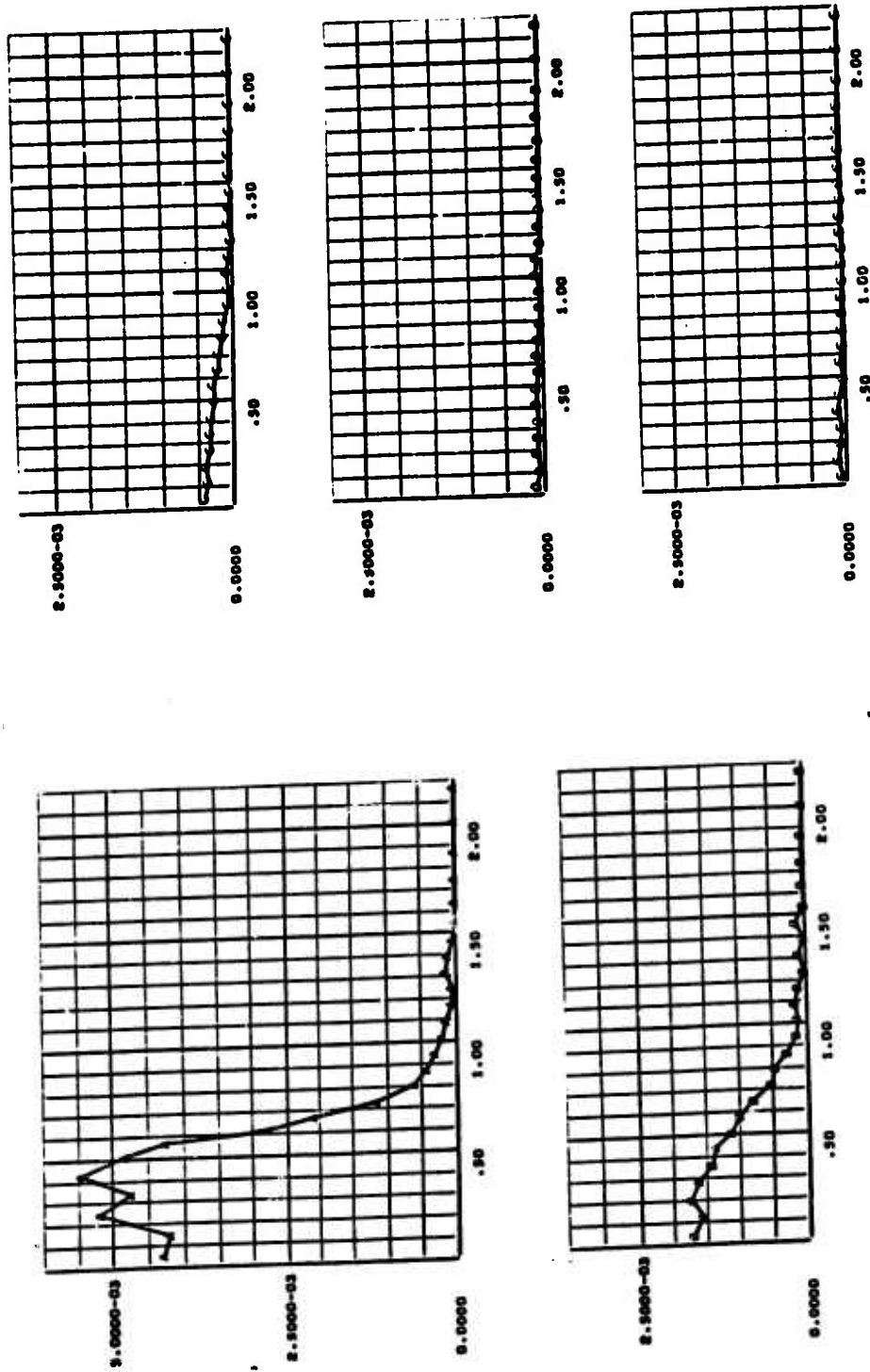
TIME= 4.5000-06

PLASTIC WORK (MB)   VS   X (CM)

Figure 82.

114

IRON - IRON IMPACT
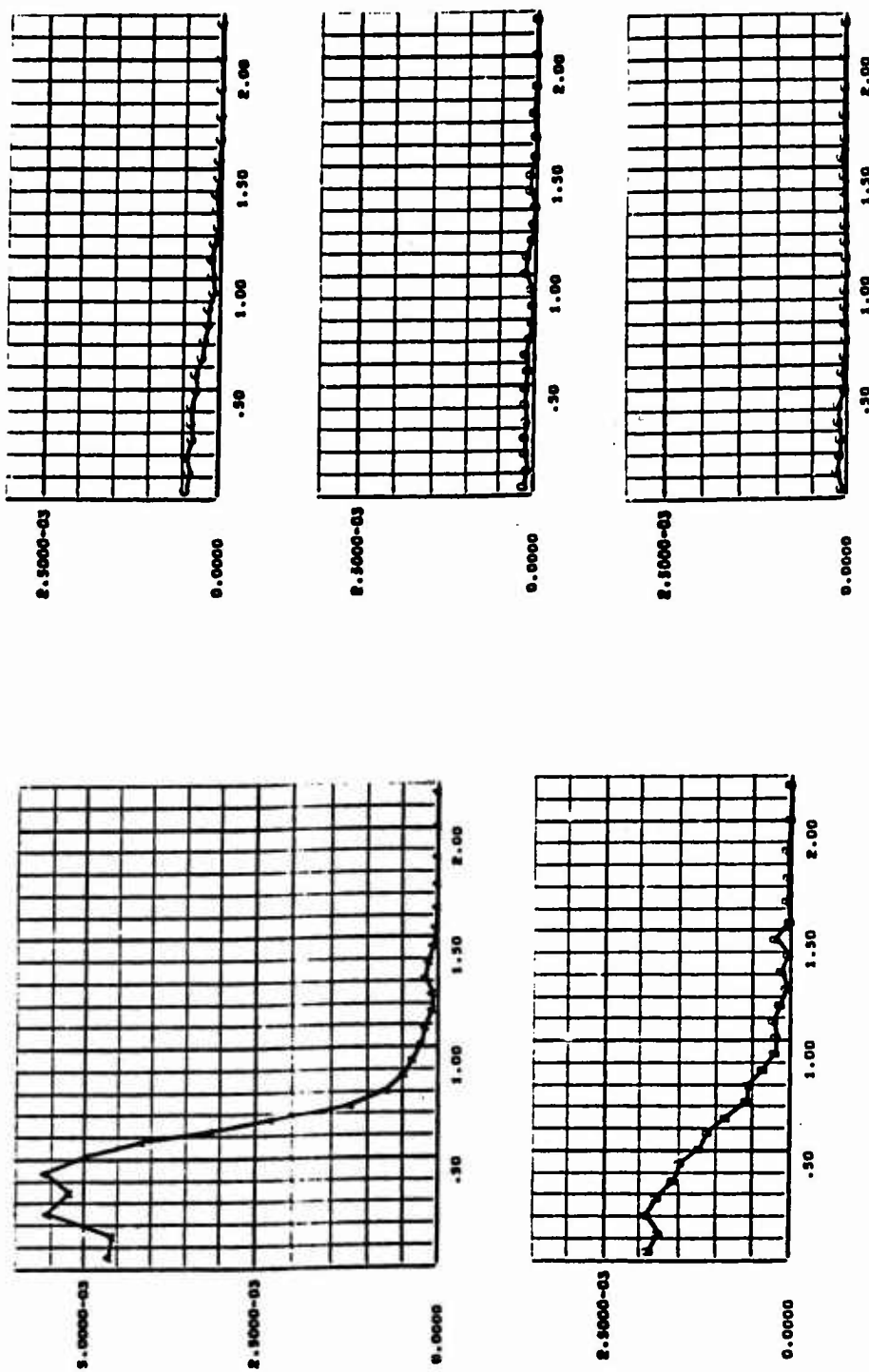
TIME= 5.0000-06

PLASTIC WORK (MB) VS X (CM)

Figure 83.

115

TEST PROBLEM NO. 2

Total Stress (Axial Direction) Versus Y
Along Axis of Symmetry

For T = 0.0, 0.5, 1.0, 1.5, 2.0, 2.5, and 3.0 μsec.

 PB = Projectile Back

PTI = Projectile Target Interface

 TB = Target Back

116

Figure 84.

IRON - ALUMINUM IMPACT   HELP-5

TIME= 5.0000-07 PROB= 2.65000+01 CYCLE NO 24

AXIAL VELOCITY (CM/MICROSEC) VS Y (CM) AT AXIS
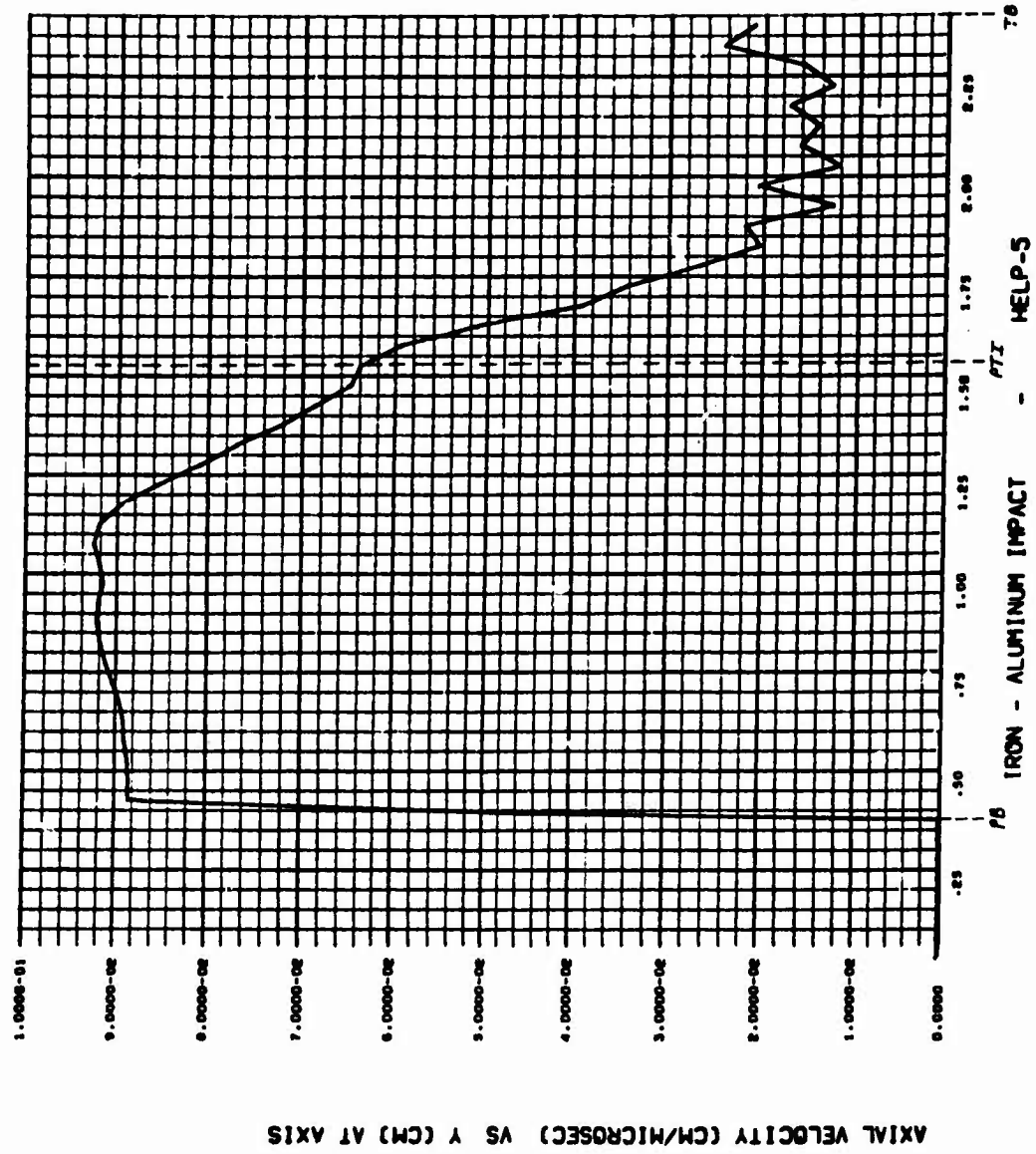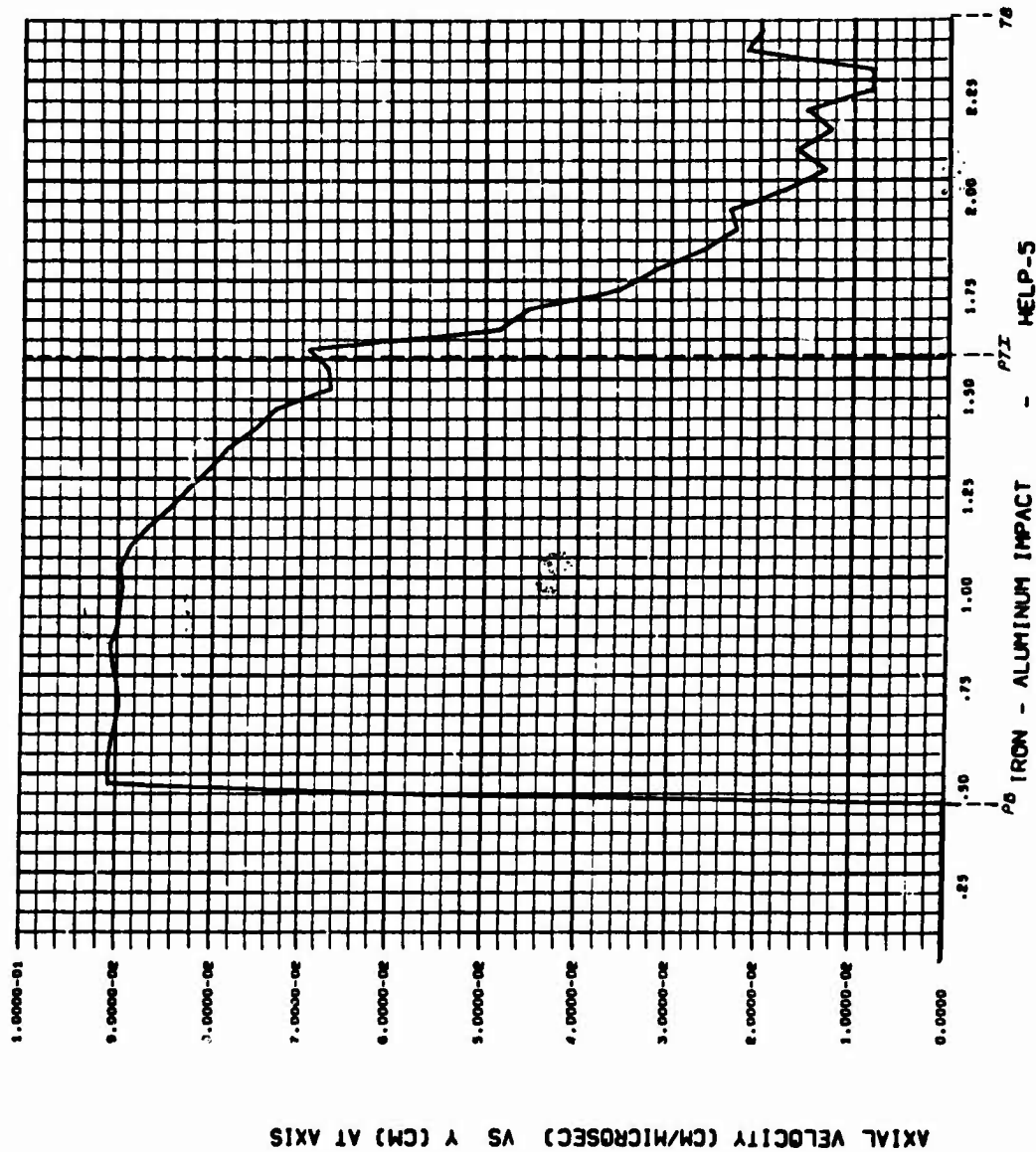
Figure 85.

Figure 86.
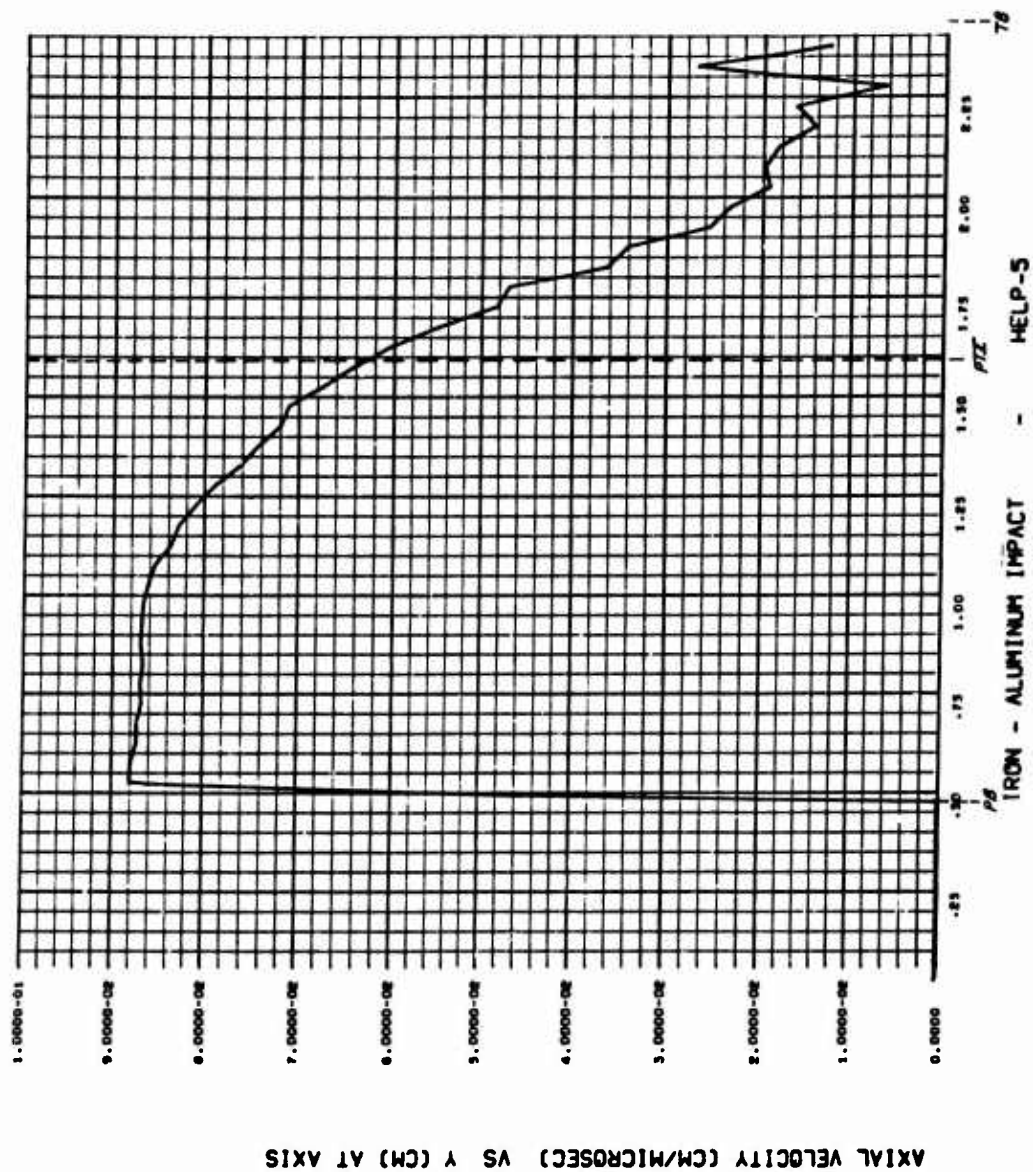
Figure 87.

Figure 88.

Figure 89.

TEST PROBLEM NO. 2

Axial Velocity Versus Y Along Axis of Symmetry

For T = 0.0, 0.5, 1.0, 1.5, 2.0, 2.5, and 3.0 μsec.

 PB = Projectile Back

PTI = Projectile Target Interface

 TB = Target Back

Figure 90.

Figure 91.

125

Figure 92.

Figure 93.

Figure 94.

128
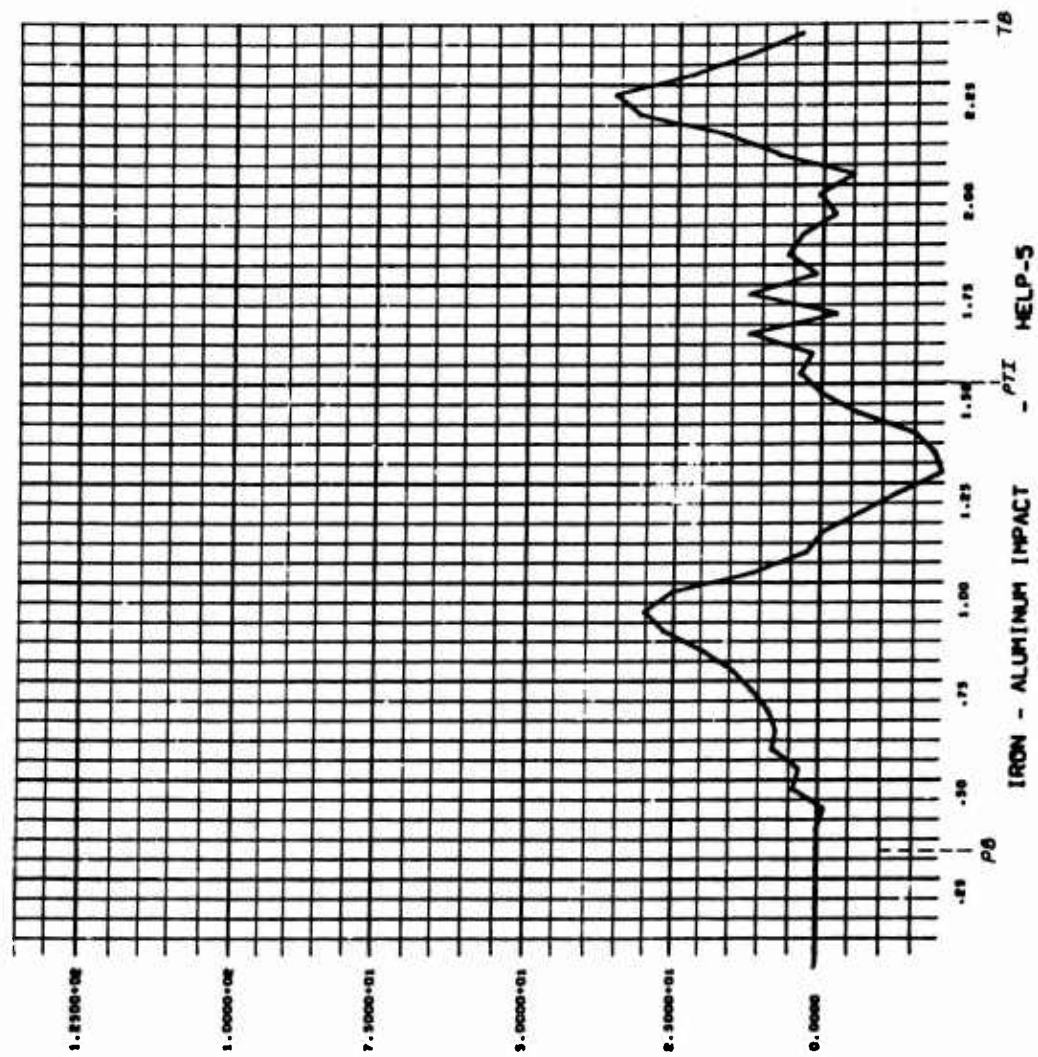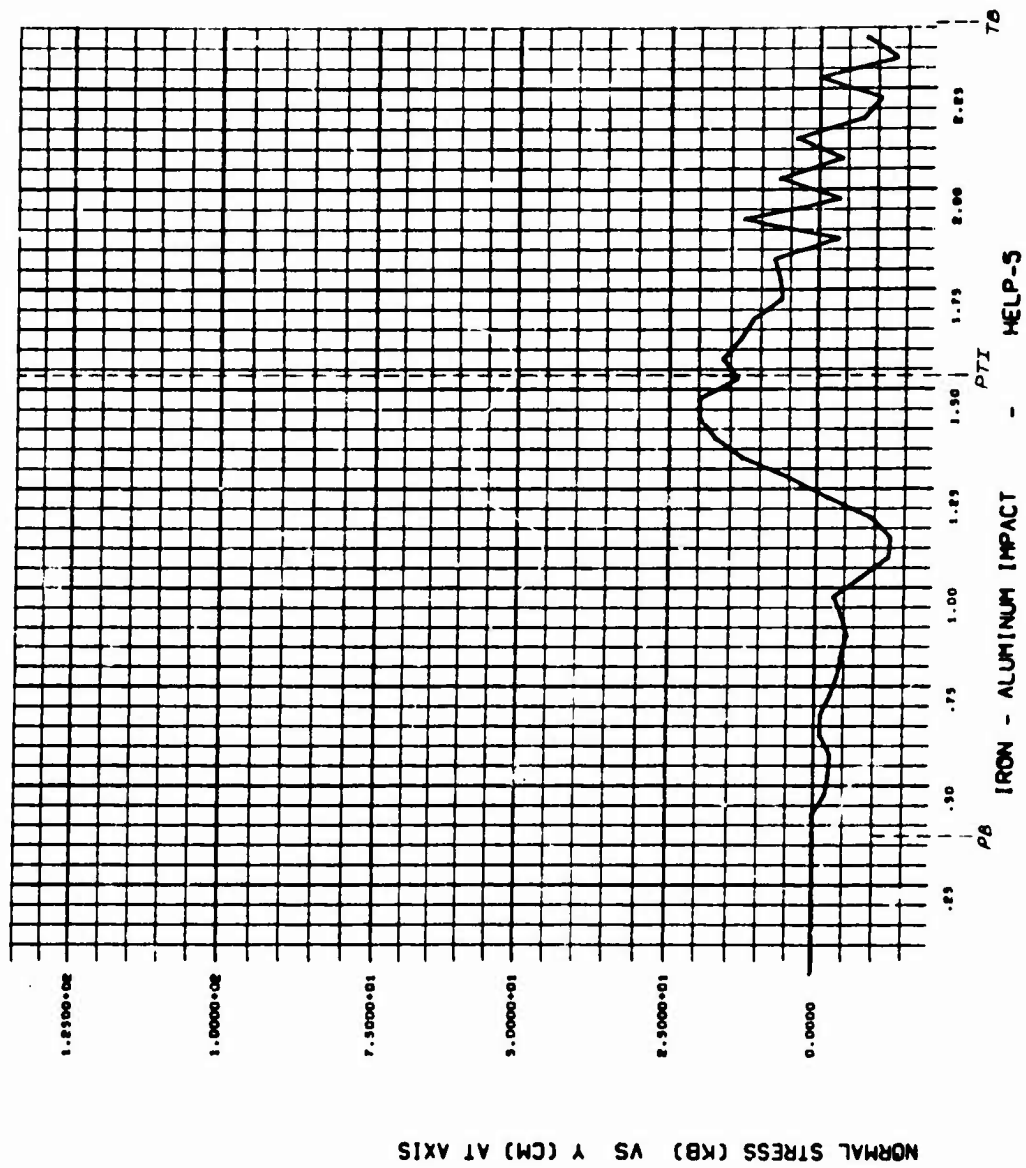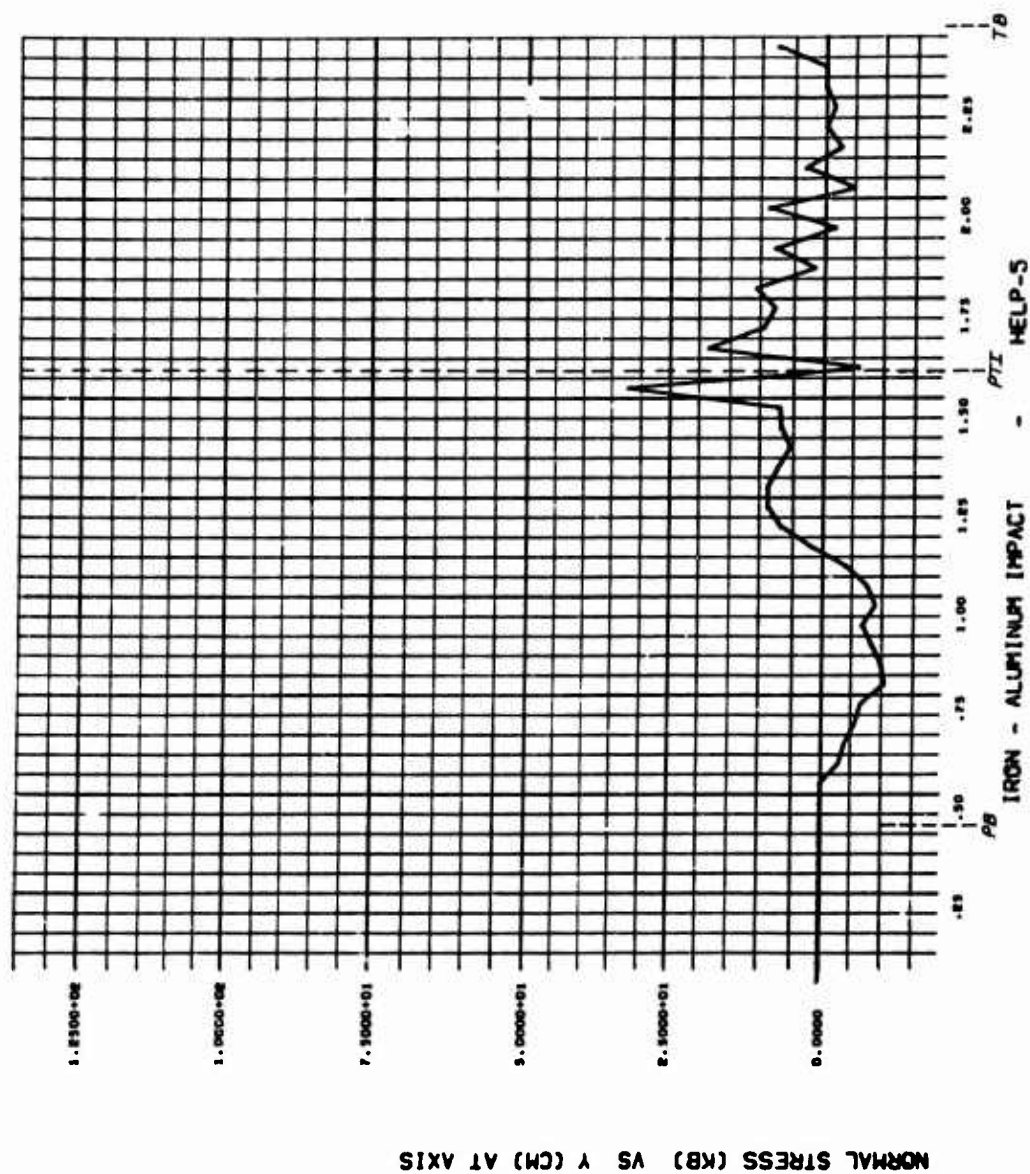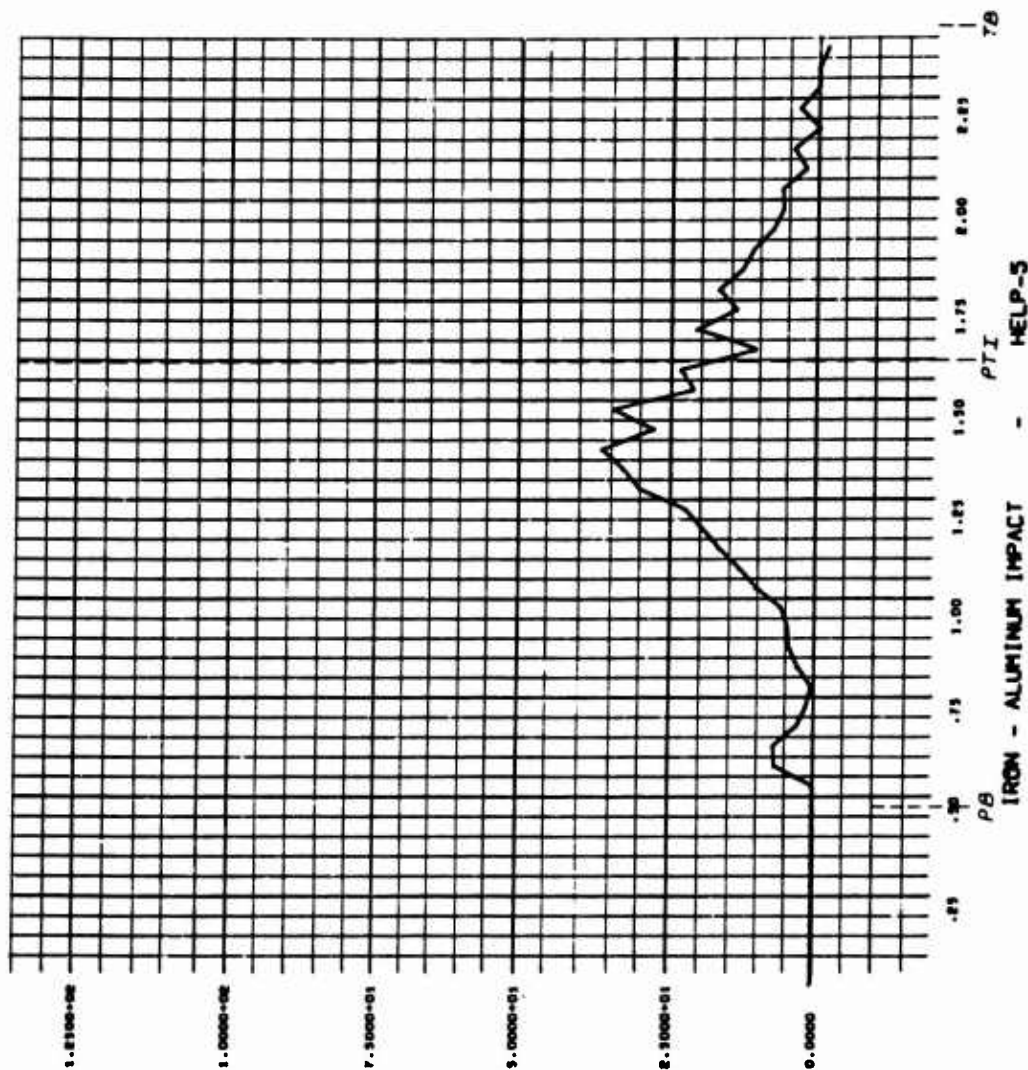
Figure 95.

TEST PROBLEM NO. 2

Relative Volume Versus Radial Distance at
Five Locations in the Target

For T = 0.0, 0.5, 1.0, 1.5, 2.0, 2.5, and 3.0 µsec.

A = Target Front Surface

B = One-Quarter Distance into Target

C = One-Half Distance into Target

D = Three-Quarters Distance into Target

E = Back Surface

IRØN - ALUMINUM IMPACT
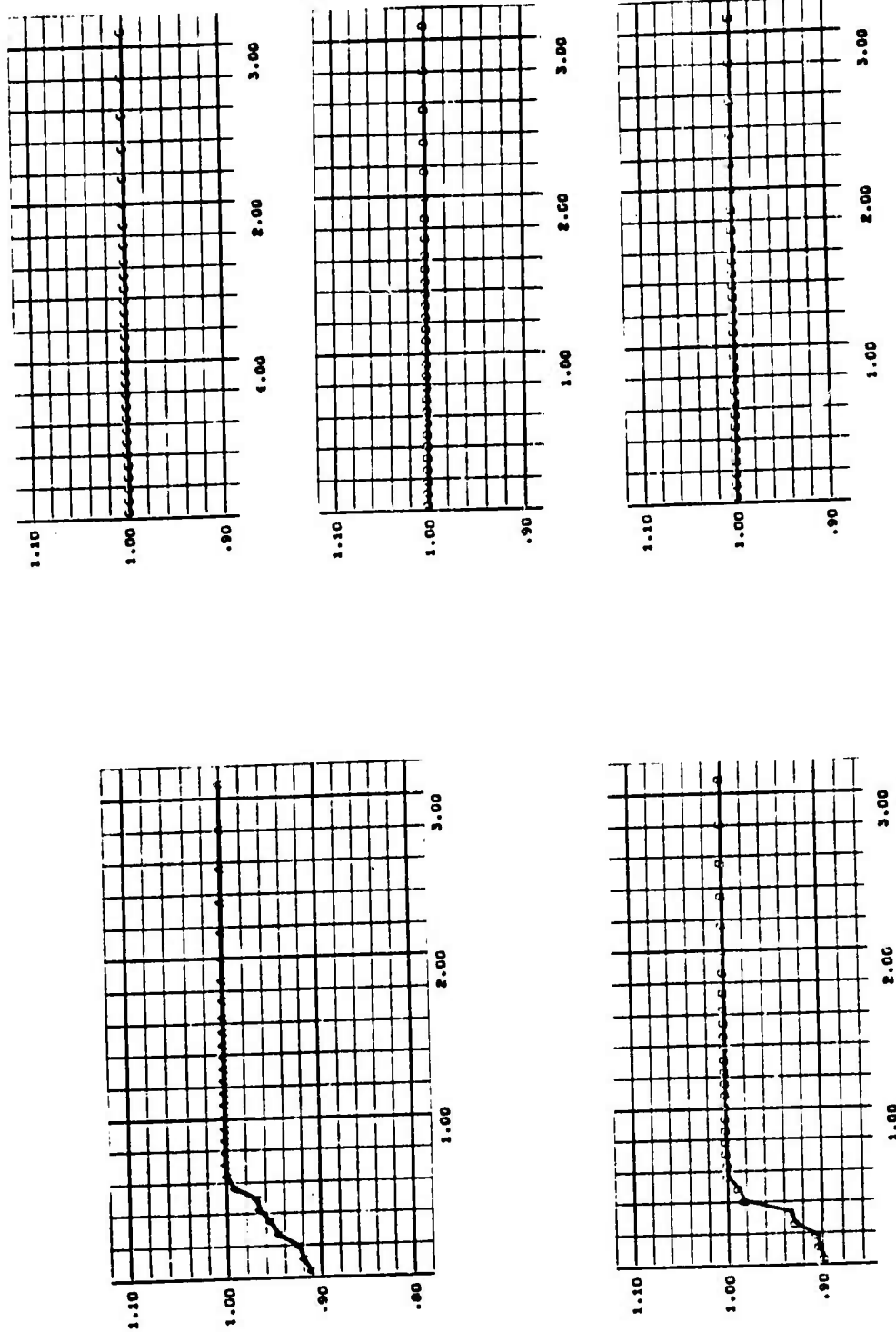
RHØZ/RHØ VS X (CM)   TIME= 5.0000-07

Figure 96.

131

IRON - ALUMINUM IMPACT
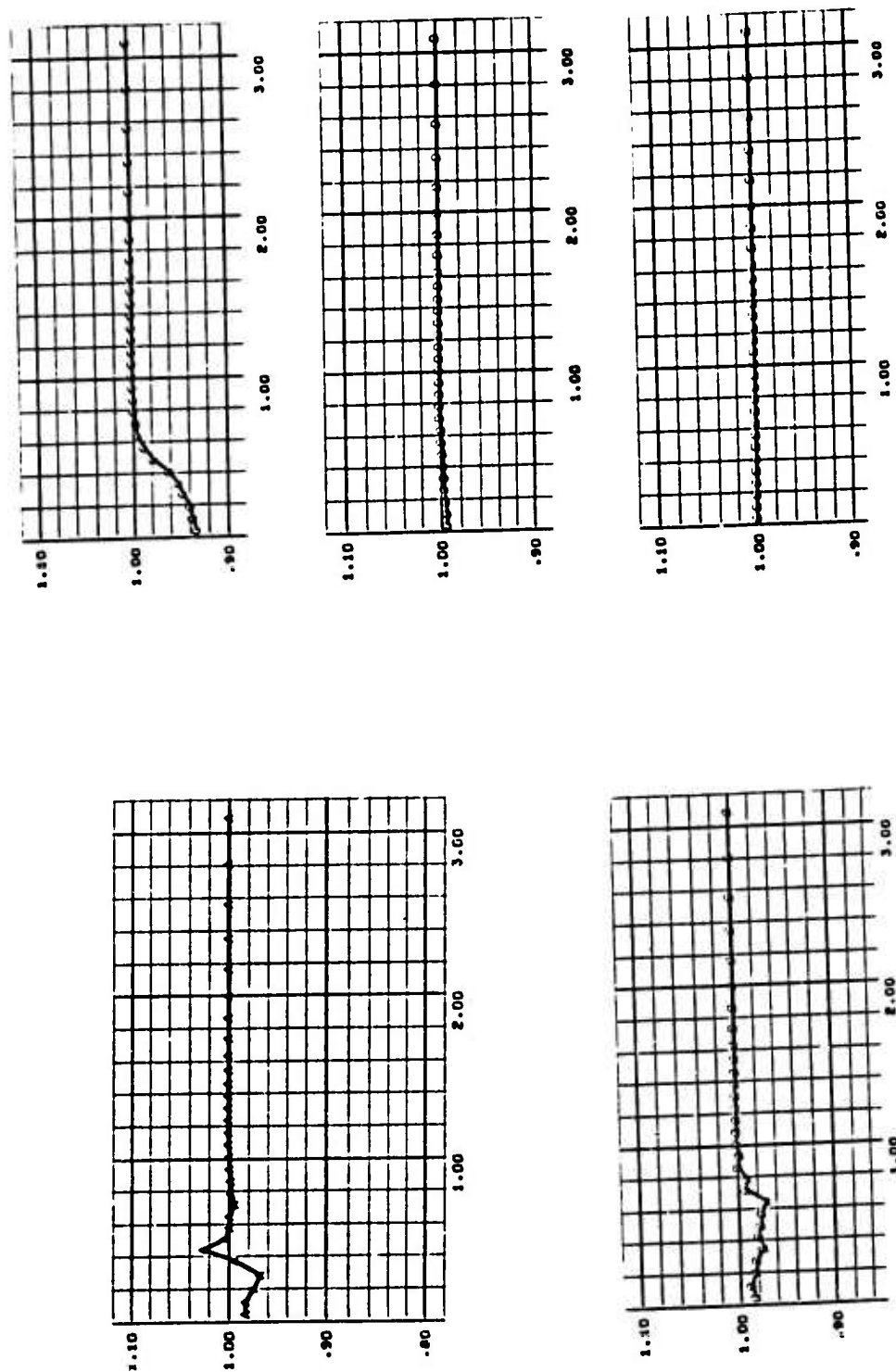
RHOZ/RHO   VS   X (CM)   TIME= 1.0000-06

Figure 97.

132

IRON - ALUMINUM IMPACT
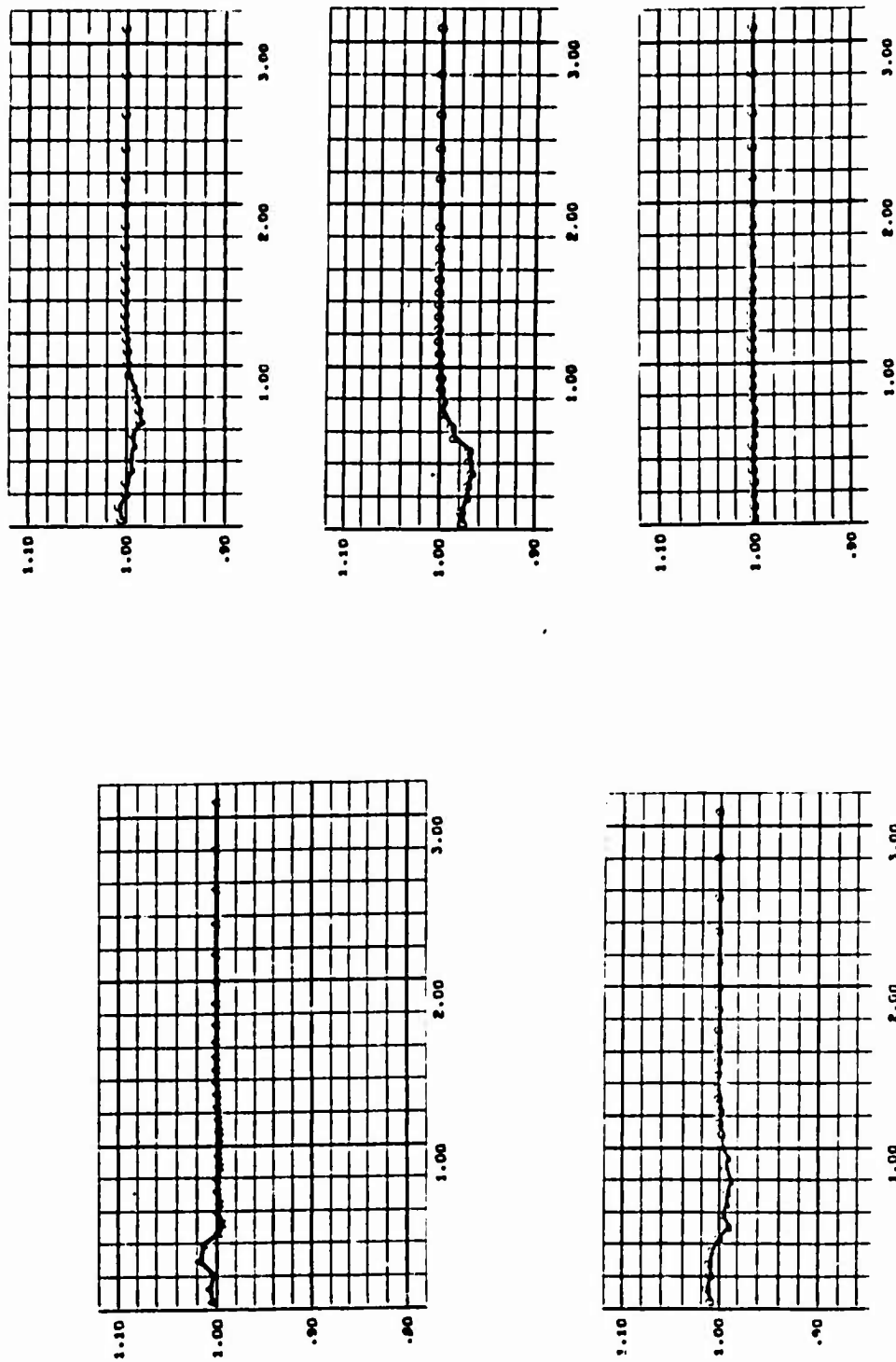
RHOZ/RHO   VS   X (CM)   TIME= 1.5000-06

Figure 98.

133

IRON - ALUMINUM IMPACT
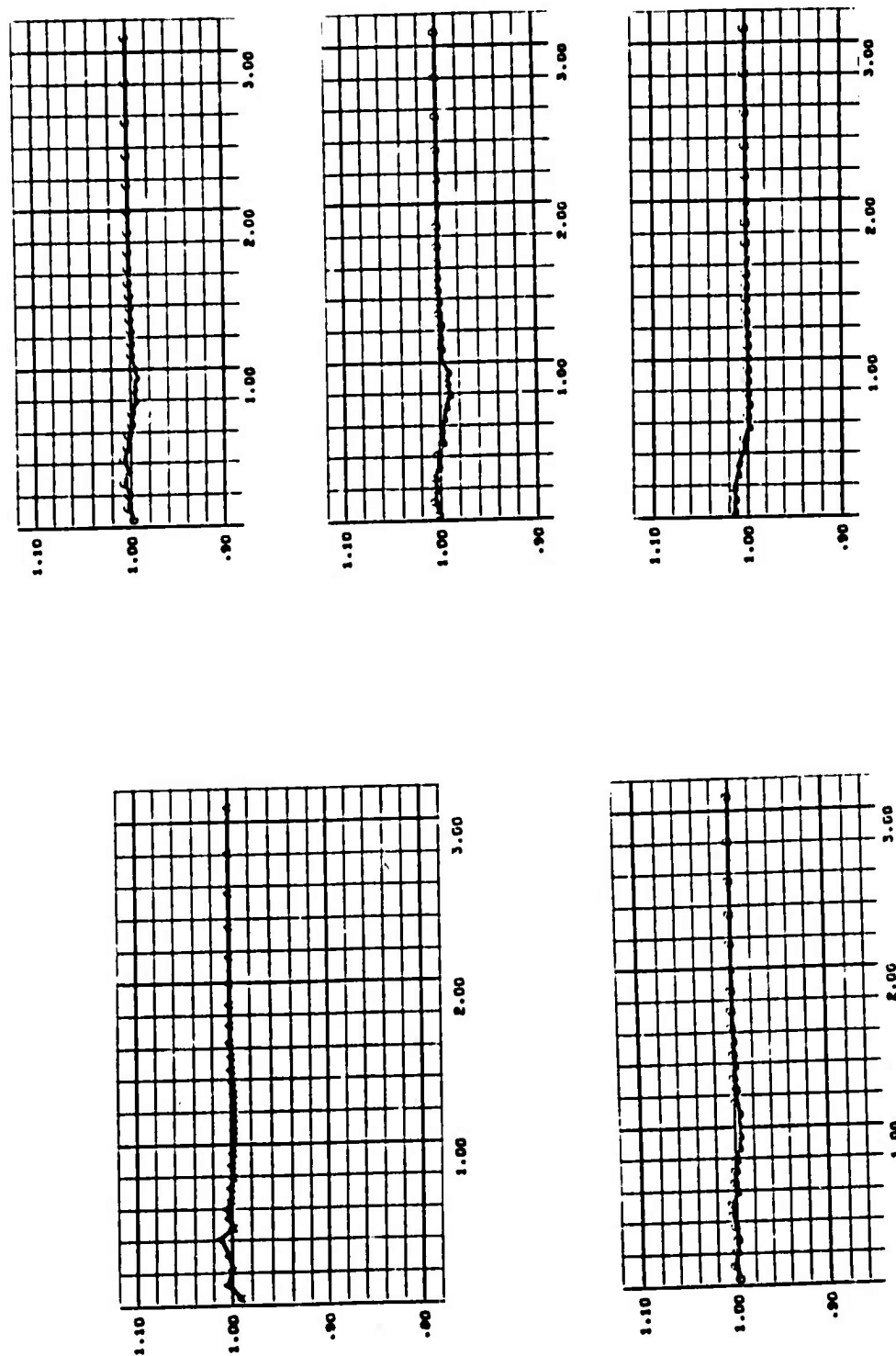
RHOZ/RHO   VS   X (CM)   TIME= 2.0000-06

Figure 99.

134

IRON - ALUMINUM IMPACT
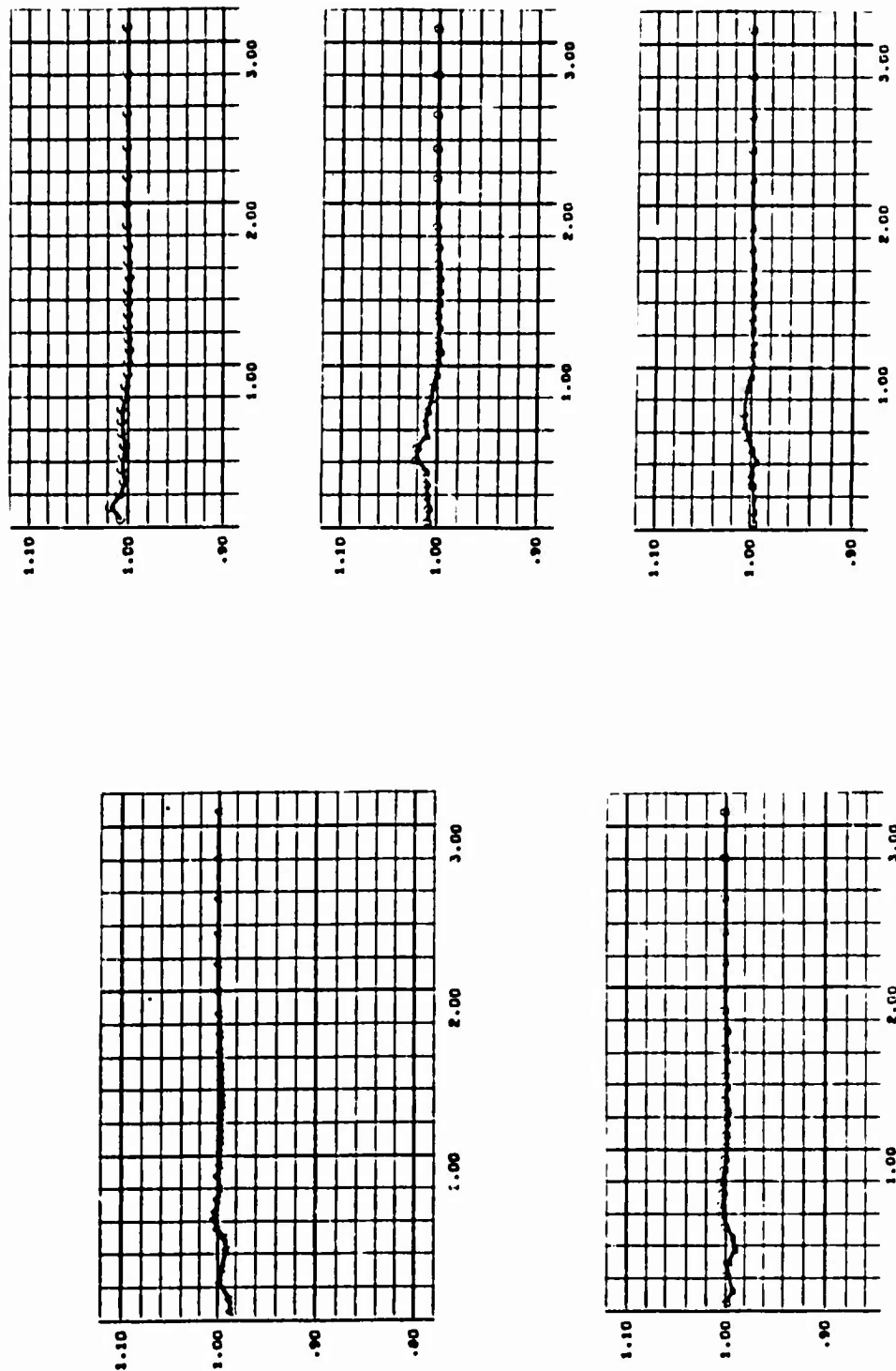
RHOZ/RHO VS X (CM) TIME= 2.5000-06

Figure 100.

135

IRON – ALUMINUM IMPACT
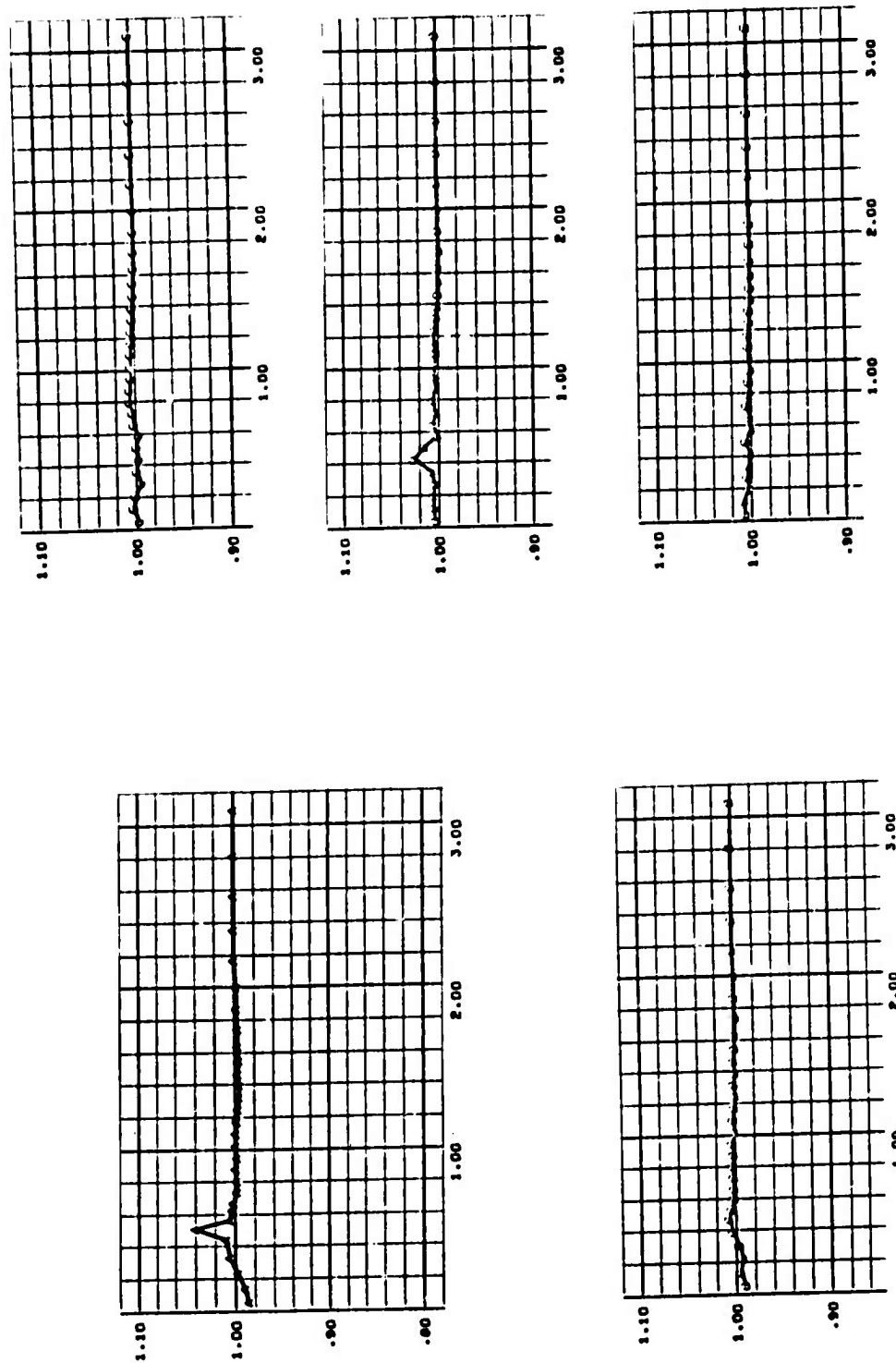
RHOZ/RHO   VS   X (CM)   TIME= 3.0000-06

Figure 101.

TEST PROBLEM NO. 2

Specific Internal Energy Versus Radial Distance
at Five Locations in the Target

For T = 0.0, 0.5, 1.0, 1.5, 2.0, 2.5, and 3.0 μsec.

A = Target Front Surface

B = One-Quarter Distance into Target

C = One-Half Distance into Target

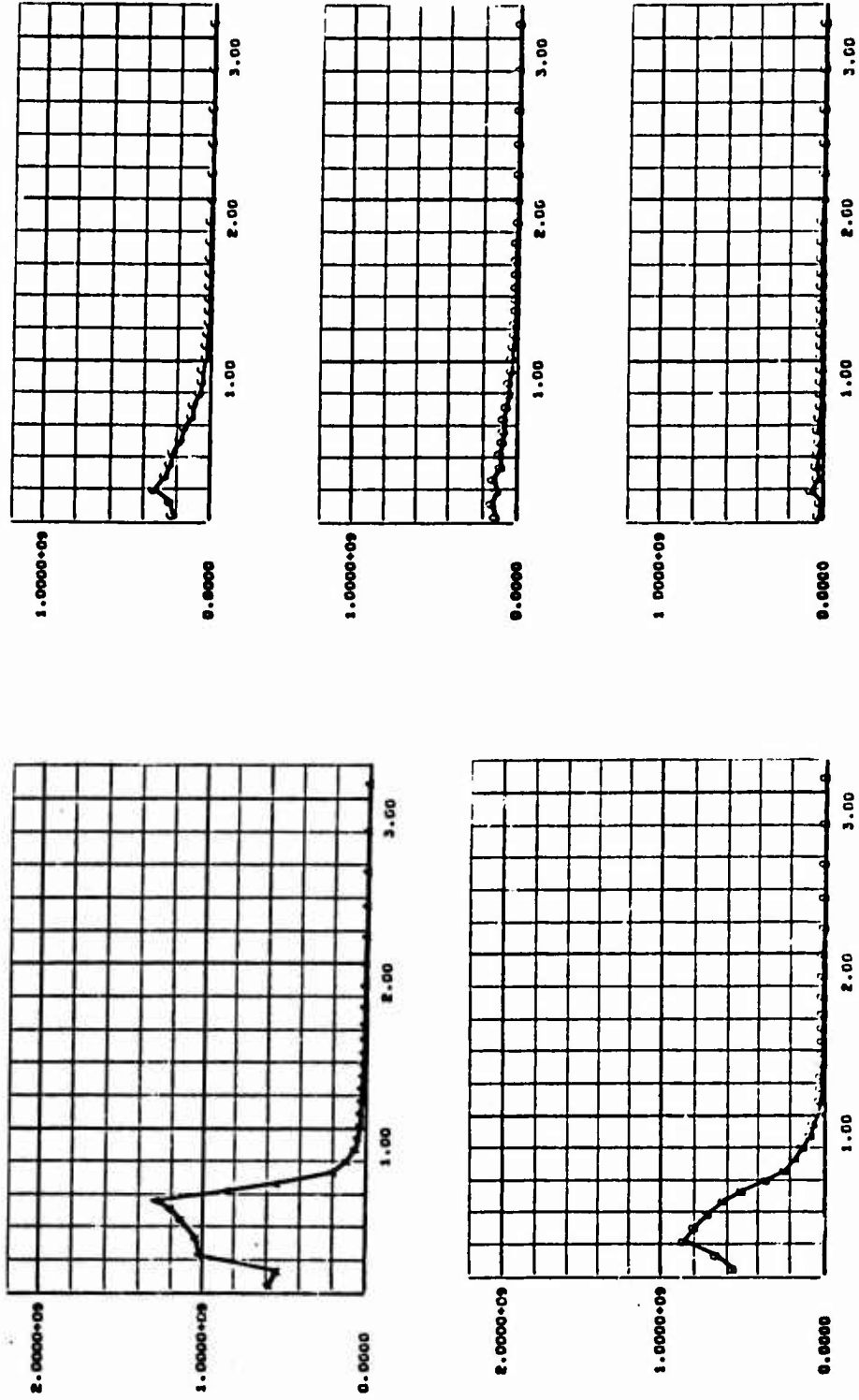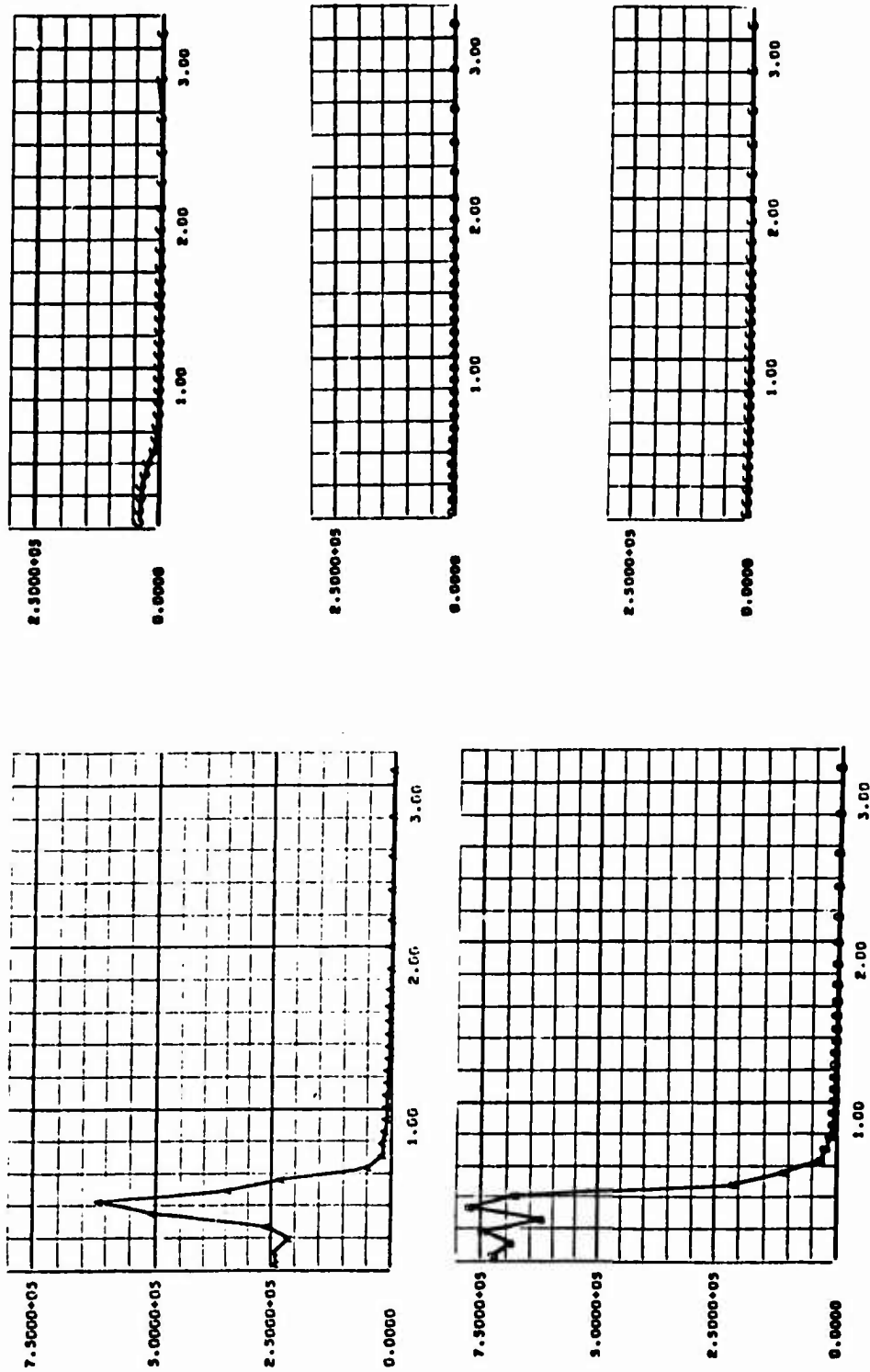D = Three-Quarters Distance into Target

E = Back Surface

137

IRON - ALUMINUM IMPACT

SPECIFIC INTERNAL ENERGY (ERGS/G) VS X (CM)   TIME= 5.0000-07

Figure 102.

138
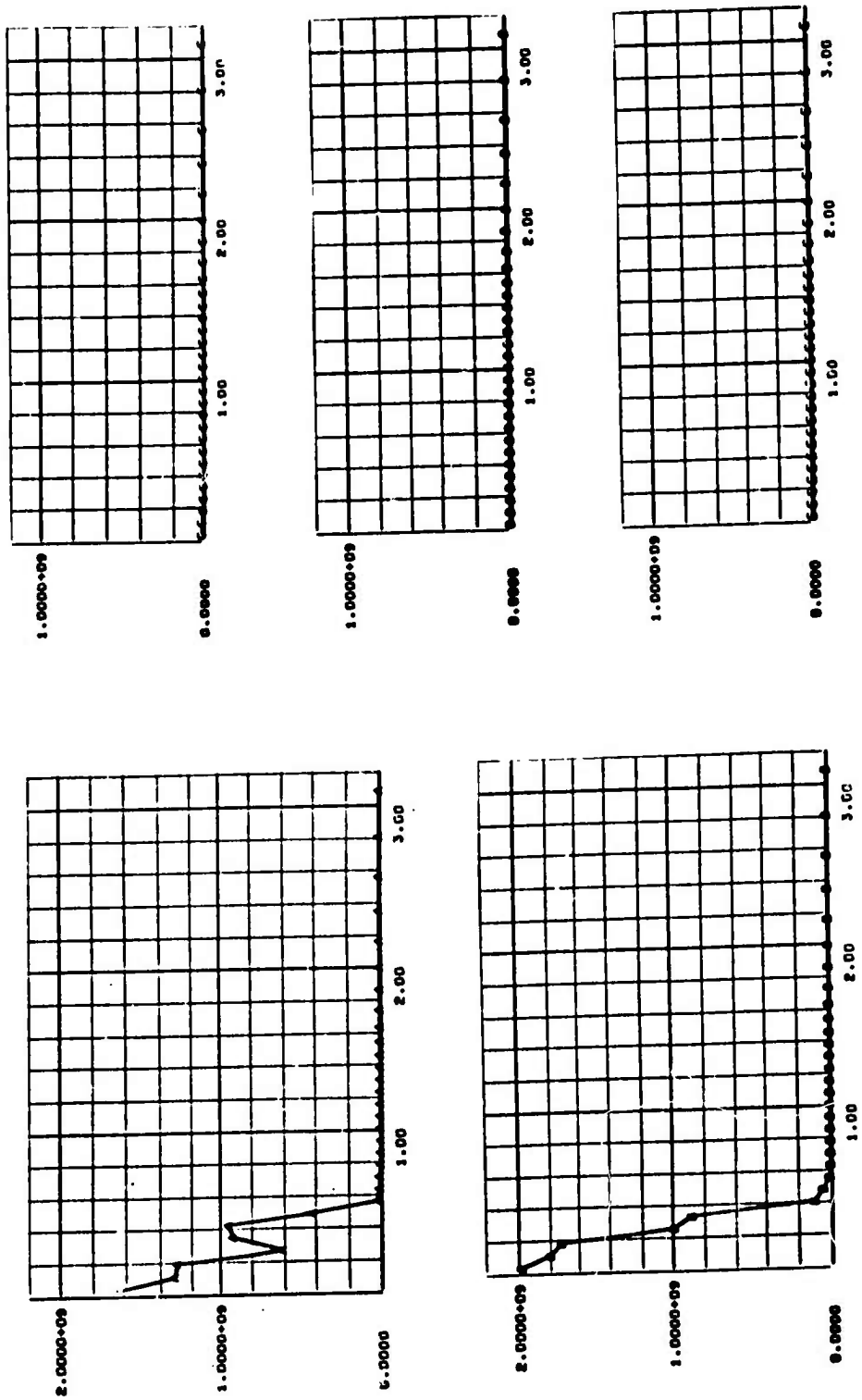
IRON - ALUMINUM IMPACT
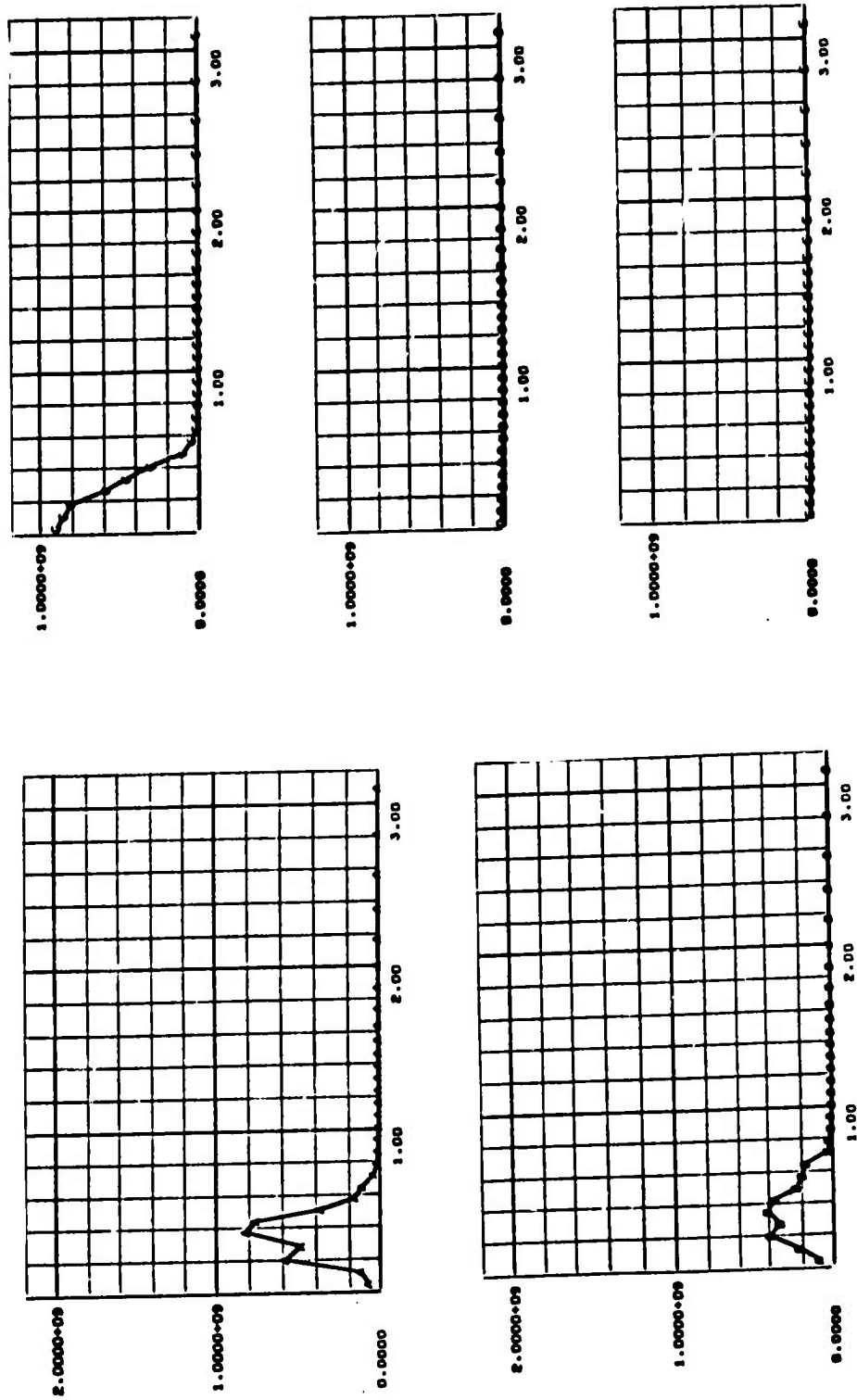
SPECIFIC INTERNAL ENERGY (ERGS/G) VS X (CM)   TIME= 1.0000-06

Figure 103.

139

IRON - ALUMINUM IMPACT
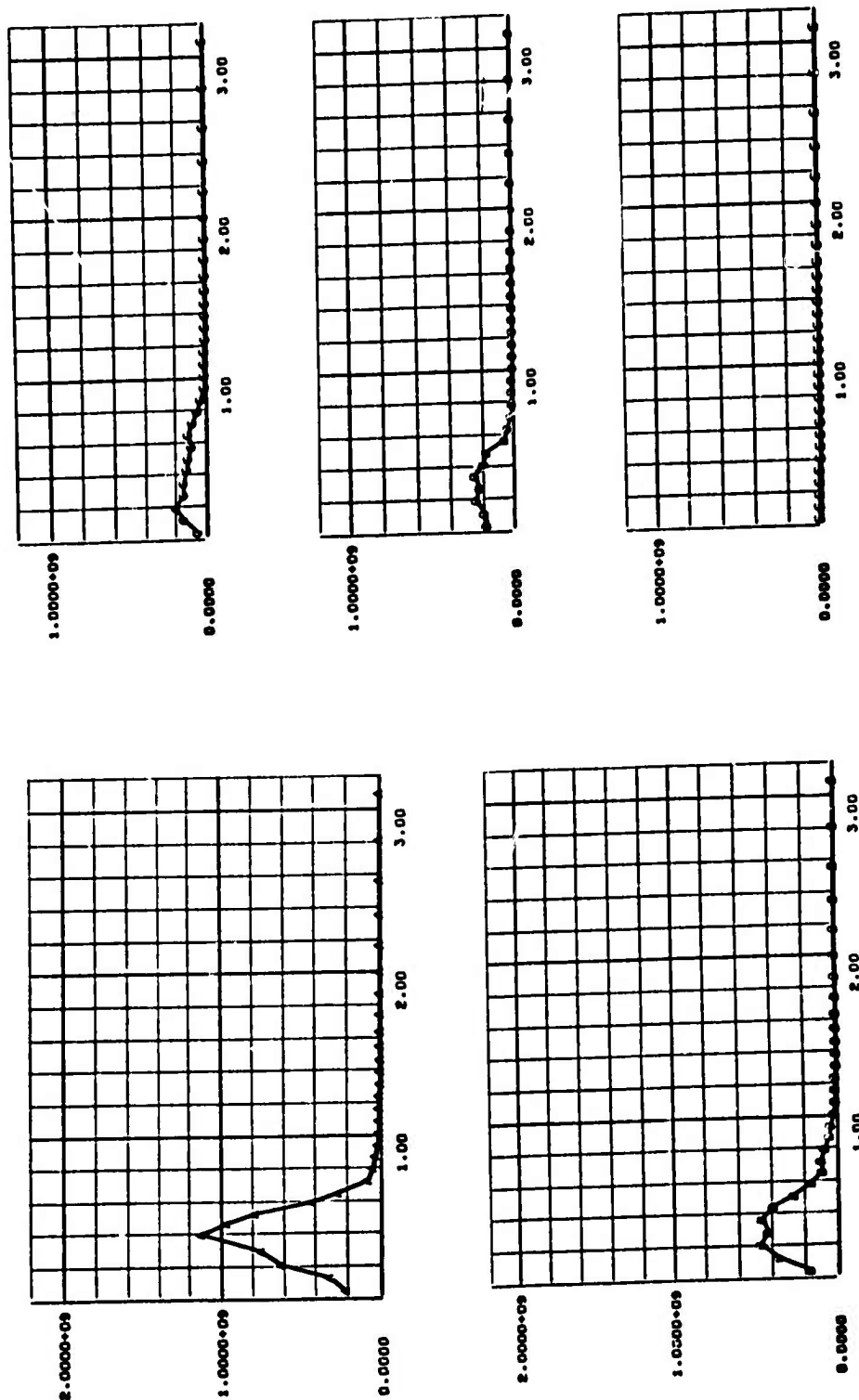
SPECIFIC INTERNAL ENERGY (ERGS/G) VS X (CM)   TIME= 1.5000-06

Figure 104.
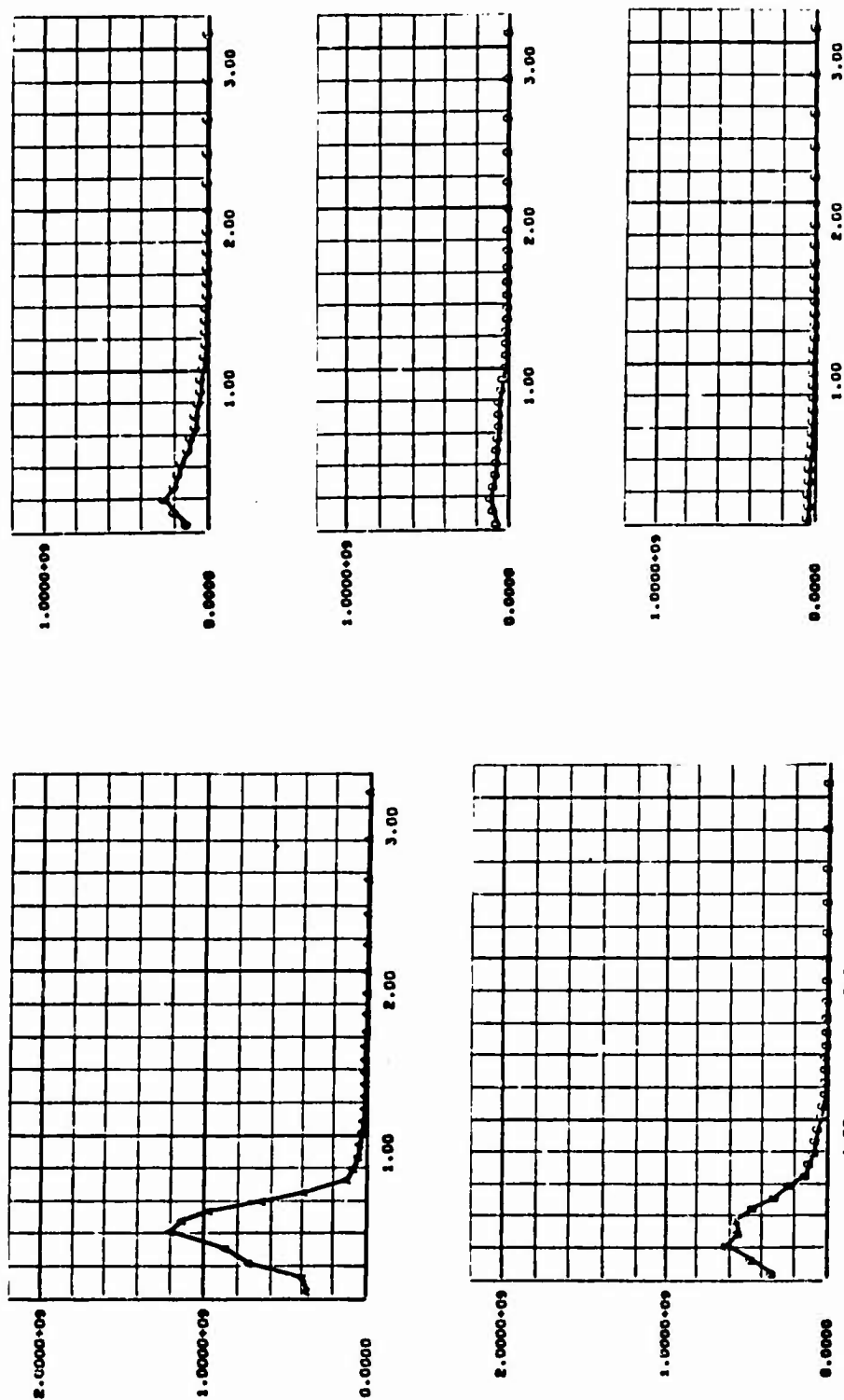
140

IRON - ALUMINUM IMPACT

SPECIFIC INTERNAL ENERGY (ERGS/G) VS X (CM)   TIME=   2.0000-06

Figure 105.

141

IRON - ALUMINUM IMPACT

SPECIFIC INTERNAL ENERGY (ERGS/G) VS X (CM)   TIME= 2.5000-06

Figure 106.

142

IRON - ALUMINUM IMPACT

SPECIFIC INTERNAL ENERGY (ERGS/G) VS X (CM)   TIME= 3.0000-06

Figure 107.

143

TEST PROBLEM NO. 2

Instantaneous Plastic Strain Rate Versus Radial Distance at Five Locations in the Target

For T = 0.0, 0.5, 1.0, 1.5, 2.0, 2.5, and 3.0 μsec.

A = Target Front Surface

B = One-Quarter Distance into Target

C = One-Half Distance into Target

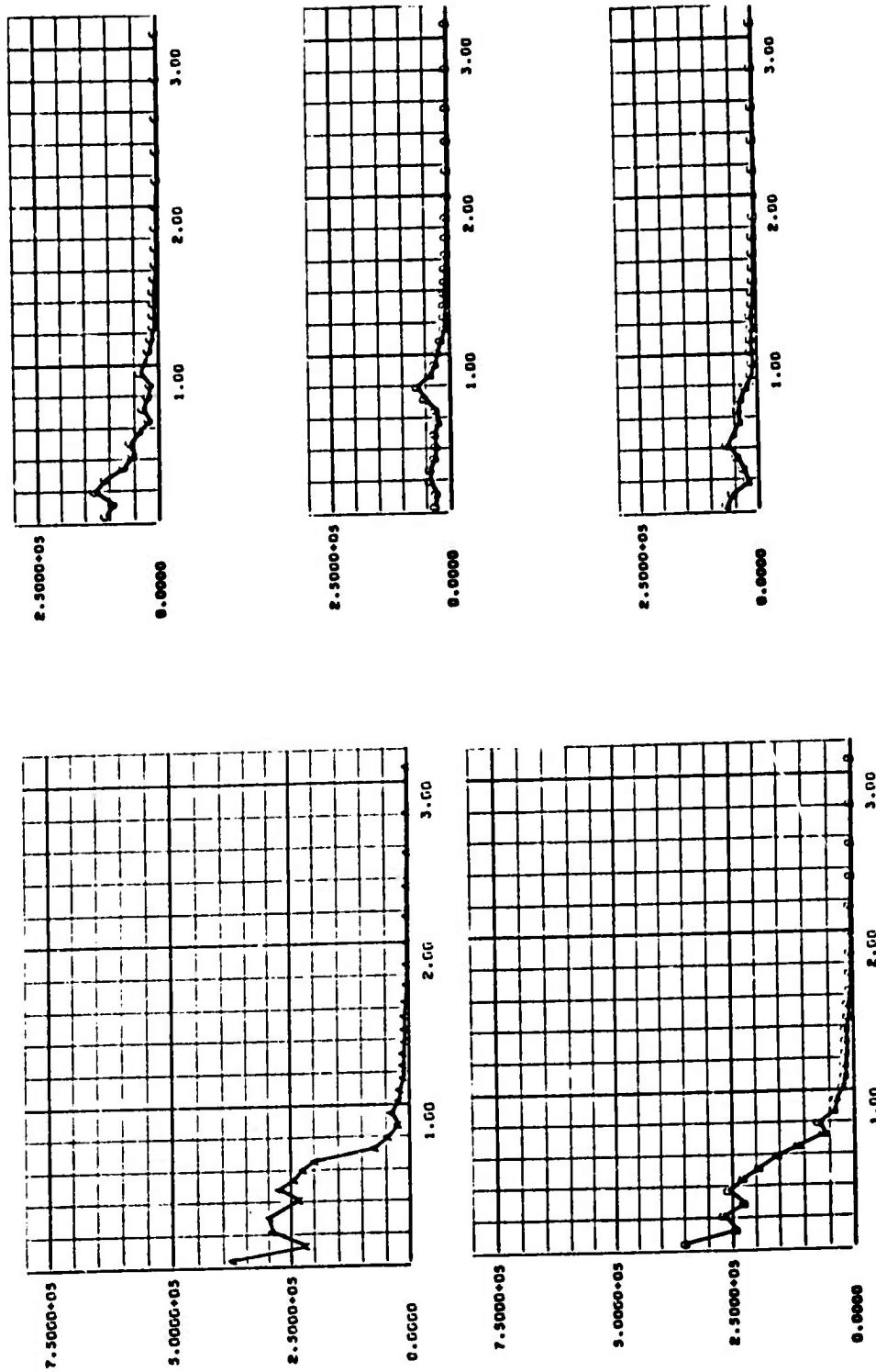D = Three-Quarters Distance into Target

E = Back Surface

IRON - ALUMINUM IMPACT

PLASTIC STRAIN RATE (1/SEC) VS X (CM)   TIME= 5.0000-07

Figure 108.

145

IRON - ALUMINUM IMPACT

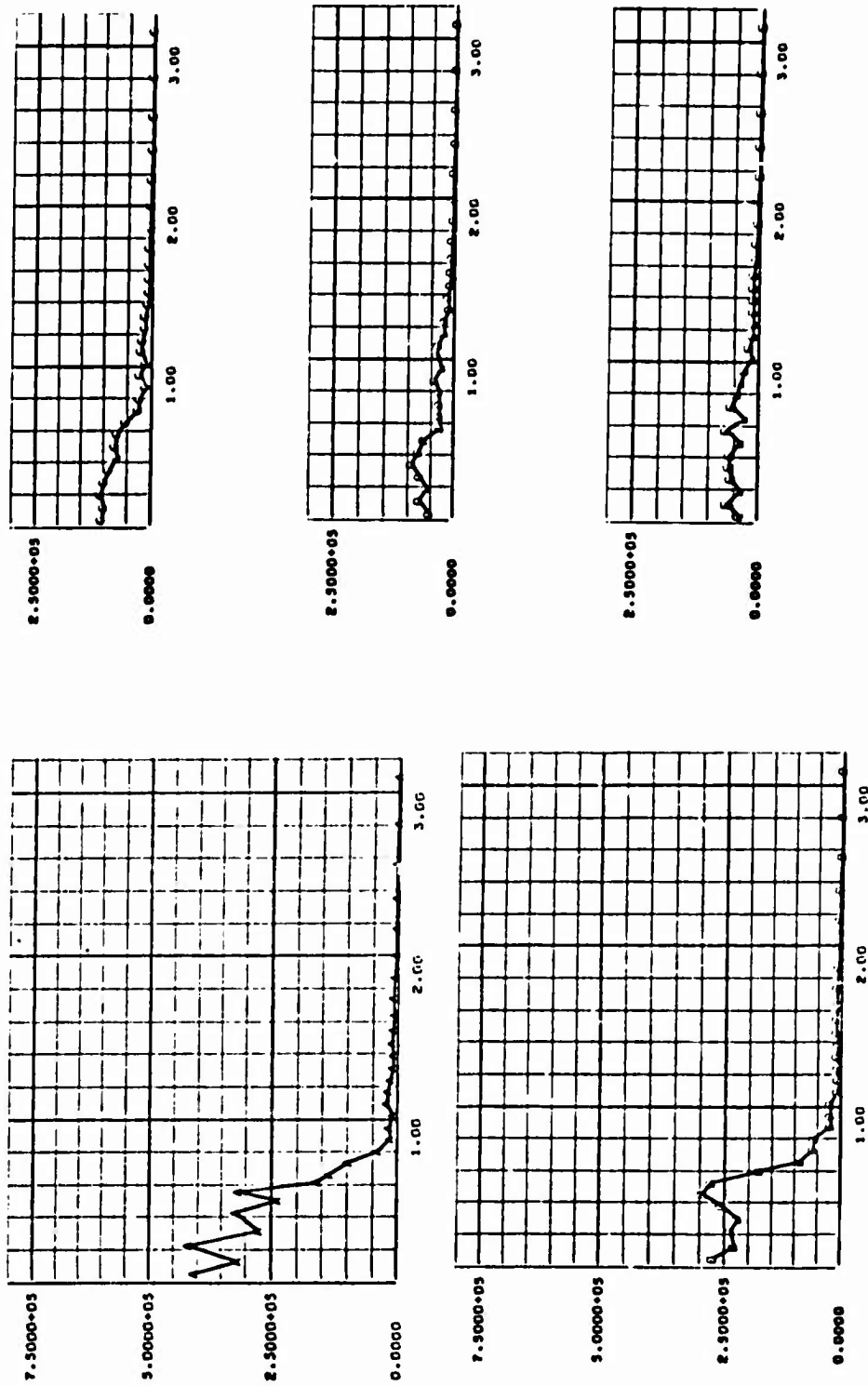PLASTIC STRAIN RATE (1/SEC) VS X (CM)   TIME= 3.3000-06

Figure 109.

146
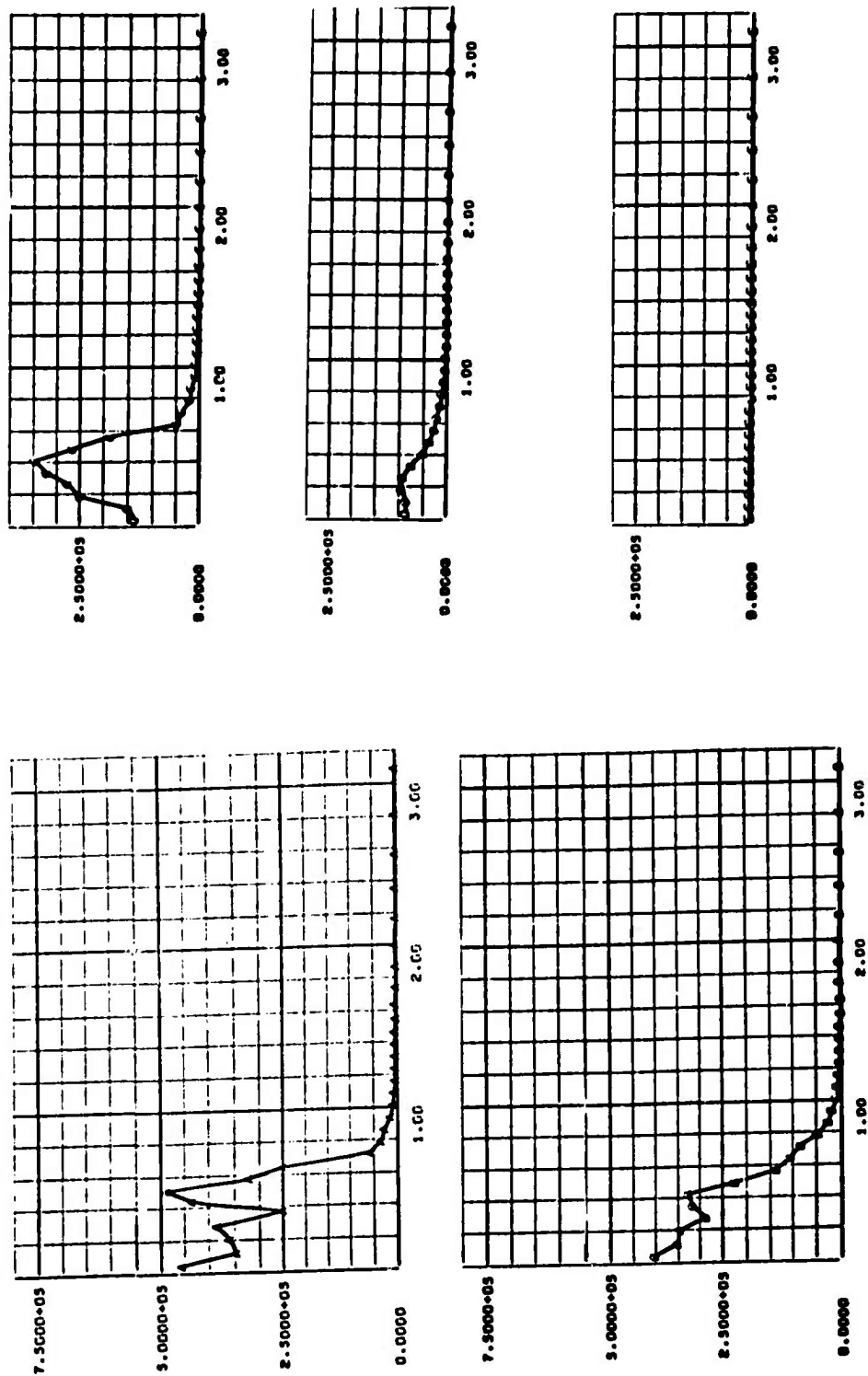
IRON - ALUMINUM IMPACT
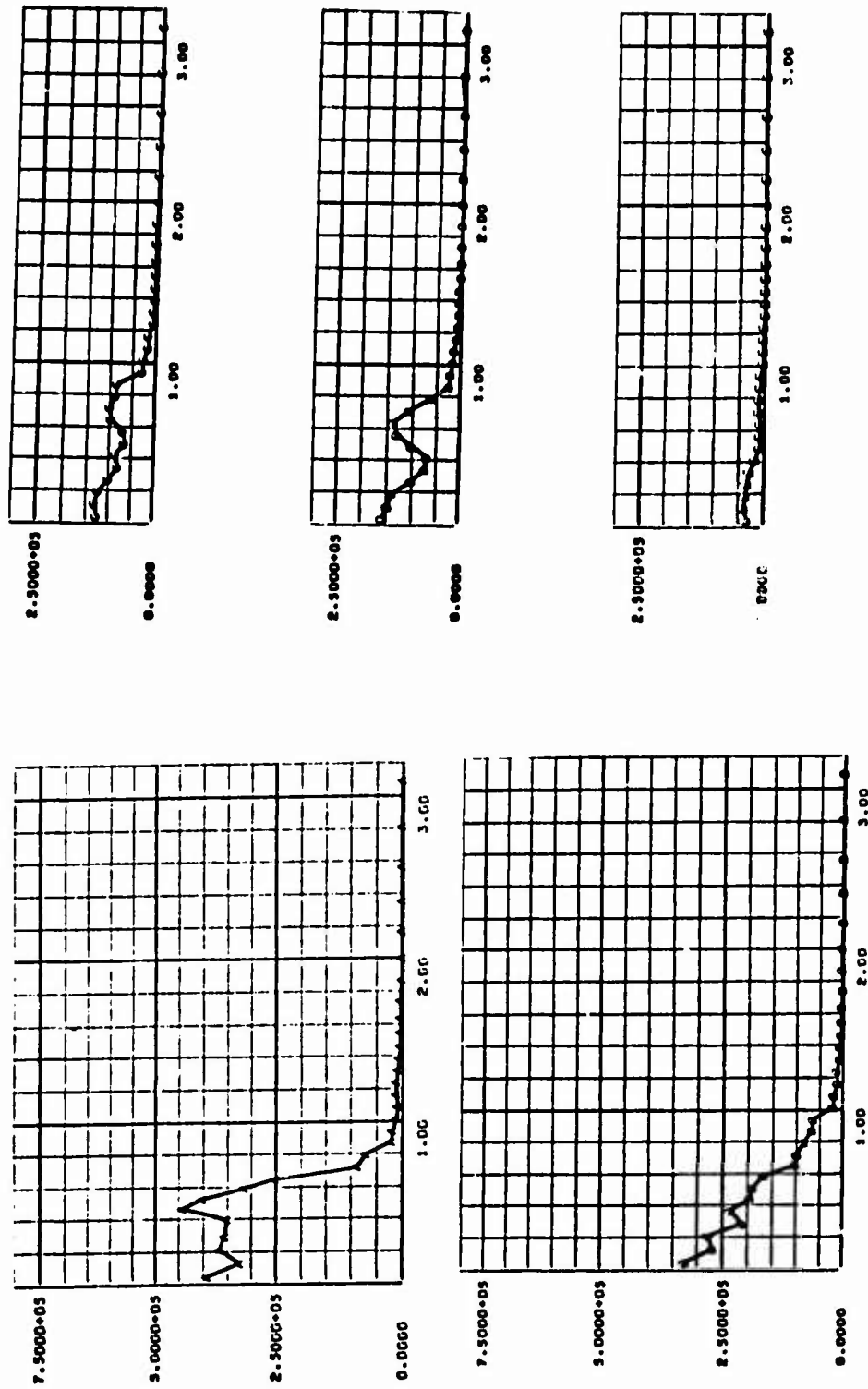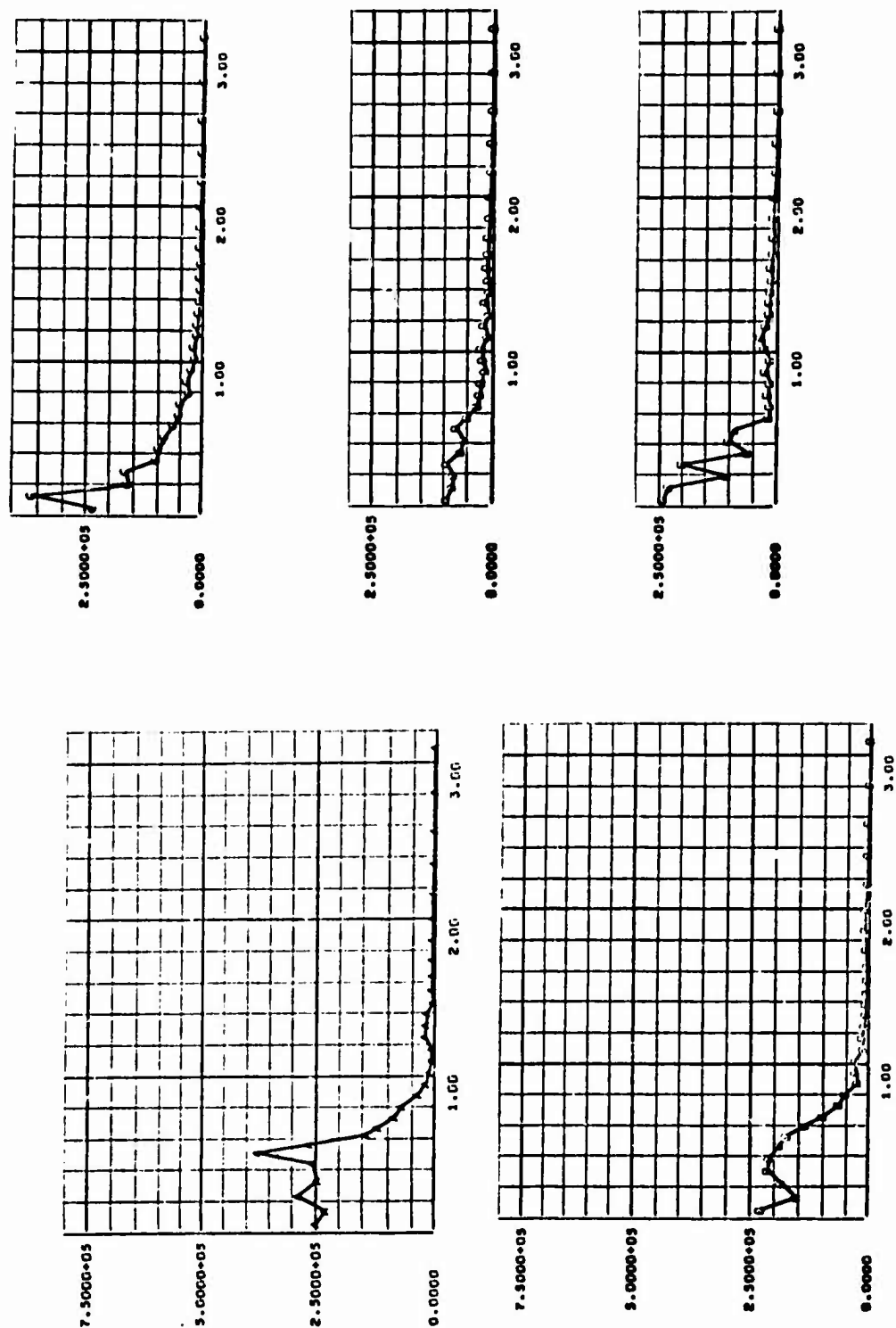
TIME= 1.5000-06

PLASTIC STRAIN RATE (1/SEC) VS X (CM)

Figure 110.

IRON - ALUMINUM IMPACT

PLASTIC STRAIN RATE (1/SEC) VS X (CM)

TIME= 2.0000-06

Figure 111.

148

IRON - ALUMINUM IMPACT

PLASTIC STRAIN RATE (1/SEC) VS X (CM)   TIME=   2.5000-06

Figure 112.

149

IRON - ALUMINUM IMPACT

TIME= 3.0000-06

PLASTIC STRAIN RATE (1/SEC) VS X (CM)

Figure 113.

150

TEST PROBLEM NO. 2

Plastic Work Versus Radial Distance at Five Locations in the Target

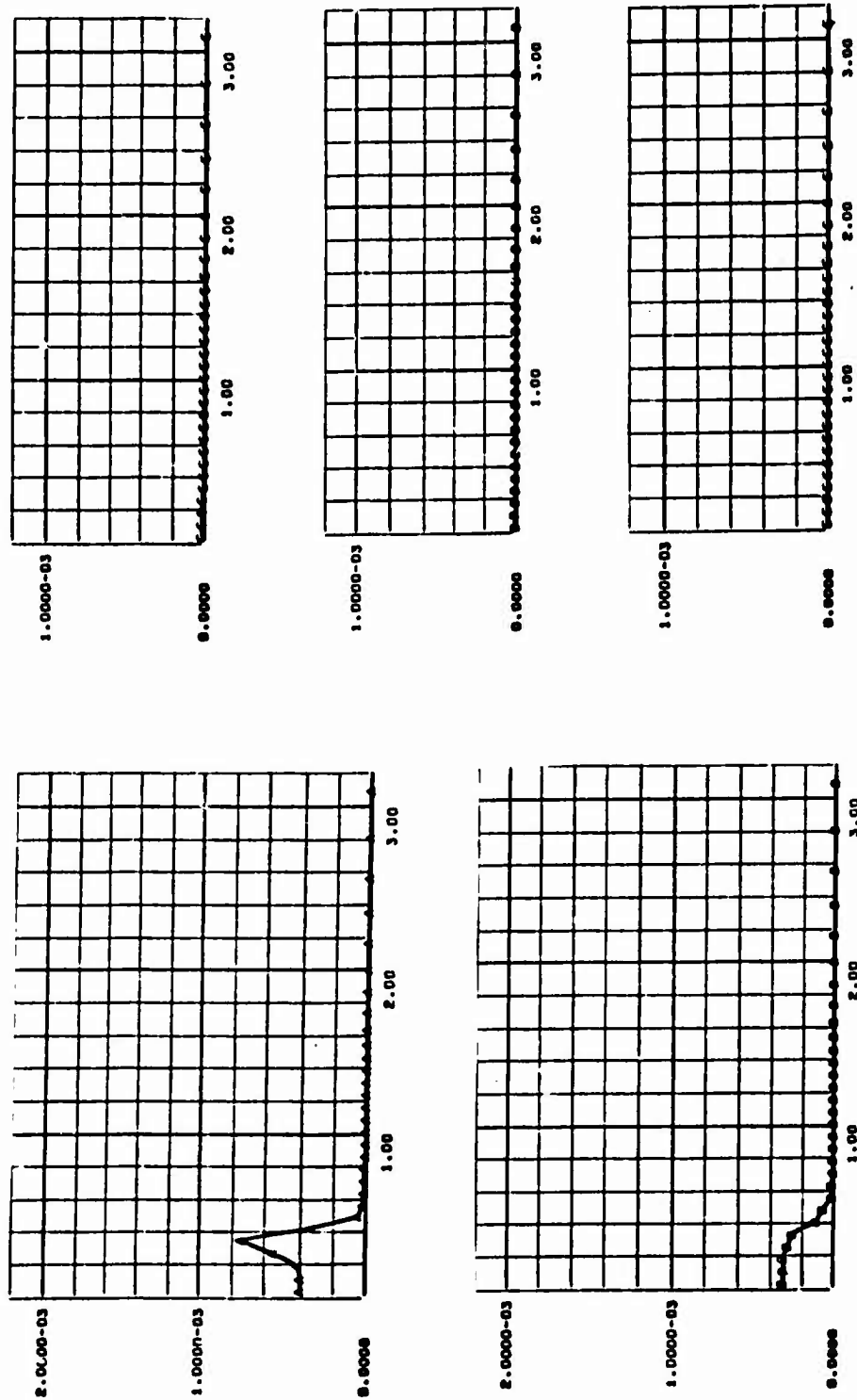For T = 0.0, 0.5, 1.0, 1.5, 2.0, 2.5, and 3.0 μsec.

A = Target Front Surface

B = One-Quarter Distance into Target

C = One-Half Distance into Target

D = Three-Quarters Distance into Target
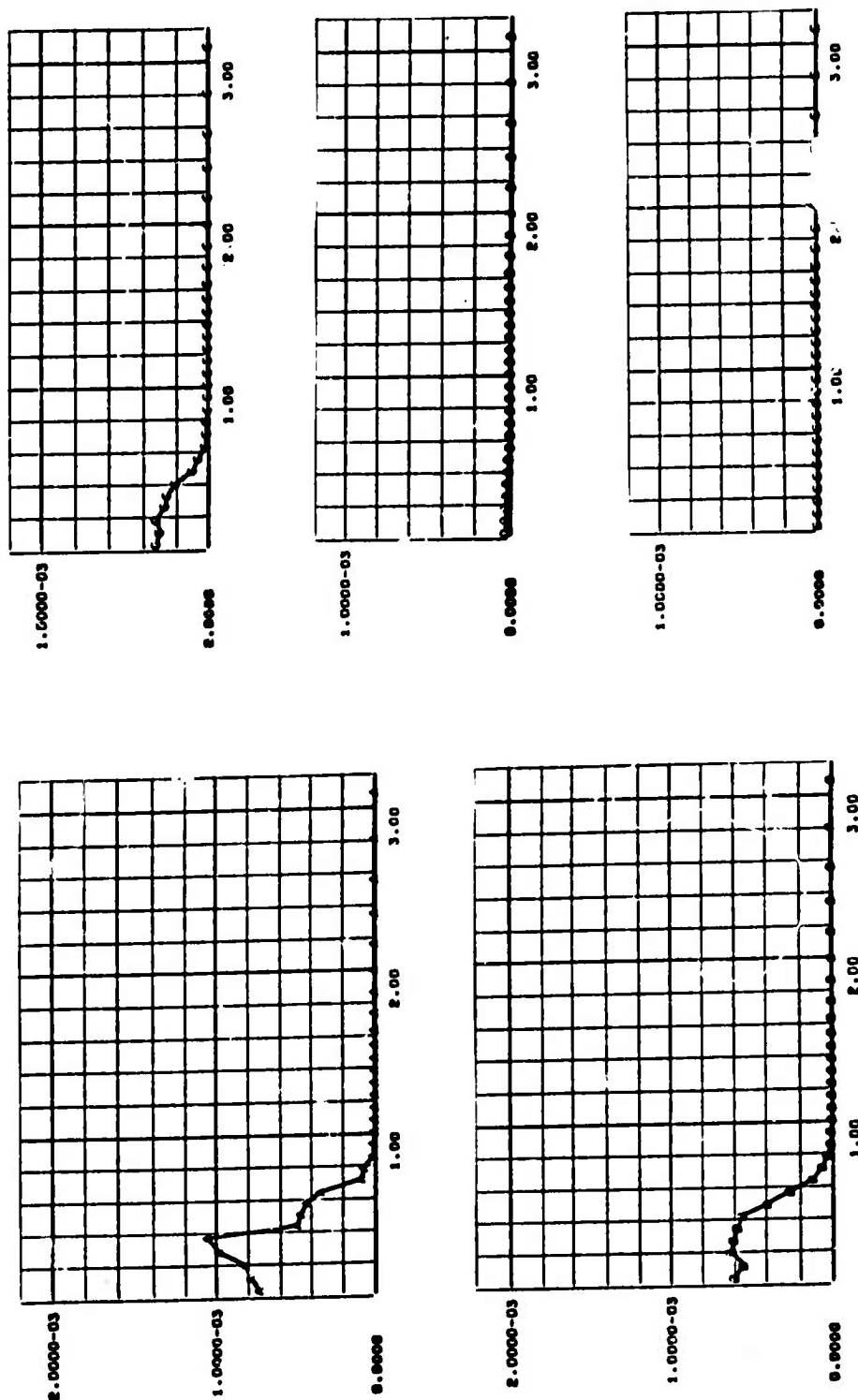
E = Back Surface

IRON - ALUMINUM IMPACT

TIME= 5.0000-07

PLASTIC WORK (MB) VS X (CM)

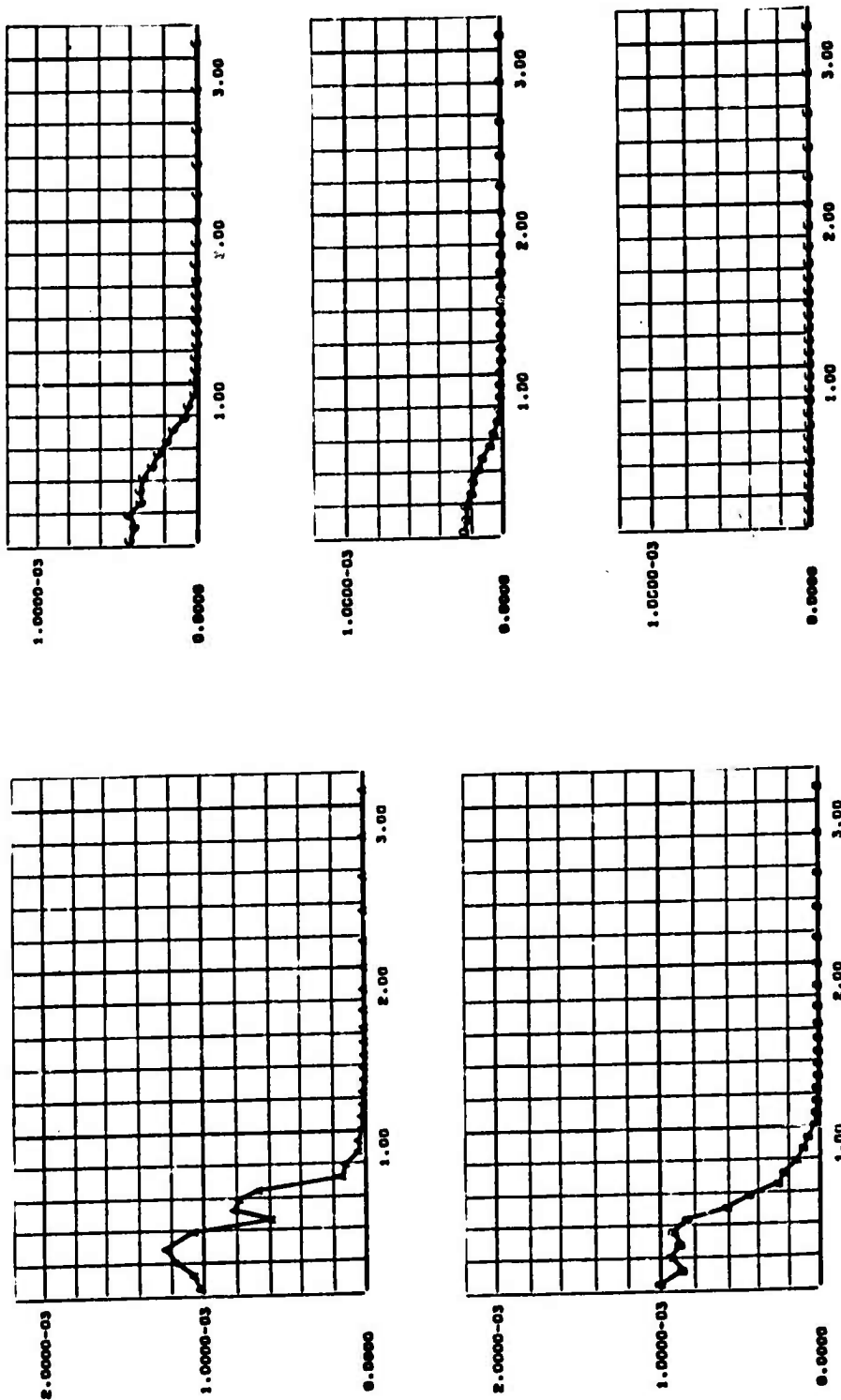Figure 114.

152

IRON - ALUMINUM IMPACT

PLASTIC WORK (MB) VS X (CM)

TIME= 1.0000-06

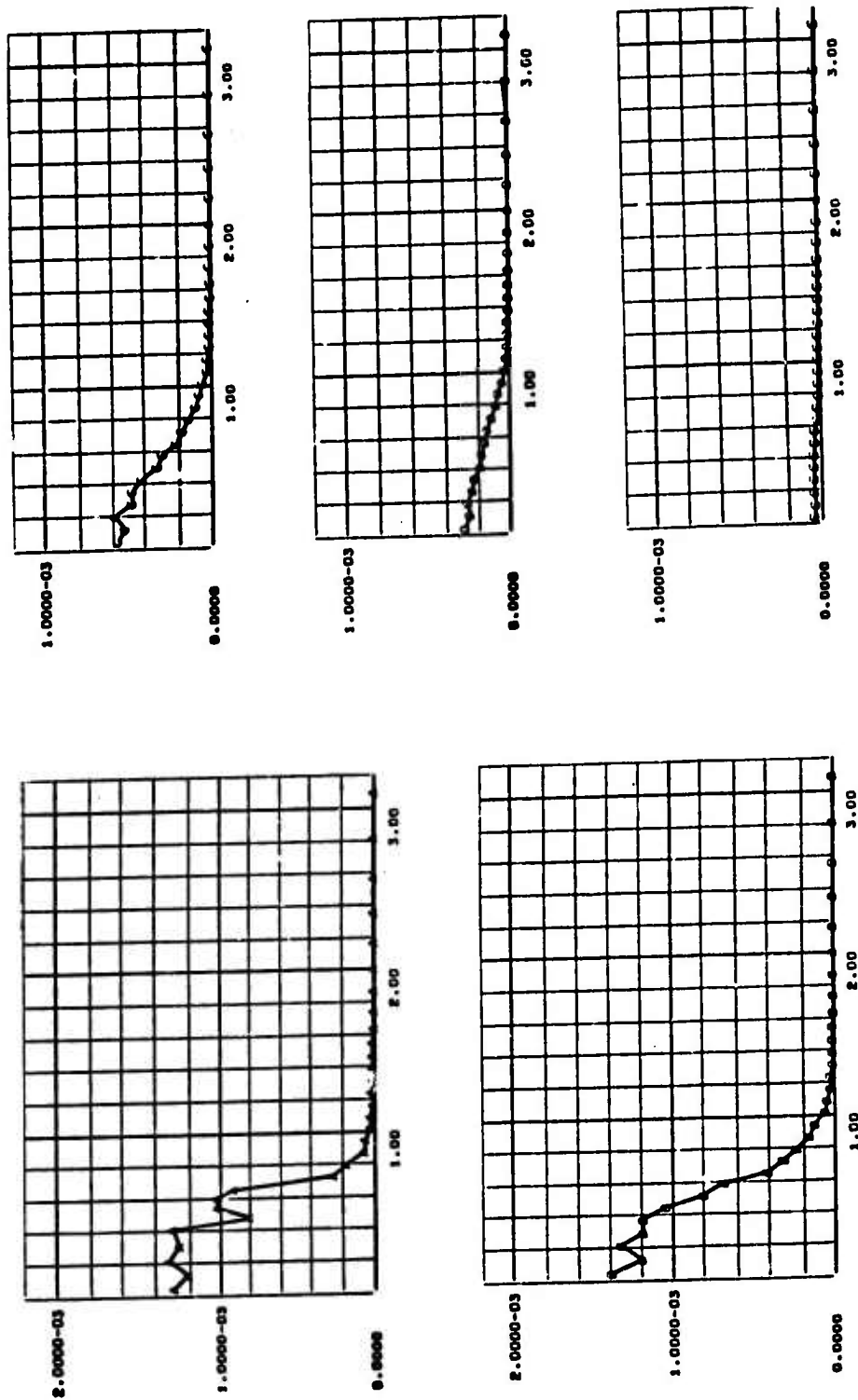Figure 115.

153

IRON - ALUMINUM IMPACT

TIME= 1.5000-06

PLASTIC WORK (MB) VS X (CM)

Figure 116.

IRON - ALUMINUM IMPACT

PLASTIC WORK (MB) VS X (CM)
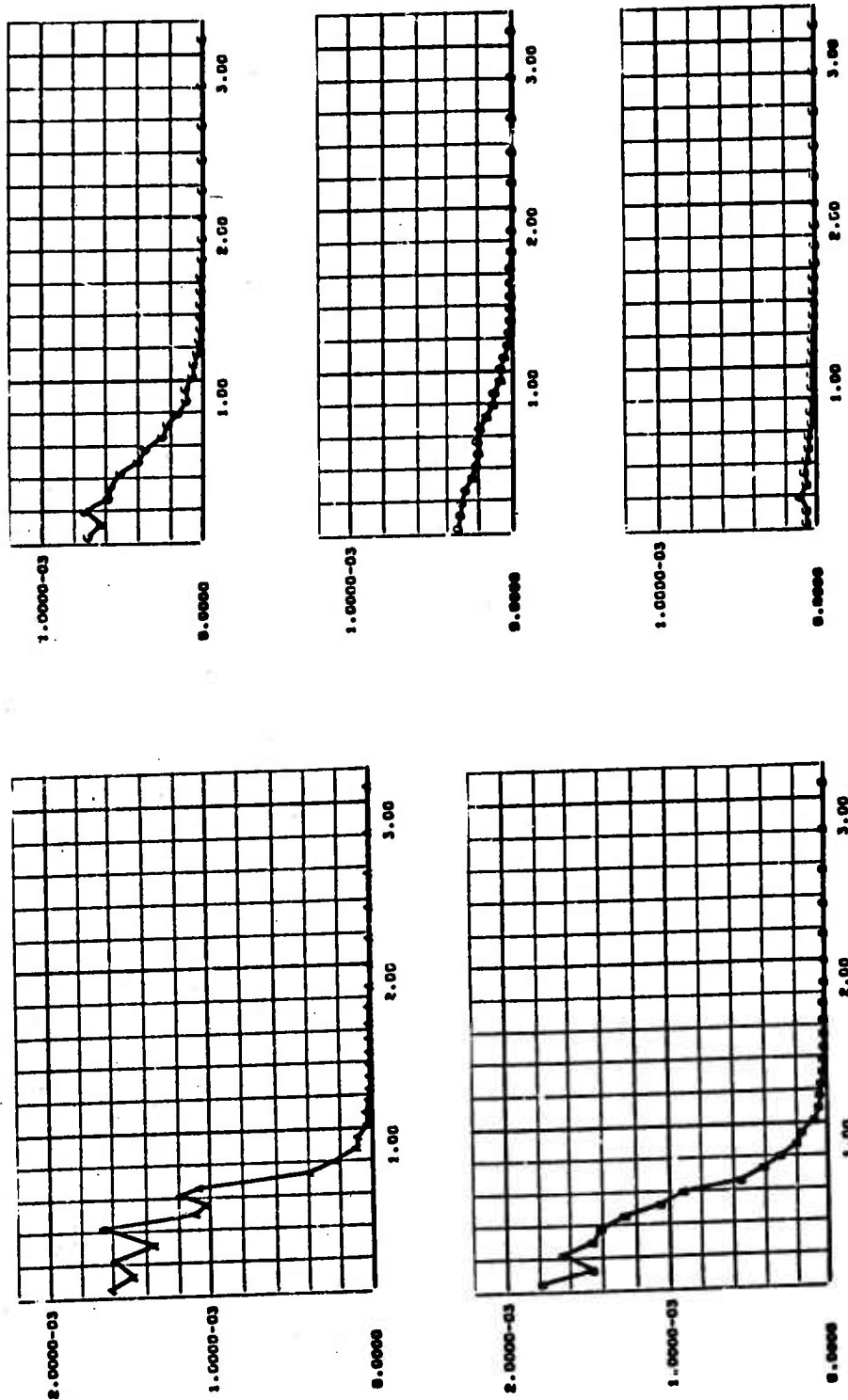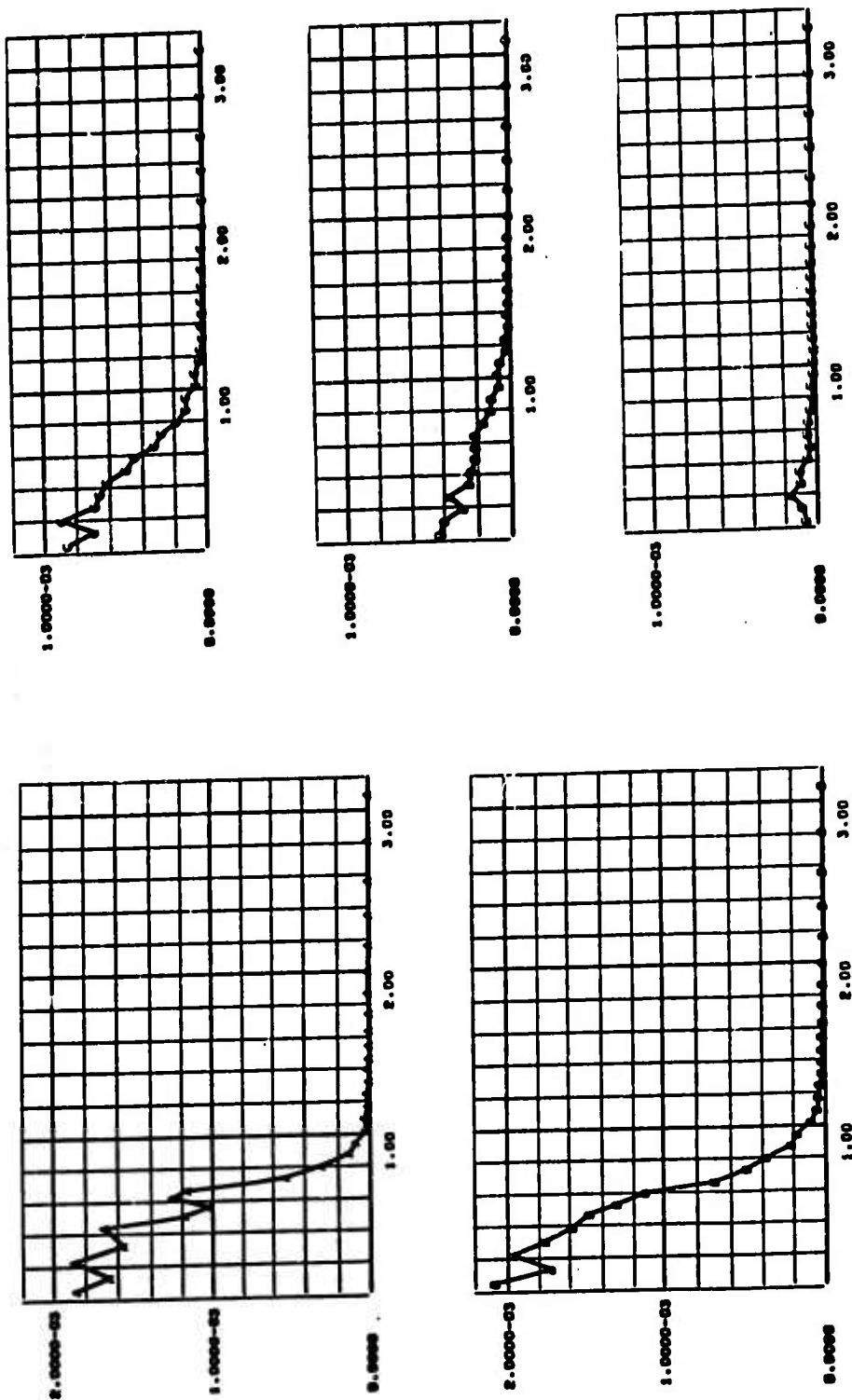
TIME= 2.0000-06

Figure 117.

IRON - ALUMINUM IMPACT

PLASTIC WORK (MB)   VS   X (CM)

TIME=   2.5000-06

Figure 118.

IRON - ALUMINUM IMPACT

PLASTIC WORK (''8) VS X (CM)

TIME= 3.0000-06

Figure 119.

157